LONG CHARACTERISTIC METHOD IN SPACE AND TIME FOR TRANSPORT PROBLEMS

A Thesis

by

TARA MARIE PANDYA

Submitted to the Office of Graduate Studies of
Texas A&M University
in partial fulfillment of the requirements for the degree of

MASTER OF SCIENCE

December 2009

Major Subject: Nuclear Engineering

LONG CHARACTERISTIC METHOD IN SPACE AND TIME FOR TRANSPORT PROBLEMS

A Thesis

by

TARA MARIE PANDYA

Submitted to the Office of Graduate Studies of
Texas A&M University
in partial fulfillment of the requirements for the degree of

MASTER OF SCIENCE

Approved by:

Chair of Committee,	Marvin Adams
Committee Members,	Jim Morel
	Nancy Amato
Head of Department,	Raymond Juzaitis

December 2009

Major Subject: Nuclear Engineering

ABSTRACT

Long Characteristic Method in Space and Time for Transport Problems. (December 2009)

Tara Marie Pandya, B.S., Texas A&M University

Chair of Advisory Committee: Dr. Marvin Adams

Discretization and solving of the transport equation has been an area of great research where many methods have been developed. Under the deterministic transport methods, the method of characteristics, MOC, is one such discretization and solution method that has been applied to large-scale problems. Although these MOC, specifically long characteristics, LC, have been thoroughly applied to discretize and solve transport problems in the spatial domain, there is a need for an equally adequate time-dependent discretization. A method has been developed that uses LC discretization of the time and space variables in solving the transport equation. This space-time long characteristic, STLC, method is a discrete ordinates method that applies LC discretization in space and time and employs a least-squares approximation of sources such as the scattering source in each cell. This method encounters the same problems that previous spatial LC methods have dealt with concerning achieving all of the following: particle conservation, exact solution along a ray, and smooth variation in reaction rate for specific problems. However, quantities that preserve conservation in each cell can also be produced with this method and compared to the non-conservative

results from this method to determine the extent to which this STLC method addresses the previous problems.

Results from several test problems show that this STLC method produces conservative and non-conservative solutions that are very similar for most cases and the difference between them vanishes as track spacing is refined. These quantities are also compared to the results produced from a traditional linear discontinuous spatial discretization with finite difference time discretization. It is found that this STLC method is more accurate for streaming-dominate and scattering-dominate test problems. Also, the solution from this STLC method approaches the steady-state diffusion limit solution from a traditional LD method. Through asymptotic analysis and test problems, this STLC method produces a time-dependent diffusion solution in the thick diffusive limit that is accurate to $O(\varepsilon)$ and is similar to a continuous linear FEM discretization method in space with time differencing. Application of this method in parallel looks promising, mostly due to the ray independence along which the solution is computed in this method.

ACKNOWLEDGEMENTS

I would like to thank my committee chair, Dr. Adams, and my committee members, Dr. Morel and Dr. Amato, for their guidance and support throughout the course of this research. Thanks also go to my friends and colleagues and the nuclear engineering department, faculty, and staff for making my time at Texas A&M University a rewarding experience. Finally, thanks to my mother and father for all of their support throughout my undergraduate and graduate career.

NOMENCLATURE

DFEM	Discontinuous Finite Element Method
FD	Finite Difference
FE	Finite Element
GMRES	General Minimum Residual
LC	Long Characteristics
LD	Linear Discontinuous
LFEM	Linear Finite Element Method
MOC	Method of Characteristics
STLC	Space-Time Long Characteristics

TABLE OF CONTENTS

Page

LIST OF FIGURES

Page

LIST OF TABLES

1. INTRODUCTION

The transport equation can be used to solve a wide range of particle transport problems including those involving radiation hydrodynamics. Discretization of the time and spatial variables is an important aspect of the method used to solve this transport equation on a problem domain. Many spatial discretization methods have been applied to multidimensional problems including finite difference (FD), finite element (FE), and the method of characteristics (MOC). In time-dependent problems the temporal variable has been discretized using FD methods and Runge-Kutta methods, which produce a sequence of steady-state problems that must be solved. Essentially, past methods discretize the spatial and time domains using two different methods and "paste" them together to solve the transport equation.

1.1 Current State of the Problem

Solving time-dependent transport problems is an important component of a wide range of applications. One of the first steps involved when solving these transport problems is discretization of the time and spatial dependence of the solution. Besides the many methods to discretize the spatial variable, there are also a variety of known methods to discretize the temporal variable, including finite difference (FD) and Runge-Kutta (RK) methods. These time discretization methods include explicit, implicit, and combination methods. The explicit methods, such as forward Euler, need very small time steps to find an adequate and stable solution and therefore require a large amount of

---

This thesis follows the style of *Journal of Computational Physics.*

computation time. The implicit methods, such as Crank Nicholson or Backward Euler, tend to be diffusive, causing unphysical spreading of the solution, and/or introduce unphysical oscillations. With both types of methods, the time-dependent solution is obtained by solving one or more steady-state transport problems for each time step. All of these methods introduce a truncation error stemming from the approximation of the time derivative operator [1].

The long characteristic (LC) method has been applied to the spatial variable in multiple spatial dimensions in a variety of applications. This LC method involves finding the desired angular solution of the transport equation along rays that pass through the problem domain in many directions. If the total source in the problem can be approximated with a simple functional form, the angular solution along each ray can be found analytically. The average scalar flux value for a cell is determined by the usual discrete ordinates approximation, as are higher angular moments if needed. The LC method has been applied extensively to relatively large-scale transport problems, especially in reactor physics analysis [1, 2, 3, 4, 5].

Application of this LC method in space leads to three properties that are not able to be achieved together. These properties include the following:

1) Cell-wise reaction rate is equal to the sum of track-wise reaction rate which will be defined as track-wise conservation, (TWC),

2) Exact solution along each ray in a problem (no arbitrary changes in track lengths),

3) Smooth variation in reaction rates between cells for problems in which the correct reaction rates are smoothly varying.

The STLC method also cannot achieve these three properties simultaneously, but can miss the first property in a benign manner which is discussed in later sections.

After employing methods for discretization of the spatial and temporal variables, there are several iterative methods that can be used to find the discrete solution. For many transport problems, source iteration suffices since the solution process is straightforward and convergent. Source iteration uses the solution from the previous iteration in the source to find the current iterate solution. However, for transport problems in optically thick regions in which particles suffer many collisions before leaking or being permanently captured, an acceleration technique is needed to converge the solution in a reasonable number of iterations. A Krylov solver such as a conjugate gradient (CG) method or the general minimum residual method (GMRES) may be employed to accelerate convergence. Krylov solvers use a basis in a Krylov subspace and find the "best" solution in the subspace at each iteration. The basic process of the CG method or biconjugate gradient method (BiCG) is an iterative method that uses a gradient of the function and the conjugates to this gradient to find the next iterate. GMRES is a particular Krylov solver that finds the "best" solution each iterate by forming a solution using the basis functions of the subspace with coefficients that minimize the norm of the residual [6, 7].

Several of the methods mentioned previously have been applied to solve large problems using parallel computing. There are two main methods used currently to solve

particle-transport problems in parallel: block-Jacobi and sweeps. Some codes combine these two methods in various ways. Block-Jacobi iteration is performed by finding the local solution on fixed subdomains using incident fluxes from the previous iterate. As subdomains are refined Block-Jacobi requires more and more iterations to converge. A sweep is performed by following a wave through the spatial domain for a given direction to find the desired solution. Iterations based upon sweeps can converge at a rate that is independent of cell and subdomain size [8].

The most useful parallel algorithms are “scalable”. An algorithm is scalable if the solution time is constant as the numbers of processors and unknowns in a problem are scaled by the same factor, when the processor count becomes large. The main drawback to sweeps and Block-Jacobi is the lack of direct scalability. Block-Jacobi iterations are not scalable due to the slow convergence that occurs as subdomains are refined for a given problem. Currently the Koch-Baker-Alcouffe (KBA) algorithm for processor partitioning of structured grids has the best results for potentially achieving scalability using sweeps. This algorithm decomposes the spatial domain into columnar partitions for each processor. The lack of scalability for this algorithm using sweeps arises from the fact that sweeps are serial in nature along the direction of propagation which leads to a lower bound on the time required to sweep a fixed grid independent of processor count. The KBA algorithm with sweeps is able to scale to a large number of processors before the loss of parallel efficiency occurs. Finding an algorithm that is sweep-based and scalable is an area of ongoing research [8, 9, 10].

1.2 Focus of this Research

The main purpose of the research proposed here is to explore the benefits of applying the method of long characteristics (LC) to discretize both the spatial and temporal variables involved in transport problems. This space-time long characteristic (STLC) method can be directly applied to a transient problem and produce the full time-dependent solution with minimal numerical error. The STLC method analytically inverts the streaming and collision operators including the time derivative. Thus, the only approximation occurs in the collisional source representation as a function expansion. Whereas most MOC implementations have used a cell-wise constant representation of the collision source, a second purpose of this research is to explore the higher-order representation of this source [1, 2].

There are several important contributions from this thesis work. First is the development of the STLC method for time-dependent slab geometry problems. Along with this development is the exploration of the linear representation of the collision source in each *x*-*t* cell ($\alpha + \beta x + \gamma t$). The second contribution is an analysis of how this STLC method satisfies conservation as well as an analysis of this method in the diffusion limit. Finally, this work shows the testing and implementation of this STLC method for various problems, especially those to test the predictions of the previous analyses.

1.3 Outline of Remainder

In the following sections the current state of solving time-dependent problems will be discussed. The basic methodology of this STLC method will be outlined

including the relation between coordinate systems, the least-squares approximation, and a specific definition of conservation of particles. Numerical results will then be presented that demonstrate the key features of this method along with a comparison to traditional discretization methods. Conclusions about this method will be presented along with recommendations for uses of this method and further research on this topic. Finally, the potential of this method for application in parallel algorithms and application to large-scale transport problems will be discussed. The main conclusion is that application of the STLC method to complex and large-scale transport problems such as those involved with radiation transport is a promising area of study.

2. DEVELOPMENT OF STLC METHOD

In this section the STLC method is developed for time-dependent slab-geometry problems. This includes deriving the basic equations for the solution along space-time characteristics and the equations for generating cell-wise collision sources from the solution along rays.

2.1 Coordinate System Definition

The STLC method seeks to solve time-dependent slab geometry transport problems using long characteristics that span space and time. The space and time domains, denoted by coordinates x and t, are discretized into cells. A characteristic that spans the problem domain is referred to as a ray, and the part of a ray in one cell is referred to as a track. Figure 1 shows the discretization of the $(i,n)^{th}$ cell with tracks passing through this cell for a particular angular direction.

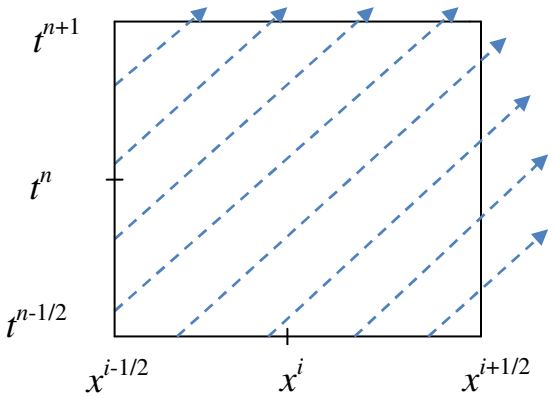

Figure 1: Space-time Cells with Tracks in One Angular Direction

In this space-time cell shown in Fig. 1, neither the tracks nor the spacing between them has units of length. This problem can be fixed by using *vt* as the vertical coordinate of the cells. In the (*x*-*vt*) system, the actual distance traveled by a particle is simply the change in its *vt* coordinate; the change in the *x* coordinate is irrelevant.

The solution along a track will now quickly be reviewed. A particle initially at position x_0 at time t_0 moving with direction cosine μ will have the following coordinates after moving a distance *s*:

$$\begin{aligned} x &= x_0 + \mu s \\ t &= t_0 + \frac{s}{v} \end{aligned} \tag{2.1}$$

where *v* is the speed of the particle. The analytic transport solution along any characteristic track is defined as the following:

$$\Psi_m(x,t) = \Psi_m(x-\mu_m\tau, t-\frac{\tau}{v})e^{-\sigma_t\tau} + \int_0^\tau ds q_{tot,m}(x-\mu_m s, t-\frac{s}{v})e^{-\sigma_t s} \tag{2.2}$$

The distance traveled along this characteristic from ($x-\mu_m\tau$, $t-\tau/v$) to (x, t) is defined as τ, and q_{tot} is the total source including scattering.

During the solution process, integration must be performed over each space-time cell using the track spacing and the solution along each track in the cell. To facilitate this, a rotated coordinate system in the *x*-*vt* plane is defined as shown in Fig. 2. In this figure, θ is related to μ by the following relation:

$$\sin\theta = \frac{1}{\sqrt{1+\mu^2}} \tag{2.3}.$$

From Fig. 2 and using the relationship in Eq. (2.1) the actual distance traveled (Δs) can be related to the distance along the u axis as shown in Eq. (2.4):

$$\Delta u = \Delta s / \sin\theta = \Delta s\sqrt{\mu^2 + 1} \tag{2.4}.$$

In this work it is assumed that the distance between adjacent parallel rays is given and is constant for a particular problem. If the ray spacing is denoted as $\Delta\omega$, then from Fig. 2 and Eq. (2.4), the starting positions for the tracks in space and time can be defined as given in Eq. (2.5).

$$\begin{aligned}
&\left.\begin{array}{l}\text{rays originating}\\ \text{at } t_{initial}\end{array}\right\}: \begin{cases} x_k = x_{k-1} + \Delta\omega_k\sqrt{1+\mu^2}, & \mu > 0 \\ x_k = x_{k-1} - \Delta\omega_k\sqrt{1+\mu^2}, & \mu < 0 \end{cases} \\
&\left.\begin{array}{l}\text{rays originating}\\ \text{on left or right}\\ \text{boundaries}\end{array}\right\}: \begin{cases} t_k = t_{k-1} + \Delta\omega_k \dfrac{\sqrt{1+\mu^2}}{v|\mu|}, & all\,\mu \end{cases}
\end{aligned} \tag{2.5}$$

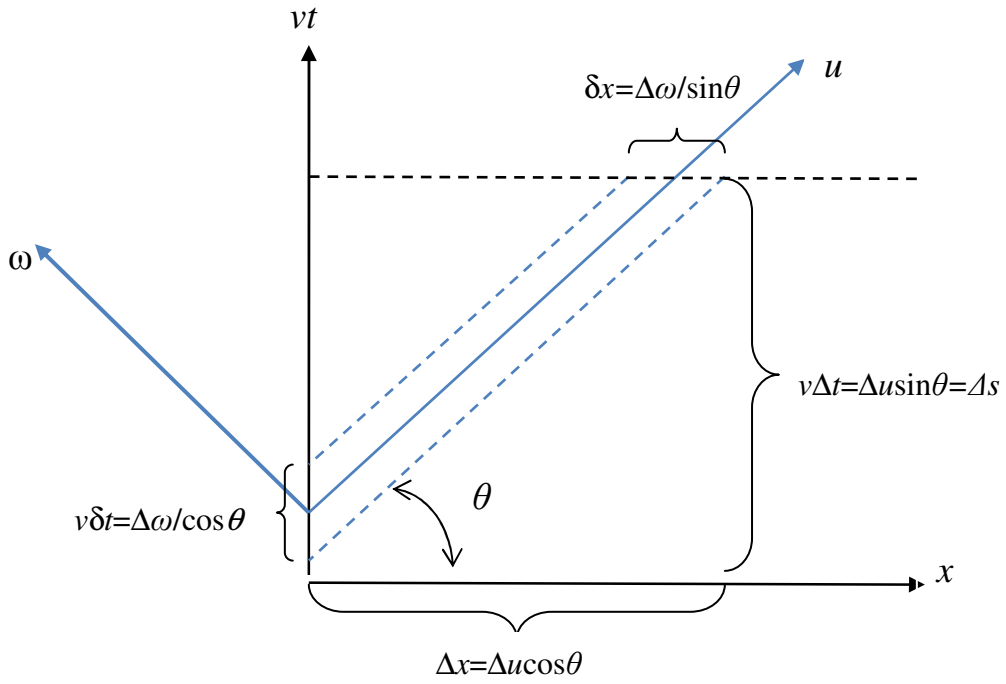

Figure 2: Rotated (*w*-*u*) Coordinate System in *x*-*vt* Plane

The relation between the integrals over (x, vt) and integrals over (ω, u) can also be determined from Fig. 2:

$$\iint\limits_{\text{area}} dx\,d(vt)\,f(x,t) = \iint\limits_{\substack{\text{same}\\ \text{area}}} d\omega\,du\,|J|\,f = \sqrt{1+\mu^2}\iint\limits_{\substack{\text{same}\\ \text{area}}} d\omega\,ds\,f \qquad (2.6).$$

The Jacobian for this coordinate system relation was used in Eq. (2.6) and is defined as shown in Eq. (2.7). Note that this integral over (ω, u) can also be written in terms of (ω, s) where s represents the length a particle traveled along a track, but with a different Jacobian as given in Eq. (2.6).

$$|J| = \begin{vmatrix} \cos\theta & -\sin\theta \\ \sin\theta & \cos\theta \end{vmatrix} = \cos^2\theta + \sin^2\theta = 1. \qquad (2.7)$$

The area integral relation given in Eq. (2.6) is the guide used to approximate the integrals over space-time cells in terms of track spacing and integrals along a track. An example of this relation is given in Eq. (2.8).

$$\int_{\Delta x} dx \int_{v\Delta t} dt\,\Psi_m(x,t) \approx \sum_{k=1}^{\#\text{ of tracks}} \frac{\Delta\omega_k}{v}\sqrt{1+\mu_m^2}\int_{\Delta s_k} ds\,\Psi_m\left(x_k+\mu_m s, t_k + s/v\right) \qquad (2.8)$$

The area that is represented by the sum over tracks in Eq. (2.8) will not be exactly equal to the actual area of the $v\Delta t\Delta x$ cell due to the characteristic discretization. Equation (2.9) shows this relation.

$$\sum_{k=1}^{\#\text{ of tracks}} \Delta\omega_k \Delta s_k \sqrt{1+\mu_m^2} \neq v\Delta t\Delta x \qquad (2.9)$$

This lack of equality for finite track spacing is the main source of the inability of this STLC method to achieve all of the desired properties described previously.

2.2 Least-Squares Method and Conservation of Particles

Next the construction of the scalar flux function that yields track-wise conservative reaction rates will be developed as well as the least-squares approximation for average quantities. As with other discrete ordinates methods, this STLC method will denote the m^{th} quadrature direction with subscript m. The characteristic solution shown in Eq. (2.2) satisfies the following conservation equation along a track:

$$\Psi_{m,k}^{out} - \Psi_{m,k}^{in} + \sigma_t \Delta s_k \bar{\Psi}_{m,k} = \frac{1}{2}\Delta s_k \left[\sigma_s \bar{\phi}_k^{SS} + \bar{Q}_k \right]. \tag{2.10}$$

The SS superscript indicates the scalar flux function used in the scattering source, and a bar denotes an average quantity (only over the track, k). Multiplying this equation by the track width, ω_k, and by $(1+\mu^2)^{1/2}$, and dividing by the speed, produces an equation in which the total number of particles that flow into and out of the space-time cell along the track appear. Summing over all tracks for all directions in the cell produces a statement of conservation for the STLC method for the cell.

$$\sum_{m=1}^{M} \sum_{k=1}^{\#\text{ of tracks}} \frac{\Delta\omega_k}{v}\sqrt{\mu_m^2+1}\left\{ \Psi_{m,k}^{out} - \Psi_{m,k}^{in} + \sigma_t \Delta s_k \bar{\Psi}_{m,k} - \frac{\sigma_s \Delta s_k}{2}\bar{\phi}_k^{SS} - \frac{\Delta s_k}{2}\bar{Q}_k \right\} = 0 \tag{2.11}$$

Looking at the limit of fine track spacing, the collision terms in Eq. (2.11) become integrals of a collision rate density over the space-time cell which is evident by the relationship in Eq. (2.8). The five terms shown in Eq. (2.11) represent (in this order) the rates at which particles stream out of, stream into, have collisions in, scatter in, and are emitted by the fixed source in a space-time cell.

For Eq. (2.11) to express conservation, the scattering term must be equal to the scattering ratio (σ_s/σ_t) multiplied by the collision term. A similar requirement applies to

the first spatial moment and the first time moment. Therefore, this condition implies the following for this STLC method where $\Psi^{x}_{m,k}$ and $\Psi^{t}_{m,k}$ represent the first spatial moment and first time moment of the angular flux along a track. The first spatial and first time moment of the scalar flux function used in the scattering source are defined as $\phi^{x,SS}_{k}$ and $\phi^{t,SS}_{k}$.

$$\sum_{m=1}^{M} w_m \sum_{k=1}^{\#\text{ of tracks}} \Delta\omega_k \sqrt{\mu_m^2+1}\Delta s_k \bar{\Psi}_{m,k} = \sum_{m=1}^{M} w_m \sum_{k=1}^{\#\text{ of tracks}} \Delta\omega_k \sqrt{\mu_m^2+1}\frac{\Delta s_k}{2}\bar{\phi}_k^{SS} \tag{2.12}$$

$$\begin{aligned}
\sum_{m=1}^{M} w_m \sum_{k=1}^{\#\text{ of tracks}} \Delta\omega_k \sqrt{\mu_m^2+1}\Delta s_k \Psi^{x}_{m,k} &= \sum_{m=1}^{M} w_m \sum_{k=1}^{\#\text{ of tracks}} \Delta\omega_k \sqrt{\mu_m^2+1}\frac{\Delta s_k}{2}\phi_k^{x,SS} \\
\sum_{m=1}^{M} w_m \sum_{k=1}^{\#\text{ of tracks}} \Delta\omega_k \sqrt{\mu_m^2+1}\Delta s_k \Psi^{t}_{m,k} &= \sum_{m=1}^{M} w_m \sum_{k=1}^{\#\text{ of tracks}} \Delta\omega_k \sqrt{\mu_m^2+1}\frac{\Delta s_k}{2}\phi_k^{t,SS}
\end{aligned} \tag{2.13}$$

When multiplied by σ_t, the left side of Eq. (2.12) is the total "track-wise" collision rate in the space-time cell multiplied by the particle velocity. A "track-wise conservative" (TWC) cell-averaged scalar flux is defined such that when we multiply it by the space-time cell area and σ_t, it yields the same collision rate. This relation for the track-wise conservative cell-averaged scalar flux is shown in Eq. (2.14).

$$\bar{\Phi}^{TWC}_{i,n}\Delta x_i \Delta t_n = \sum_{m=1}^{M} w_m \sum_{k=1}^{\#\text{ of tracks}} \frac{\Delta\omega_k}{v}\sqrt{\mu_m^2+1}\Delta s_k \bar{\Psi}_{m,k} \tag{2.14}$$

Similarly, there are track-wise conservative expressions for the *x* and *t* moments of the scalar flux as given in Eq. (2.15).

$$\begin{aligned}
\Phi^{x,TWC}_{i,n}\Delta x_i \Delta t_n &= \sum_{m=1}^{M} w_m \sum_{k=1}^{\#\text{ of tracks}} \frac{\Delta\omega_k}{v}\sqrt{\mu_m^2+1}\Delta s_k \Psi^{x}_{m,k} \\
\Phi^{t,TWC}_{i,n}\Delta x_i \Delta t_n &= \sum_{m=1}^{M} w_m \sum_{k=1}^{\#\text{ of tracks}} \frac{\Delta\omega_k}{v}\sqrt{\mu_m^2+1}\Delta s_k \Psi^{t}_{m,k}
\end{aligned} \tag{2.15}$$

Although these previous expressions show that this STLC method can be conservative, they do not show what function should be used for ϕ^{SS} in the scattering source to make this conservation statement correct. If a constant flux were assumed in each cell, this ϕ^{SS} function would be the conservative average given in Eq. (2.12). We are interesting in higher-order treatments. In this work we let the scattering source in a space-time cell be a linear function of x and t as shown in Eq. (2.16), where x_i is the spatial midpoint of a cell and t_n is the midpoint of a time step.

$$\phi_{i,n}^{SS}(x,t) = \bar{\phi}_{i,n}^{SS} + \phi_{i,n}^{x,SS}\frac{2(x-x_i)}{\Delta x_i} + \phi_{i,n}^{t,SS}\frac{2(t-t_n)}{\Delta t_n} \tag{2.16}$$

The three coefficients in Eq. (2.16), $\bar{\phi}_{i,n}^{SS}$, $\phi_{i,n}^{x,SS}$, and $\phi_{i,n}^{t,SS}$, must be determined such that Eqs. (2.12) and (2.13) are satisfied. Using intuition, one might suggest that the conservative flux values given in Eqs. (2.14) and (2.15) are the coefficients that are needed; however, this intuition is not correct. These coefficients are determined by satisfying the following average, x-moment, and t-moment equations:

$$\begin{aligned}
&\sum_{m=1}^{M} w_m \sum_{k=1}^{\#\text{ of tracks}} \Delta\omega_k \sqrt{1+\mu_m^2} \int_0^{\Delta s_k} ds \left[\Psi_{m,k}(s) - \frac{1}{2}\phi_{i,n}^{SS}(x(s),t(s)) \right] = 0 \\
&\sum_{m=1}^{M} w_m \sum_{k=1}^{\#\text{ of tracks}} \Delta\omega_k \sqrt{1+\mu_m^2} \int_0^{\Delta s_k} ds \left[x(s)-x_i \right] \left[\Psi_{m,k}(s) - \frac{1}{2}\phi_{i,n}^{SS}(x(s),t(s)) \right] = 0 . \\
&\sum_{m=1}^{M} w_m \sum_{k=1}^{\#\text{ of tracks}} \Delta\omega_k \sqrt{1+\mu_m^2} \int_0^{\Delta s_k} ds \left[t(s)-t_n \right] \left[\Psi_{m,k}(s) - \frac{1}{2}\phi_{i,n}^{SS}(x(s),t(s)) \right] = 0
\end{aligned} \tag{2.17}$$

The expressions shown in Eq. (2.17) are equivalent to a least-squares determination of the linear (in x and t) scalar flux function: they minimize the squared difference between

the scalar flux function and the STLC solution when integrated along each track and summed over all tracks and quadrature directions.

The track-wise conservative values for the scalar flux and its moments given in Eqs. (2.14) and (2.15) are the values that must be used in an analytic integral over the space-time cell to produce reaction rates equal to the total reaction rates along all of the tracks multiplied by track width. But as seen from Eq. (2.17) these are not the values that should be used in the scattering (or fission) source in the characteristic equation. The function produced from Eq. (2.17) would not give the same reaction rates, if analytically integrated over a space-time cell, as the sum of the track-wise rates. This "perceived" non-conservatism occurs because this function generates conservative reaction rates in the *approximate* integration over a cell; this approximation obviously being the track-based summation in many of the previous equations. If the function defined in Eq. (2.16) is used in the scattering source, the STLC method obtained has the following properties:

- Track-wise particle conservation which was defined previously (TWC),
- Exact solution along a ray (no changes in track lengths),
- Possible unsmooth cell-to-cell variation in reaction rates for problems with correct reaction rates are smoothly varying

It should be noted that these unsmooth reaction rates do not affect the exiting flux from a particular cell because a smooth function, ϕ^{SS}, is used in the scattering (and fission) source in the characteristic equation. Therefore, although the reaction-rate based

quantities may not be smooth, there is not a lack of smoothness in the angular fluxes from the STLC method.

2.3 Implementation of STLC Least-Squares Method

Implementation of this method to solve various problems is relatively straightforward. A summary of the basic steps coded in implementation of this method to find the angular flux and scalar flux in each cell of a problem is described below with a flowchart of the code layout included in Appendix A. Also the specification of track width and the technique used to accelerate convergence is discussed.

The first step is to read the problem definition and assign material properties to each region of the problem. From this input the necessary track width is defined as described in the following paragraph. Also the starting points of the rays in space and time for every direction are established. Next the iteration over each time step starts. After initializing and resetting variables the iteration over each quadrature direction begins. Inside this quadrature loop, a loop over each cell is performed. For a cell, each track through the cell is looped over in order to form the source along the track and the exiting angular flux from each track. From this information, the average angular flux along with the x-moment and t-moment of the angular flux are determined for the cell. Also the contribution to the average, x-moment, and t-moment of the TWC scalar flux is stored. After looping through all cells and angular directions, the non-TWC scalar flux and its moments are found by using the previously found TWC flux quantities. Finally, this time step iteration is repeated until convergence of these non-TWC fluxes and moments is reached.

To form the scattering source properly in each space-time cell, this method requires a minimum of two rays passing through each cell for each quadrature direction. The determination of this minimum ray spacing is simple. For a particular quadrature direction, the ray spacing must meet the following criteria:

$$\Delta w_{m,k}^{i} <= \Delta w_{\max}^{i,n} = \frac{\Delta x_i + v\left|\mu_m\right|\Delta t_n}{2\sqrt{\mu_m^2 + 1}}. \tag{2.18}$$

Equation (2.18) suggests that each region and time step with uniform cell spacing can have a different ray spacing. However, for this STLC method implementation, only the first time step is considered in determination of the ray spacing. If the user-input ray spacing does not meet the specified ray spacing requirement in Eq. (2.18), the ray spacing is set to the maximum allowable spacing. For simplicity, the minimum track spacing amongst all directions and cells can be used for every direction as given in Eq. (2.19).

$$\Delta w_k = \min_{\substack{m=1,\ldots,M \\ i=1,\ldots,\#cells}} \Delta w_{m,k}^{i} \tag{2.19}$$

For problems in which source iteration requires many iterations for convergence or may not converge, such as those involving highly diffusive regions, the GMRES (Generalized Minimum Residual) method is used to achieve convergence of the scalar flux and its moments faster than source iteration. Therefore in reference to the previous steps employed to solve a problem, the GMRES algorithm is implemented in the following manner. For each time step iteration, first the uncollided non-TWC flux and its moments are determined by doing one iteration of the previous steps with a zero

scattering source. The output from this iteration will be designated as Q. GMRES solves a system in the following form:

$$A\phi^{SS} = Q\,. \tag{2.20}$$

The previous STLC method solves a problem of the following form, where l denotes the iteration step within each time step.

$$\begin{aligned} L\psi^{(l+1)} &= K\phi^{(l)} + q \\ \phi^{(l+1)} &= M\psi^{(l+1)} \end{aligned} \tag{2.21}$$

Rearranging Eq. (2.21) leads to Eq.(2.22),

$$\begin{aligned} \phi^{(l+1)} &= M\left(L^{-1}K\psi^{(l+1)} + L^{-1}q\right) \\ \phi^{(l+1)} &= ML^{-1}K\phi^{(l)} + Q \end{aligned}\,. \tag{2.22}$$

The A matrix is defined as the following:

$$A = I - ML^{-1}K\,. \tag{2.23}$$

Substituting this definition into Eq. (2.22), the solution at the new iterate is found in terms of known values.

$$\begin{aligned} \phi^{(l+1)} &= \left(I - A\right)\phi^{(l)} + Q \\ \phi^{(l+1)} &= \phi^{(l)} - A\phi^{(l)} + Q \end{aligned} \tag{2.24}$$

The GMRES method implemented is matrix-free, therefore only the action of A on a vector needs to be known. Equation (2.25) shows the action of this matrix on a known vector, v, which is given by GMRES [6, 7].

$$\begin{aligned} Ly &= Kv + q \\ u &= My = ML^{-1}Kv + Q \\ Av &= \left(I - ML^{-1}K\right)v = v - u + Q \end{aligned} \tag{2.25}$$

Following this iteration, the non-TWC and TWC scalar flux values can be produced using the STLC method previously developed.

Another method employed to be able to run the STLC code for thick problems with high scattering is the use of a preconditioner with GMRES. A preconditioner was sought that was straightforward to implement and relied upon previous experience with transport precondtioners. Previous experience has shown that a diffusion equation that is nearly consistent with the transport equation works well as a preconditioner. Therefore the S_2 LD time-dependent equations were chosen to serve as the preconditioner for GMRES. For problems in 1-D space and time these equations have six unknowns in each cell (three for each angle): the average angular flux, the spatial moment of the angular flux, and the time moment of the angular flux. The conservation, x-moment, and t-moment LD equations are given in Eqs. (2.26)-(2.28) where T, B, R, and L represent the top, bottom, right, and left values in a cell respectively. Equation (2.29) gives the relations for the angular flux values along the top, bottom, left, and right of each cell. Along with the discrete ordinates definition given in Eq. (2.30), the unknowns in each cell can be determined from Eqs. (2.26)-(2.30).

$$\begin{aligned}&\frac{1}{v}\left(\frac{\psi^{T}_{i,m,n}-\psi^{B}_{i,m,n}}{\Delta t_n}\right)+\mu_m\left(\frac{\psi^{R}_{i,m,n}-\psi^{L}_{i,m,n}}{\Delta x_i}\right)+\sigma_t\bar{\psi}_{i,m,n}\\&=\frac{\sigma_s}{2}\left(\bar{\psi}_{i,1,n}+\bar{\psi}_{i,2,n}\right)+\frac{Q_{i,n}}{2},\qquad \begin{matrix} m=1,2\\ i=1,\ldots I\end{matrix}\end{aligned} \tag{2.26}$$

$$\begin{aligned}&\frac{1}{v}\left(\frac{\psi^{T,x}_{i,m,n}-\psi^{B,x}_{i,m,n}}{\Delta t_n}\right)+3\mu_m\left(\frac{\psi^{R}_{i,m,n}-2\bar{\psi}_{i,m,n}+\psi^{L}_{i,m,n}}{\Delta x_i}\right)+\sigma_t\psi^{x}_{i,m,n}\\&=\frac{\sigma_s}{2}\left(\psi^{x}_{i,1,n}+\psi^{x}_{i,2,n}\right)+\frac{Q^{x}_{i,n}}{2},\qquad \begin{matrix} m=1,2\\ i=1,\ldots I\end{matrix}\end{aligned} \tag{2.27}$$

$$\frac{3}{v}\left(\frac{\psi^{T}_{i,m,n}-2\bar{\psi}_{i,m,n}+\psi^{B}_{i,m,n}}{\Delta t_n}\right)+\mu_m\left(\frac{\psi^{R,t}_{i,m,n}-\psi^{L,t}_{i,m,n}}{\Delta x_i}\right)+\sigma_t\psi^{t}_{i,m,n}$$
$$=\frac{\sigma_s}{2}\left(\psi^{t}_{i,1,n}+\psi^{t}_{i,2,n}\right)+\frac{Q^{t}_{i,n}}{2},\qquad \begin{matrix} m=1,2 \\ i=1,\ldots I \end{matrix} \tag{2.28}$$

$$\begin{aligned}
&\psi^{R}_{i,m,n}=\bar{\psi}_{i,m,n}+\psi^{x}_{i,m,n}, && \psi^{L}_{i,m,n}=\bar{\psi}_{i-1,m,n}+\psi^{x}_{i-1,m,n}, && \mu_m>0\\
&\psi^{R}_{i,m,n}=\bar{\psi}_{i+1,m,n}-\psi^{x}_{i+1,m,n}, && \psi^{L}_{i,m,n}=\bar{\psi}_{i,m,n}-\psi^{x}_{i,m,n}, && \mu_m<0\\
&\psi^{T}_{i,m,n}=\bar{\psi}_{i,m,n}+\psi^{t}_{i,m,n}, && \psi^{B}_{i,m,n}=\bar{\psi}_{i,m,n-1}+\psi^{t}_{i,m,n-1}, && m=1,2
\end{aligned} \tag{2.29}$$

Boundary Conditions:

$$\psi^{R}_{I,m,n}=\psi_{inc} \qquad \mu_m<0$$
$$\psi^{L}_{1,m,n}=\psi_{inc} \qquad \mu_m>0$$

$$\begin{aligned}
\bar{\phi}_{i,n}&=\sum_{m=1}^{2}w_m\bar{\psi}_{i,m,n}\\
\phi^{x}_{i,n}&=\sum_{m=1}^{2}w_m\psi^{x}_{i,m,n}\\
\phi^{t}_{i,n}&=\sum_{m=1}^{2}w_m\psi^{t}_{i,m,n}
\end{aligned} \tag{2.30}$$

Application of this LD preconditioner into the GMRES framework is fairly straightforward and builds upon the previous matrix framework. First, the new "uncollided" source is determined from these LD equations by adding a correction to the previous uncollided source. Equation (2.31) shows how to find this corrected source where the 2 index represents the matrices for the S_2 LD equations.

$$\begin{aligned}
&L_2 y-K_2M_2 y=K_2Q\\
&F=M_2 y\\
&\tilde{Q}=Q+F
\end{aligned} \tag{2.31}$$

Second a correction to the scalar flux iterate is determined using these LD equations as shown in Eq. (2.32).

$$\begin{aligned}
&\phi^{(l+1/2)} = \left(I - A\right)\phi^{(l)} + Q \\
&\delta\phi = \phi^{(l+1/2)} - \phi^{(l)} \\
&L_2 y - K_2 M_2 y = K_2 \delta\phi \\
&F = M_2 y \\
&\phi_{new} = \phi^{(l+1/2)} + F
\end{aligned} \tag{2.32}$$

Finally the action of the preconditioned system matrix is found using this correction, similar to Eq. (2.25), as shown in Eq. (2.33).

$$PA\phi^{(l)} = \phi^{(l)} - \phi_{new} + \tilde{Q} \tag{2.33}$$

A short proof is presented here which shows that this preconditioning matrix is correct for solving this transport equation. First note that the preconditioned iteration being sought should be of the form represented in Eq. (2.34) where the preconditioner, P, should be an approximation of the inverse of the A matrix.

$$\phi^{(l+1)} = \left(I - PA\right)\phi^{(l)} + Pb \tag{2.34}$$

The correction term found in Eq. (2.32) can be expanded to find the iteration being sought in Eq.(2.34). Equation (2.35) shows this expansion in terms of the LD equations.

$$\begin{aligned}
\phi_{new} &= \phi^{(l+1/2)} + F \\
&= \phi^{(l+1/2)} + M_2\left[L_2 - K_2 M_2\right]^{-1} K_2\left(\phi^{(l+1/2)} - \phi^{(l)}\right) \\
&= \left[I + M_2\left(L_2 - K_2 M_2\right)^{-1} K_2\right]\phi^{(l+1/2)} + M_2\left[L_2 - K_2 M_2\right]^{-1} K_2\phi^{(l)}
\end{aligned} \tag{2.35}$$

Defining the preconditioner as given in Eq. (2.36) and expanding the half iterate flux value in terms of the original STLC transport matrices leads to Eq. (2.37).

$$P = \left[I + M_2\left(L_2 - K_2 M_2\right)^{-1} K_2\right] \tag{2.36}$$

$$\phi_{new} = P\left[\left(I - A\right)\phi^{(l)} + b\right] - M_2\left[L_2 - K_2 M_2\right]^{-1} K_2\phi^{(l)} \tag{2.37}$$

Further simplification of Eq. (2.37) leads to Eq. (2.38) which is equivalent to the preconditioned system sought in Eq. (2.34).

$$\begin{aligned} \phi_{new} &= Pb + \left[P\left(I - A\right) - M_2 \left[L_2 - K_2 M_2 \right]^{-1} K_2 \right] \phi^{(l)} \\ \phi_{new} &= \left(I - PA\right)\phi^{(l)} + Pb \end{aligned} \tag{2.38}$$

The definition of the preconditioner can be expanded to show it satisfies the condition of being an approximate inverse of the A matrix. Factoring out the inverse of L in Eq. (2.36) leads to Eq. (2.39).

$$P = \left[I + M_2 \left(I - L_2^{-1} K_2 M_2 \right)^{-1} L_2^{-1} K_2 \right] \tag{2.39}$$

With this equation, the following identity for the inverse can be applied.

$$\begin{aligned} &\left\| B \right\| < 1 \\ &\left(I - B\right)^{-1} = I + B + B^2 + B^3 + \ldots \end{aligned} \tag{2.40}$$

Applying this definition to the preconditioner leads to the inverse of the A matrix for the S_2 LD equations as shown in Eq. (2.41).

$$\begin{aligned} P &= I + M_2 \left\{ I + L_2^{-1} K_2 M_2 + \left(L_2^{-1} K_2 M_2 \right)^2 + \left(L_2^{-1} K_2 M_2 \right)^3 + \ldots \right\} \\ P &= \left(I - M_2 L_2^{-1} K_2 \right)^{-1} \\ P &= A_2^{-1} \end{aligned} \tag{2.41}$$

In this section we have developed a space-time LC method with several desirable properties. These include track-wise particle conservation, exact solution along a ray with no artificial changes in track lengths, and possible unsmooth cell-to-cell reaction rates for problems in which they should be smoothly varying. This STLC method

approximates the collision source by a linear function in x and t. In the next section an analysis of this method's performance in particular limits of interest will be performed.

3. ANALYSIS OF STLC LEAST-SQUARES METHOD

In this section, the STLC method previously developed is analyzed to gain insight into how it should perform on problems of interest. We examine problems with linear solutions and explore how "unsmooth" the TWC flux solution may be in certain scenarios. Considerable attention is then devoted to the asymptotic "thick diffusion limit" as applied to this STLC method. To our knowledge this is the first such analysis being reported for an LC method. The basis for this diffusion limit analysis is taken from papers by Larsen and Morel [11] [12].

3.1 Linear Solution

This section investigates the behavior of this STLC method for problems with a linear solution. From the previous method development we showed that the angular flux along each track is found exactly because we know the analytic solution along each track. If the solution of a problem is linear in x and t then the angular flux along each track will also be linear and exact in x and t. From the least-squares approximation shown in Eq. (2.17), the scalar flux solution in each cell is determined from the angular flux along each track in a cell by minimizing the squared difference between the scalar flux function and the STLC solution integrated along each track and summed over all tracks and quadrature directions. Since the collision source is represented as a linear function of x and t, this least-squares method will produce an exact linear solution for $\phi_{i,n}^{SS}$ in x and t because the angular flux along each track is linear.

3.2 Bumpy Conservative Solution

This section seeks to show by a very simple example why the TWC solution produced from the STLC method deviates from a correct smooth solution for problems in which the solution should be smooth. Consider a problem with a constant solution. Also consider a ray spacing for a particular quadrature angle such that one cell has two tracks in it and the adjacent cell has three tracks in it; this leads to a track pattern in the cells of 2,3,2,3,etc. The angular flux along each track is found exactly for this constant solution and is the same along each track. Summing the angular flux over all tracks in each cell for this particular direction will lead to reaction rates for each cell in the following pattern: 2γ, 3γ, 2γ, 3γ, etc. Therefore we see that this STLC method produces a conservative solution with unsmooth reaction rates for a problem in which the reaction rates should be smooth.

3.3 Steady-State LC Diffusion Limit

We begin with a quick review of the diffusion limit for steady-state LC as applied to slab geometry. The standard steady-state transport equation will be analyzed in the limit as $\varepsilon \to 0$ where ε is a small parameter that controls the sizes of various terms in the equation. Equation (3.1) shows this transport equation and Eq. (3.2) shows the scaling that will be used to represent the "thick" diffusion limit.

$$\begin{aligned} &\mu \frac{\partial \psi(x,\mu)}{\partial x} + \sigma_t \psi(x,\mu) = \frac{1}{2}\left[\sigma_s \phi(x) + q(x)\right], \\ &\phi(x) = \sum_{m=1}^{M} w_m \psi(x,\mu_m) = \sum_{m=1}^{M} w_m \psi_m(x) \end{aligned} \tag{3.1}$$

$$\begin{aligned} \sigma_t &\to \frac{\sigma_t}{\varepsilon} \\ \sigma_s &\to \frac{\sigma_t}{\varepsilon} - \varepsilon\sigma_a \\ q &\to \varepsilon q \end{aligned} \tag{3.2}$$

Applying the scaling in Eq. (3.2) the transport equation in Eq. (3.1) becomes the following.

$$\mu\frac{\partial\psi(x,\mu)}{\partial x} + \frac{\sigma_t}{\varepsilon}\psi(x,\mu) = \frac{1}{2}\left[\left(\frac{\sigma_t}{\varepsilon} - \varepsilon\sigma_a\right)\phi(x) + \varepsilon q(x)\right] \tag{3.3}$$

The flux terms will be expanded as shown in Eq. (3.4). Applying this expansion to Eq. (3.3) yields the following transport equation to manipulate.

$$\begin{aligned} \phi &= \phi^{(0)} + \varepsilon\phi^{(1)} + \varepsilon^2\phi^{(2)} + \ldots, \\ \psi &= \psi^{(0)} + \varepsilon\psi^{(1)} + \varepsilon^2\psi^{(2)} + \ldots \end{aligned} \tag{3.4}$$

$$\begin{aligned} &\mu\frac{\partial}{\partial x}\left(\psi^{(0)} + \varepsilon\psi^{(1)} + \varepsilon^2\psi^{(2)} + \ldots\right) + \frac{\sigma_t}{\varepsilon}\left(\psi^{(0)} + \varepsilon\psi^{(1)} + \varepsilon^2\psi^{(2)} + \ldots\right) \\ &= \frac{1}{2}\left[\left(\frac{\sigma_t}{\varepsilon} - \varepsilon\sigma_a\right)\left(\phi^{(0)} + \varepsilon\phi^{(1)} + \varepsilon^2\phi^{(2)} + \ldots\right) + \varepsilon q(x)\right] \end{aligned} \tag{3.5}$$

Now applying the cellular and angular designations described in section 2.1, Eq. (3.5) becomes valid for each cell as given in Eq. (3.6).

$$\begin{aligned} &\mu_m\frac{\partial}{\partial x}\left(\psi_{i,m}^{(0)} + \varepsilon\psi_{i,m}^{(1)} + \varepsilon^2\psi_{i,m}^{(2)} + \ldots\right) + \frac{\sigma_t}{\varepsilon}\left(\psi_{i,m}^{(0)} + \varepsilon\psi_{i,m}^{(1)} + \varepsilon^2\psi_{i,m}^{(2)} + \ldots\right) \\ &= \frac{1}{2}\left[\left(\frac{\sigma_t}{\varepsilon} - \varepsilon\sigma_a\right)\left(\phi_i^{(0)} + \varepsilon\phi_i^{(1)} + \varepsilon^2\phi_i^{(2)} + \ldots\right) + \varepsilon q_i(x)\right] \end{aligned} \tag{3.6}$$

The first spatial moment of Eq. (3.6) therefore looks like the following:

$$\begin{aligned}
&\mu_m\left(\psi^{(0)}_{i+1/2,m}+\varepsilon\psi^{(1)}_{i+1/2,m}+\varepsilon^2\psi^{(2)}_{i+1/2,m}+\ldots\right)+\mu_m\left(\psi^{(0)}_{i-1/2,m}+\varepsilon\psi^{(1)}_{i-1/2,m}+\varepsilon^2\psi^{(2)}_{i-1/2,m}+\ldots\right)\\
&-2\mu_m\left(\psi^{(0)}_{i,m}+\varepsilon\psi^{(1)}_{i,m}+\varepsilon^2\psi^{(2)}_{i,m}+\ldots\right)+\frac{\sigma_t}{\varepsilon}\Delta x_i\left(\psi^{x,(0)}_{i,m}+\varepsilon\psi^{x,(1)}_{i,m}+\varepsilon^2\psi^{x,(2)}_{i,m}+\ldots\right) \qquad (3.7)\\
&=\frac{1}{2}\Delta x_i\left[\left(\frac{\sigma_t}{\varepsilon}-\varepsilon\sigma_a\right)\left(\phi^{x,(0)}_i+\varepsilon\phi^{x,(1)}_i+\varepsilon^2\phi^{x,(2)}_i+\ldots\right)+\varepsilon q^x_i(x)\right]
\end{aligned}$$

Looking at the $O(\varepsilon^{-1})$ terms from Eq. (3.6), it is found that the leading order solution is isotropic as given in Eq. (3.8). Also, from Eq. (3.7) the $O(\varepsilon^{-1})$ terms show that the leading order spatial moment is isotropic as well.

$$\psi^{(0)}_{i,m}=\frac{1}{2}\phi^{(0)}_i \qquad (3.8)$$

$$\psi^{x,(0)}_{i,m}=\frac{1}{2}\phi^{x,(0)}_i \qquad (3.9)$$

The definition of the average and first spatial moment of the flux in a cell is given in Eq. (3.10).

$$\begin{aligned}
\phi_i &=\frac{1}{2}\left(\phi_{i,L}+\phi_{i,R}\right)\\
\phi^x_i &=\frac{1}{2}\left(\phi_{i,R}-\phi_{i,L}\right)
\end{aligned} \qquad (3.10)$$

Combining this equation with Eq. (3.8) the half-range isotropic nature of the leading order angular flux at a cell edge is found.

$$\psi^{(0)}_{i+1/2,m}=\begin{Bmatrix}\phi^{(0)}_{i,R} & \mu_m>0,\\ \phi^{(0)}_{i+1,L} & \mu_m<0\end{Bmatrix}\text{for i = 1,...,I-1} \qquad (3.11)$$

Looking at the O(1) terms from Eq. (3.6), the following balance equation arises.

$$\mu_m\left[\psi^{(0)}_{i+1/2,m}-\psi^{(0)}_{i-1/2,m}\right]+\sigma_t\Delta x_i\psi^{(1)}_{i,m}=\frac{1}{2}\sigma_t\Delta x_i\phi^{(1)}_i \qquad (3.12)$$

Multiplying Eq. (3.12) by a quadrature weight and summing over all angles leads to Eq. (3.13). Performing the same action to the O(1) terms from Eq. (3.7) arrives at Eq. (3.14)

.

$$\begin{aligned}
&\sum_{m=1}^{M} w_m \mu_m \left[\psi^{(0)}_{i+1/2,m} - \psi^{(0)}_{i-1/2,m} \right] + \sum_{m=1}^{M} w_m \sigma_t \Delta x_i \psi^{(1)}_{i,m} = \sum_{m=1}^{M} w_m \frac{1}{2} \sigma_t \Delta x_i \phi^{(1)}_i \\
&\sum_{m=1}^{M} w_m \mu_m \left[\psi^{(0)}_{i+1/2,m} - \psi^{(0)}_{i-1/2,m} \right] + \sigma_t \Delta x_i \phi^{(1)}_i = \sigma_t \Delta x_i \phi^{(1)}_i \\
&\sum_{m=1}^{M} w_m \mu_m \left[\psi^{(0)}_{i+1/2,m} - \psi^{(0)}_{i-1/2,m} \right] = 0
\end{aligned} \tag{3.13}$$

$$\begin{aligned}
&\sum_{m=1}^{M} w_m \mu_m \left[3\psi^{(0)}_{i+1/2,m} + 3\psi^{(0)}_{i-1/2,m} - 6\psi^{(0)}_{i,m} \right] + \sigma_t \Delta x_i \phi^{x,(1)}_i = \sigma_t \Delta x_i \phi^{x,(1)}_i \\
&\sum_{m=1}^{M} w_m \mu_m \left[3\psi^{(0)}_{i+1/2,m} + 3\psi^{(0)}_{i-1/2,m} - 6\psi^{(0)}_{i,m} \right] = 0 \\
&\sum_{m=1}^{M} w_m \mu_m \left[\psi^{(0)}_{i+1/2,m} + \psi^{(0)}_{i-1/2,m} - 2\psi^{(0)}_{i,m} \right] = 0
\end{aligned} \tag{3.14}$$

Adding Eq. (3.13) and Eq. (3.14) and substituting the relation from Eq. (3.11), continuity of the leading order scalar flux is found as shown in Eq. (3.15).

$$\begin{aligned}
&\sum_{m=1}^{M} w_m \mu_m \psi^{(0)}_{i+1/2,m} = 0, \\
&\sum_{\mu_m > 0} w_m \mu_m \left(\frac{1}{2} \phi^{(0)}_{i,R} \right) = \sum_{\mu_m < 0} w_m \left| \mu_m \right| \left(\frac{1}{2} \phi^{(0)}_{i+1,L} \right) \\
&\phi^{(0)}_{i,R} = \phi^{(0)}_{i+1,L} = \phi^{(0)}_{i+1/2}
\end{aligned} \tag{3.15}$$

This scalar flux identity shown in Eq. (3.15) holds for all interior edges. For the boundary edges there is a different relation set by the boundary condition for the problem. Considering the left boundary, Eq. (3.16) shows the corresponding condition for the scalar flux with a similar argument for the right boundary given in Eq. (3.17) where ρ is defined as a normalization constant for the angular quadrature.

$$\sum_{\mu_m>0} w_m \mu_m \psi_{m,inc}^{(0)} = \sum_{\mu_m<0} w_m \left|\mu_m\right| \frac{1}{2} \phi_{1,L}^{(0)}$$
$$\phi_{1,L}^{(0)} = \phi_{1/2}^{(0)} = \sum_{\mu_m>0} w_m \frac{4\mu_m}{\rho} \psi_{m,inc}^{(0)} \tag{3.16}$$

$$\phi_{I+1,R}^{(0)} = \phi_{I+1/2}^{(0)} = \sum_{\mu_m<0} w_m \frac{4\left|\mu_m\right|}{\rho} \psi_{m,inc}^{(0)} \tag{3.17}$$

Looking at the O(ε) terms from Eq. (3.6) and Eq. (3.7) the following balance and first spatial moment equations arise.

$$\mu_m \left[\psi_{i+1/2,m}^{(1)} - \psi_{i-1/2,m}^{(1)}\right] + \sigma_t \Delta x_i \psi_{i,m}^{(2)} = \frac{1}{2}\sigma_t \Delta x_i \phi_i^{(2)} - \frac{1}{2}\sigma_a \Delta x_i \phi_i^{(0)} + \frac{1}{2}\Delta x_i Q_i \tag{3.18}$$

$$\mu_m \left[\psi_{i+1/2,m}^{(1)} + \psi_{i-1/2,m}^{(1)} - 2\psi_{i,m}^{(1)}\right] + \frac{1}{3}\sigma_t \Delta x_i \psi_{i,m}^{x,(2)}$$
$$= \frac{1}{6}\sigma_t \Delta x_i \phi_i^{x,(2)} - \frac{1}{6}\sigma_a \Delta x_i \phi_i^{x,(0)} + \frac{1}{6}\Delta x_i Q_i^x \tag{3.19}$$

Adding Eqs. (3.18) and (3.19) centered around cell *i* and then again multiplying by a quadrature weight and summing over angles, the following balance equation is found.

$$2\left(J_{i+1/2}^{(1)} - J_i^{(1)}\right) + \sigma_a \Delta x_i \left(\phi_i^{(0)} + \frac{1}{3}\phi_i^{x,(0)}\right) = \Delta x_i \left(Q_i + \frac{1}{3}Q_i^x\right) \tag{3.20}$$

A different balance equation is found by subtracting Eq. (3.18) from Eq. (3.19) centered about the cell *i+1* with the same quadrature sum.

$$2\left(J_{i+1}^{(1)} - J_{i+1/2}^{(1)}\right) + \sigma_a \Delta x_{i+1} \left(\phi_{i+1}^{(0)} - \frac{1}{3}\phi_{i+1}^{x,(0)}\right) = \Delta x_{i+1} \left(Q_{i+1} - \frac{1}{3}Q_{i+1}^x\right) \tag{3.21}$$

Now adding Eqs. (3.20) and (3.21) and dividing by two, Eq. (3.22) is found.

$$J_{i+1}^{(1)} - J_i^{(1)} + \frac{1}{2}\sigma_a \Delta x_i \left(\phi_i^{(0)} + \frac{1}{3}\phi_i^{x,(0)} \right) + \frac{1}{2}\sigma_a \Delta x_{i+1} \left(\phi_{i+1}^{(0)} - \frac{1}{3}\phi_{i+1}^{x,(0)} \right) = \frac{1}{2}\Delta x_{i+1} \left(Q_{i+1} - \frac{1}{3}Q_{i+1}^{x} \right) + \frac{1}{2}\Delta x_i \left(Q_i + \frac{1}{3}Q_i^{x} \right) \tag{3.22}$$

Substituting from Eq. (3.10), Eq. (3.22) leads to Eq. (3.23) which contains an unknown, the first order current density.

$$J_{i+1}^{(1)} - J_i^{(1)} + \sigma_a \Delta x_i \left(\frac{1}{6}\phi_{i-1/2}^{(0)} + \frac{1}{3}\phi_{i+1/2}^{(0)} \right) + \sigma_a \Delta x_{i+1} \left(\frac{1}{3}\phi_{i+1/2}^{(0)} + \frac{1}{6}\phi_{i+3/2}^{(0)} \right) = \frac{1}{2}\Delta x_{i+1} \left(Q_{i+1} - \frac{1}{3}Q_{i+1}^{x} \right) + \frac{1}{2}\Delta x_i \left(Q_i + \frac{1}{3}Q_i^{x} \right) \tag{3.23}$$

Looking back at the balance equation from the O(1) terms given in Eq. (3.12)and taking the first angular moment of this equation leads to an expression for the first order current density.

$$\begin{aligned} &\sum_{m=1}^{M} w_m \mu_m^2 \left[\psi_{i+1/2,m}^{(0)} - \psi_{i-1/2,m}^{(0)} \right] + \sum_{m=1}^{M} w_m \mu_m \sigma_t \Delta x_i \psi_{i,m}^{(1)} = \sum_{m=1}^{M} w_m \mu_m \frac{1}{2}\sigma_t \Delta x_i \phi_i^{(1)} \\ &\sum_{m=1}^{M} w_m \mu_m^2 \left[\psi_{i+1/2,m}^{(0)} - \psi_{i-1/2,m}^{(0)} \right] + \sigma_t \Delta x_i J_i^{(1)} = 0 \\ &\Rightarrow \\ &J_i^{(1)} = -\frac{1}{3\sigma_t \Delta x_i} \sum_{m=1}^{M} 3 w_m \mu_m^2 \left[\psi_{i+1/2,m}^{(0)} - \psi_{i-1/2,m}^{(0)} \right] \end{aligned} \tag{3.24}$$

Bringing in the boundary conditions defined previously, the first term in Eq. (3.24) becomes the following.

$$\sum_{m=1}^{M} w_m \mu_m^2 \left[\psi_{i+1/2,m}^{(0)} \right] = \begin{Bmatrix} \sum_{\mu_m > 0} w_m \mu_m^2 \psi_{m,inc} + \frac{1}{6}\phi_{1,L}^{(0)} & i = 0, \\ \frac{1}{3}\phi_{i+1/2}^{(0)} & i = 1, \ldots, I-1, \\ \sum_{\mu_m < 0} w_m \mu_m^2 \psi_{m,inc} + \frac{1}{6}\phi_{I+1,R}^{(0)} & i = I \end{Bmatrix} \tag{3.25}$$

Substituting Eq. (3.25) into Eq. (3.24) yields the following expression for the current density.

$$J_i^{(1)} = \begin{Bmatrix} -\frac{1}{3\sigma_t \Delta x_i}\left[\phi_{3/2}^{(0)} - \sum_{\mu_m>0} w_m\left(3\mu_m^2 + 2\frac{|\mu_m|}{\rho}\right)\psi_{m,inc}\right] & i=1, \\ -\frac{1}{3\sigma_t \Delta x_i}\left[\phi_{i+1/2}^{(0)} - \phi_{i-1/2}^{(0)}\right] & i=2,...,I-1, \\ -\frac{1}{3\sigma_t \Delta x_i}\left[\sum_{\mu_m<0} w_m\left(3\mu_m^2 + 2\frac{|\mu_m|}{\rho}\right)\psi_{m,inc} - \phi_{I-1/2}^{(0)}\right] & i=I \end{Bmatrix} \tag{3.26}$$

With this current density definition, Eq. (3.26) can be substituted into Eq. (3.23). Equation (3.27) shows the relation for the first cell with the left boundary current condition substituted and a definition for the fixed source terms.

$$\begin{aligned} &J_2^{(1)} + \frac{1}{3\sigma_t \Delta x_1}\left[\phi_{3/2}^{(0)} - \sum_{\mu_m>0} w_m\left(3\mu_m^2 + 2\frac{|\mu_m|}{\rho}\right)\psi_{m,inc}\right] \\ &+\sigma_a \Delta x_1\left(\frac{1}{6}\sum_{\mu_m>0} w_m\left(4\frac{\mu_m}{\rho}\right)\psi_{m,inc} + \frac{1}{3}\phi_{3/2}^{(0)}\right) + \sigma_a \Delta x_2\left(\frac{1}{3}\phi_{3/2}^{(0)} + \frac{1}{6}\phi_{5/2}^{(0)}\right) \\ &= \frac{1}{2}\Delta x_2\left(Q_2 - \frac{1}{3}Q_2^x\right) + \frac{1}{2}\Delta x_1\left(Q_1 + \frac{1}{3}Q_1^x\right) = \left(\Delta x Q\right)_{3/2} \end{aligned} \tag{3.27}$$

Since the diffusion equation that is desired has a three point stencil, the scalar flux in the left cell will be redefined to meet the condition in Eq. (3.28)

$$\begin{aligned} &\frac{1}{3\sigma_t \Delta x_1}\left[-\sum_{\mu_m>0} w_m\left(3\mu_m^2 + 2\frac{|\mu_m|}{\rho}\right)\psi_{m,inc}\right] + \frac{\sigma_a \Delta x_1}{6}\sum_{\mu_m>0} w_m 4\frac{\mu_m}{\rho}\psi_{m,inc} \\ &= -\frac{1}{3\sigma_t \Delta x_i}\Phi_{1/2} + \frac{\sigma_a \Delta x_1}{6}\Phi_{1/2} \end{aligned} \tag{3.28}$$

Therefore, the scalar flux on the left edge is defined as the following.

$$\Phi_{1/2}=\frac{\sum_{\mu_m>0} w_m\left(3\mu_m^2+2\frac{|\mu_m|}{\rho}\left(1-\sigma_t\sigma_a\Delta x_1^2\right)\right)\psi_{m,inc}}{1-\frac{1}{2}\sigma_t\sigma_a\Delta x_1^2} \tag{3.29}$$

In general this redefined scalar flux can be defined at every edge in a similar manner as given in Eq. (3.30).

$$\Phi_{i-1/2}=\begin{cases}\dfrac{\sum_{\mu_m>0} w_m\left(3\mu_m^2+2\frac{|\mu_m|}{\rho}\left(1-\sigma_t\sigma_a\Delta x_1^2\right)\right)\psi_{m,inc}}{1-\frac{1}{2}\sigma_t\sigma_a\Delta x_1^2} & i=1,\\ \phi_{i-1/2} & i=2,...,I,\\ \dfrac{\sum_{\mu_m<0} w_m\left(3\mu_m^2+2\frac{|\mu_m|}{\rho}\left(1-\sigma_t\sigma_a\Delta x_I^2\right)\right)\psi_{m,inc}}{1-\frac{1}{2}\sigma_t\sigma_a\Delta x_I^2} & i=I+1\end{cases} \tag{3.30}$$

Equation (3.23) for interior nodes with the current density definition is the following.

$$\begin{aligned}&-\frac{1}{3\sigma_t\Delta x_{i+1}}\left[\phi_{i+3/2}^{(0)}-\phi_{i+1/2}^{(0)}\right]+\frac{1}{3\sigma_t\Delta x_i}\left[\phi_{i+1/2}^{(0)}-\phi_{i-1/2}^{(0)}\right]\\&+\sigma_a\Delta x_i\left(\frac{1}{6}\phi_{i-1/2}^{(0)}+\frac{1}{3}\phi_{i+1/2}^{(0)}\right)+\sigma_a\Delta x_{i+1}\left(\frac{1}{3}\phi_{i+1/2}^{(0)}+\frac{1}{6}\phi_{i+3/2}^{(0)}\right)=\left(Q\Delta x\right)_{i+1/2}\end{aligned} \tag{3.31}$$

Simplifying Eq. (3.31) and substituting the definition in Eq. (3.30), the desired three point diffusion equation is found from the LC transport equation.

$$\begin{aligned}&-\frac{\Phi_{i+3/2}-\Phi_{i+1/2}}{3\sigma_t\Delta x_{i+1}}+\frac{\Phi_{i+1/2}-\Phi_{i-1/2}}{3\sigma_t\Delta x_i}+\sigma_a\Delta x_i\left(\frac{1}{6}\Phi_{i-1/2}+\frac{1}{3}\Phi_{i+1/2}\right)\\&+\sigma_a\Delta x_{i+1}\left(\frac{1}{6}\Phi_{i+3/2}+\frac{1}{3}\Phi_{i+1/2}\right)=\left(Q\Delta x\right)_{i+1/2},\qquad i=1,...,I-1\end{aligned} \tag{3.32}$$

Thus we see that as a problem becomes thick and highly scattering, the leading-order LC angular flux becomes isotropic, and the leading-order scalar flux satisfies a linear continuous FEM discretization of the diffusion equation.

3.4 STLC Diffusion Limit

Now the asymptotic analysis of the STLC transport equation will be discussed. It should be noted that the diffusion limit of this equation should collapse in a steady-state problem to the steady-state diffusion limit found in Eq. (3.32); this will be checked in the next section. The transport equation of interest is given in Eq. (3.33).

$$\begin{aligned} &\frac{1}{v}\frac{\partial\psi(x,\mu,t)}{\partial t}+\mu\frac{\partial\psi(x,\mu,t)}{\partial x}+\sigma_t\psi(x,\mu,t)=\frac{1}{2}\left[\sigma_s\phi(x,t)+q(x,t)\right], \\ &\phi(x,t)=\sum_{m=1}^{M}w_m\psi(x,\mu_m,t)=\sum_{m=1}^{M}w_m\psi_m(x,t) \end{aligned} \tag{3.33}$$

The same scaling to represent the "thick" diffusion limit as in the previous section will be used but with an addition given in Eq. (3.34).

$$\begin{aligned} &\sigma_t\to\frac{\sigma_t}{\varepsilon} \\ &\sigma_s\to\frac{\sigma_t}{\varepsilon}-\varepsilon\sigma_a \\ &q\to\varepsilon q \\ &v\to\frac{v}{\varepsilon} \end{aligned} \tag{3.34}$$

With this scaling, the time axis is essentially stretched so in the limit as $\varepsilon\to 0$ the number of tracks starting on the cell boundary becomes infinite. This representation of a scaling of a cell and a set of tracks through this cell is shown in Fig. 3.

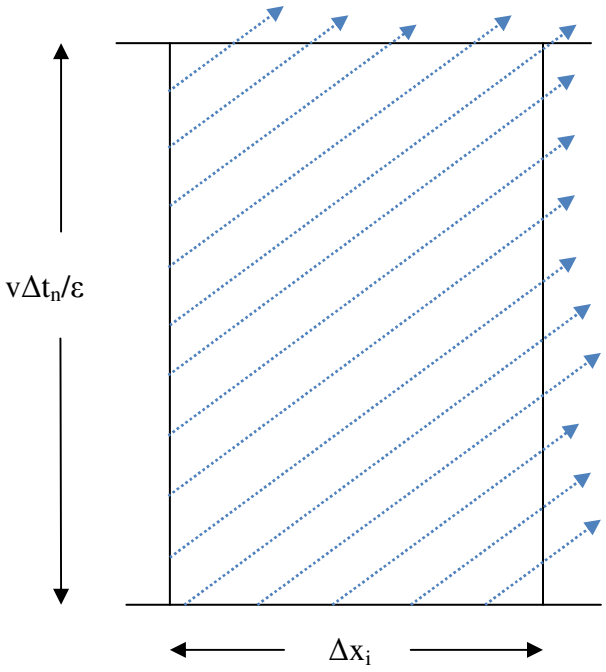

Figure 3: Representative (x,t) Cell with Tracks and Stretching Along the Time Axis for One Angular Direction

For reference in the following derivation, four types of tracks shown in Fig. 3 are defined. Tracks that pass through the corner of a cell occurring at the angular direction $\mu = 0$ will be ignored because they are not included in the quadrature set used for calculation. These four types of tracks are defined as the following:

1) tracks cross $x_{i-1/2}$ and $x_{i+1/2}$ (across Δx_i),

2) tracks cross $t_{n-1/2}$ and $t_{n+1/2}$ (across Δt_n),

3) tracks cross $t_{n-1/2}$ and $x_{i\pm1/2}$,

4) tracks cross $x_{i\pm1/2}$ and $t_{n+1/2}$.

It is important to note that as $\varepsilon \to 0$, the term $\frac{v\Delta t_n}{\varepsilon}$ becomes large, so the *(i,n)* cell is dominated by tracks of type 1. The tracks of types 3 and 4 will make up an O(ε) fraction of the total tracks. The tracks of type 2 should vanish given a fixed minimum angle in the quadrature and a sufficiently small ε, so they are not considered in this derivation.

The scaling given in Eq. (3.34) is applied to the transport equation in Eq. (3.33) along with discretization in the defined track notation with a linear representation of the scattering source as previously defined. For simplicity of notation, the asymptotic expansion of the flux as given in Eq. (3.4) will not be applied until further in the derivation.

$$\frac{d\Psi_{m,k}(s)}{ds}+\frac{\sigma_t}{\varepsilon}\Psi_{m,k}(s)-\frac{1}{2}\left(\frac{\sigma_t}{\varepsilon}-\varepsilon\sigma_a\right)\phi_k^{SS}\left(x(s),t(s)\right)-\varepsilon q_k\left(x(s),t(s)\right)=0 \tag{3.35}$$

In this discretization, the approximate integral over cells takes the form of weighted summations as given in Eq. (3.36).

$$\frac{\varepsilon}{v}\sum_{m=1}^{M}w_m\sum_{k=1}^{\#\text{ in (i,n,m)}}\omega_k\sqrt{1+\mu_m^2}\int_0^{\Delta s_k}dsF(x(s),t(s))\left[f(s)\right]=0 \tag{3.36}$$

As per the least-squares approximation for this method given in Eq. (2.17), first the case of F = 1 is considered. The following balance equation is produced when applying Eq. (3.36) to Eq. (3.35) with the aforementioned weighting function.

$$\begin{aligned}
&\frac{\varepsilon}{v}\sum_{m=1}^{M} w_m \sum_{k=1}^{\#\text{ in (i,n,m)}} \omega_k \sqrt{1+\mu_m^2}\left(\Psi_{m,k}\left(\Delta s_k\right)-\Psi_{m,k}\left(0\right)\right) \\
&+\frac{\sigma_t}{v}\sum_{m=1}^{M} w_m \sum_{k=1}^{\#\text{ in (i,n,m)}} \omega_k \sqrt{1+\mu_m^2}\int_0^{\Delta s_k} ds\left(\Psi_{m,k}\left(s\right)-\frac{1}{2}\phi_k^{SS}\right) \\
&+\frac{\varepsilon^2}{v}\sum_{m=1}^{M} w_m \sum_{k=1}^{\#\text{ in (i,n,m)}} \omega_k \sqrt{1+\mu_m^2}\int_0^{\Delta s_k} ds\left(\frac{\sigma_a}{2}\phi_k^{SS}-\frac{1}{2}q_k\right)=0
\end{aligned} \tag{3.37}$$

The same action will be performed on Eq. (3.35) with the following weighting function.

$$F(x(s),t(s))=\frac{2\left(x-x_i\right)}{\Delta x_i}=\frac{2\left(x_{k,0}-x_i+\mu_m s\right)}{\Delta x_i} \tag{3.38}$$

The first term in Eq. (3.35) becomes the following:

$$\begin{aligned}
&\int_0^{\Delta s_k} ds F\frac{d\Psi_{m,k}\left(s\right)}{ds}= \\
&=\frac{2\left(x_{k,0}-x_i\right)}{\Delta x_i}\int_0^{\Delta s_k} ds\frac{d\Psi_{m,k}\left(s\right)}{ds}+\int_0^{\Delta s_k} ds\frac{2\mu_m}{\Delta x_i}s\frac{d\Psi_{m,k}\left(s\right)}{ds} \\
&=\frac{2\left(x_{k,0}-x_i\right)}{\Delta x_i}\left(\Psi_{m,k}\left(\Delta s_k\right)-\Psi_{m,k}\left(0\right)\right)+\frac{2\mu_m}{\Delta x_i}\Delta s_k\left(\Psi_{m,k}\left(\Delta s_k\right)-\bar{\Psi}_{m,k}\right)
\end{aligned} \tag{3.39}$$

Therefore with this first term, the first spatial moment equation is given in Eq. (3.40).

$$\begin{aligned}
&\frac{\varepsilon}{v}\sum_{m=1}^{M} w_m \sum_{k=1}^{\#\text{ in (i,n,m)}} \omega_k \sqrt{1+\mu_m^2}\left[\begin{array}{l}\frac{2\left(x_{k,0}-x_i\right)}{\Delta x_i}\left(\Psi_{m,k}\left(\Delta s_k\right)-\Psi_{m,k}\left(0\right)\right) \\ +\frac{2\mu_m}{\Delta x_i}\Delta s_k\left(\Psi_{m,k}\left(\Delta s_k\right)-\bar{\Psi}_{m,k}\right)\end{array}\right] \\
&+\frac{\sigma_t}{v}\sum_{m=1}^{M} w_m \sum_{k=1}^{\#\text{ in (i,n,m)}} \omega_k \sqrt{1+\mu_m^2}\int_0^{\Delta s_k} ds\left[\frac{2\left(x-x_i\right)}{\Delta x_i}\left(\Psi_{m,k}\left(s\right)-\frac{1}{2}\phi_k^{SS}\right)\right] \\
&+\frac{\varepsilon^2}{v}\sum_{m=1}^{M} w_m \sum_{k=1}^{\#\text{ in (i,n,m)}} \omega_k \sqrt{1+\mu_m^2}\int_0^{\Delta s_k} ds\frac{2\left(x-x_i\right)}{\Delta x_i}\left(\frac{\sigma_a}{2}\phi_k^{SS}-\frac{1}{2}q_k\right)=0
\end{aligned} \tag{3.40}$$

Finally, the same action will be performed on the discretized transport equation with the following weighting function.

$$F(x(s),t(s)) = \frac{2\left(t-t_n\right)}{\Delta t_n} = \frac{2\left(t_{k,0}-t_n+\dfrac{\varepsilon}{v}s\right)}{\Delta t_n} \tag{3.41}$$

The first term, when applying Eq. (3.36) with this weighting function, is given in Eq. (3.42) and is similar to the first term of the spatial moment equation.

$$\begin{aligned}
&\int_0^{\Delta s_k} ds F \frac{d\Psi_{m,k}(s)}{ds} = \\
&= \frac{2\left(t_{k,0}-t_n\right)}{\Delta t_n}\int_0^{\Delta s_k} ds \frac{d\Psi_{m,k}(s)}{ds} + \int_0^{\Delta s_k} ds \frac{2\varepsilon}{v\Delta t_n} s \frac{d\Psi_{m,k}(s)}{ds} \\
&= \frac{2\left(t_{k,0}-t_n\right)}{\Delta t_n}\left(\Psi_{m,k}(\Delta s_k) - \Psi_{m,k}(0)\right) + \frac{2\varepsilon}{v\Delta t_n}\Delta s_k\left(\Psi_{m,k}(\Delta s_k) - \bar{\Psi}_{m,k}\right)
\end{aligned} \tag{3.42}$$

The full time moment equation is given in Eq. (3.43).

$$\begin{aligned}
&\frac{\varepsilon}{v}\sum_{m=1}^{M} w_m \sum_{k=1}^{\#\text{ in (i,n,m)}} \omega_k \sqrt{1+\mu_m^2}\left[\begin{array}{l}\dfrac{2\left(t_{k,0}-t_n\right)}{\Delta t_n}\left(\Psi_{m,k}(\Delta s_k) - \Psi_{m,k}(0)\right) \\ +\dfrac{2\varepsilon}{v\Delta t_n}\Delta s_k\left(\Psi_{m,k}(\Delta s_k) - \bar{\Psi}_{m,k}\right)\end{array}\right] \\
&+\frac{\sigma_t}{v}\sum_{m=1}^{M} w_m \sum_{k=1}^{\#\text{ in (i,n,m)}} \omega_k \sqrt{1+\mu_m^2}\int_0^{\Delta s_k} ds\left[\frac{2\left(t-t_n\right)}{\Delta t_n}\left(\Psi_{m,k}(s) - \frac{1}{2}\phi_k^{SS}\right)\right] \\
&+\frac{\varepsilon^2}{v}\sum_{m=1}^{M} w_m \sum_{k=1}^{\#\text{ in (i,n,m)}} \omega_k \sqrt{1+\mu_m^2}\int_0^{\Delta s_k} ds\frac{2\left(t-t_n\right)}{\Delta t_n}\left(\frac{\sigma_a}{2}\phi_k^{SS} - \frac{1}{2}q_k\right) = 0
\end{aligned} \tag{3.43}$$

The asymptotic expansions of the flux as given in Eq. (3.4) will now be applied to Eqs. (3.35), (3.37), (3.40), and (3.43). First the $O(\varepsilon^{-1})$ terms will be analyzed. From Eq. (3.35), these terms give the isotropic nature of the leading order angular flux as given in Eq. (3.44).

$$\Psi_{m,k}^{(0)}(s) = \frac{1}{2}\phi_k^{(0),SS}\left(x(s),t(s)\right) \tag{3.44}$$

From Eq. (3.37), for these $O(\varepsilon^{-1})$ terms, only the tracks of type 1 contribute. Multiplying these terms by an angle in the quadrature and summing, the following equation is found:

$$\begin{aligned}&\frac{1}{v}\sum_{m=1}^{M} w_m \mu_m \sum_{k=\text{type 1}} \omega_k \sqrt{1+\mu_m^2}\,\Delta s_k \bar{\Psi}_{m,k}^{(0)}(s) \\ &= \frac{1}{v}\sum_{m=1}^{M} w_m \mu_m \sum_{k=\text{type 1}} \omega_k \sqrt{1+\mu_m^2}\,\Delta s_k \frac{1}{2}\bar{\phi}_k^{(0),SS}\end{aligned} . \tag{3.45}$$

To evaluate the summations in Eq. (3.45), the properties of tracks of type 1 must be exploited. Equation (3.46) shows two important relations for tracks of type 1 that will be employed throughout this diffusion-limit analysis.

$$\begin{aligned}&\frac{\varepsilon}{v}\omega_k\sqrt{1+\mu_m^2} = |\mu_m|\,\delta t \\ &\Delta s_k = \frac{\Delta x_i}{|\mu_m|}\end{aligned} \tag{3.46}$$

Therefore, applying the relations in Eq. (3.46), the terms in Eq. (3.45) show that the leading order average current is zero as given in Eq. (3.47).

$$\begin{aligned}&\Delta x_i \Delta t_n \bar{J}_{i,n}^{(0)} = \Delta x_i \Delta t_n \frac{1}{2}\sum_{m=1}^{M} w_m \mu_m \bar{\phi}_k^{(0),SS} \\ &\bar{J}_{i,n}^{(0)} = 0\end{aligned} \tag{3.47}$$

The $O(\varepsilon^{-1})$ terms from the spatial moment equation, Eq. (3.40), are given in Eq. (3.48) where the integral over the *s* variable has been converted to an integral over the *x* variable. As previously, only tracks of type 1 contribute to leading order.

$$\begin{aligned}&\frac{1}{v}\sum_{m=1}^{M} w_m \sum_{k=\text{type 1}} \omega_k \sqrt{1+\mu_m^2}\,\frac{1}{\mu_m}\int_{x_{i-1/2}}^{x_{i+1/2}} dx \frac{2(x-x_i)}{\Delta x_i}\Psi_{m,k}^{(0)}(s) \\ &= \frac{1}{v}\sum_{m=1}^{M} w_m \sum_{k=\text{type 1}} \omega_k \sqrt{1+\mu_m^2}\,\frac{1}{\mu_m}\int_{x_{i-1/2}}^{x_{i+1/2}} dx \frac{2(x-x_i)}{\Delta x_i}\frac{1}{2}\phi_k^{(0),SS}\end{aligned} \tag{3.48}$$

Applying the relations in Eq. (3.46) and multiplying by a quadrature angle before summing over all angles, these terms become the following:

$$\sum_{m=1}^{M} w_m \mu_m \sum_{k=\text{type 1}} \delta t \Delta x_i \Psi_{m,k}^{x,(0)} = \sum_{m=1}^{M} w_m \mu_m \frac{1}{2} \sum_{k=\text{type 1}} \delta t \Delta x_i \phi_{i,n}^{x,(0),SS} \,. \tag{3.49}$$

Therefore, it is seen that the first spatial moment of the leading order current is zero as given in Eq. (3.50).

$$J_{i,n}^{x,(0)} = 0 \tag{3.50}$$

Finally from the time moment equation, Eq. (3.43), the $O(\varepsilon^{-1})$ terms are given in Eq. (3.51) where, again, only tracks of type 1 are of interest.

$$\begin{aligned} &\frac{1}{v} \sum_{m=1}^{M} w_m \sum_{k=\text{type 1}} \omega_k \sqrt{1+\mu_m^2} \int_0^{\Delta s_k} ds \frac{2\left(t-t_n\right)}{\Delta t_n} \Psi_{m,k}^{(0)}\left(s\right) \\ &= \frac{1}{v} \sum_{m=1}^{M} w_m \sum_{k=\text{type 1}} \omega_k \sqrt{1+\mu_m^2} \int_0^{\Delta s_k} ds \frac{2\left(t-t_n\right)}{\Delta t_n} \frac{1}{2} \phi_k^{(0),SS} \end{aligned} \tag{3.51}$$

Multiplying by a quadrature angle before summing over all angles and applying relations in Eq. (3.46) these terms in Eq. (3.51) become the following.

$$\begin{aligned} &\sum_{m=1}^{M} w_m \mu_m \sum_{k=\text{type 1}} \left|\mu_m\right| \delta t \int_0^{\Delta s_k} ds \frac{2\left(t-t_n\right)}{\Delta t_n} \Psi_{m,k}^{(0)}\left(s\right) \\ &= \sum_{m=1}^{M} w_m \mu_m \frac{1}{2} \sum_{k=\text{type 1}} \left|\mu_m\right| \delta t \int_0^{\Delta s_k} ds \frac{2\left(t-t_n\right)}{\Delta t_n} \phi_k^{(0),SS} \end{aligned} \tag{3.52}$$

Therefore, Eq. (3.52) has now become the following relation which shows that the leading order time moment of the current in the center of a cell is zero.

$$\Delta x_i \Delta t_n J_{i,n}^{t,(0)} = 0 \tag{3.53}$$

Applying the results of Eq. (3.47) and Eq. (3.50), the half-range isotropic nature of the angular flux at the center of a cell edge is found as given in Eq. (3.54).

$$\Psi^{(0)}_{i+1/2,m,n} = \frac{1}{2}\begin{Bmatrix} \overline{\phi}^{(0)}_{i,n} + \phi^{x,(0)}_{i,n} & \mu_m > 0, \\ \overline{\phi}^{(0)}_{i+1,n} - \phi^{x,(0)}_{i+1,n} & \mu_m < 0 \end{Bmatrix} \text{for i = 1,...,I-1} \tag{3.54}$$

Now the O(1) terms will be analyzed from applying the asymptotic expansions to Eqs. (3.37), (3.40), and (3.43). From Eq. (3.37), the O(1) terms are given in Eq. (3.55) where only tracks of type 1 contribute:

$$\begin{aligned} &\frac{1}{v}\sum_{m=1}^{M} w_m \sum_{k=\text{type 1}} \omega_k \sqrt{1+\mu_m^2}\left(\Psi^{(0)}_{m,k}\left(\Delta s_k\right) - \Psi^{(0)}_{m,k}\left(0\right)\right) \\ &+\frac{\sigma_t}{v}\sum_{m=1}^{M} w_m \sum_{k=\text{type 1}} \omega_k \sqrt{1+\mu_m^2}\int_0^{\Delta s_k} ds\left(\Psi^{(1)}_{m,k}\left(s\right) - \frac{1}{2}\phi^{(1),SS}_k\right) = 0 \end{aligned} \tag{3.55}$$

From the least squares definition in Eq. (2.17) the second term in Eq. (3.55) is zero. Applying the relation in Eq. (3.46), these terms show that all of the leading-order cell-edge current are equal.

$$\begin{aligned} &\sum_{m=1}^{M} w_m \sum_{k=\text{type 1}} \left|\mu_m\right| \delta t\left(\Psi^{(0)}_{m,k}\left(\Delta s_k\right) - \Psi^{(0)}_{m,k}\left(0\right)\right) = 0 \\ &\Delta t_n\left(J^{(0)}_{i+1/2,n} - J^{(0)}_{i-1/2,n}\right) = 0 \\ &J^{(0)}_{i+1/2,n} = J^{(0)}_{i-1/2,n} \end{aligned} \tag{3.56}$$

The O(1) terms from Eq. (3.40) are given in Eq. (3.57).

$$\begin{aligned} &\frac{\varepsilon}{v}\sum_{m=1}^{M} w_m \sum_{k=\text{type 1}} \omega_k \sqrt{1+\mu_m^2}\left[\begin{aligned} &\frac{2\left(x_{k,0} - x_i\right)}{\Delta x_i}\left(\Psi^{(0)}_{m,k}\left(\Delta s_k\right) - \Psi^{(0)}_{m,k}\left(0\right)\right) \\ &+\frac{2\mu_m}{\Delta x_i}\Delta s_k\left(\Psi^{(0)}_{m,k}\left(\Delta s_k\right) - \overline{\Psi}^{(0)}_{m,k}\right) \end{aligned}\right] \\ &+\frac{\sigma_t}{v}\sum_{m=1}^{M} w_m \sum_{k=\text{type 1}} \omega_k \sqrt{1+\mu_m^2}\int_0^{\Delta s_k} ds\,\frac{2\left(x - x_i\right)}{\Delta x_i}\left(\Psi^{(1)}_{m,k}\left(s\right) - \frac{1}{2}\phi^{(1),SS}_k\right) = 0 \end{aligned} \tag{3.57}$$

Again from the least squares definition the second term is zero. The first summation needs a closer evaluation. Since only tracks of type 1 need to be considered, the following relation applies:

$$\frac{2\left(x_{k,0}-x_i\right)}{\Delta x_i}=\frac{2\left(x_{i\pm1/2}-x_i\right)}{\Delta x_i}=\pm1 \tag{3.58}$$

Applying this relation and the one in Eq. (3.46), the first term in Eq. (3.57) becomes the following:

$$\sum_{m=1}^{M} w_m \sum_{k=\text{type 1}} \left|\mu_m\right| \delta t \left[\begin{cases} \Psi_{m,k}\left(\Delta s_k\right)+\Psi_{m,k}\left(0\right)-2\overline{\Psi}_{m,k}, & \mu_m>0, \\ -\Psi_{m,k}\left(\Delta s_k\right)-\Psi_{m,k}\left(0\right)+2\overline{\Psi}_{m,k}, & \mu_m<0 \end{cases} \right] \tag{3.59}$$

Considering the properties of tracks of type 1 and the summation over all angles, Eq. (3.59) yields the relation shown in Eq. (3.60).

$$\begin{aligned} &\Delta t_n\left(J^{(0)}_{i+1/2,n}+J^{(0)}_{i-1/2,n}-2\overline{J}^{(0)}_{i,n}\right)=0 \\ &J^{(0)}_{i+1/2,n}+J^{(0)}_{i-1/2,n}-2\overline{J}^{(0)}_{i,n}=0 \end{aligned} \tag{3.60}$$

Applying the results in Eq. (3.47) and Eq. (3.56) to Eq. (3.60) yields the following equality which holds for interior cell edges.

$$\begin{aligned} &J^{(0)}_{i+1/2,n}=0 \\ &\Rightarrow \sum_{m=1}^{M} w_m\mu_m\psi^{(0)}_{i+1/2,m,n}=0 \\ &\Rightarrow \sum_{\mu_m>0} w_m\mu_m\frac{1}{2}\left(\overline{\phi}^{(0)}_{i,n}+\phi^{x,(0)}_{i,n}\right)=\sum_{\mu_m<0} w_m\left|\mu_m\right|\frac{1}{2}\left(\overline{\phi}^{(0)}_{i+1,n}-\phi^{x,(0)}_{i+1,n}\right) \\ &\Rightarrow \overline{\phi}^{(0)}_{i,n}+\phi^{x,(0)}_{i,n}=\overline{\phi}^{(0)}_{i+1,n}-\phi^{x,(0)}_{i+1,n} \end{aligned} \tag{3.61}$$

Equation (3.61) shows that the leading-order least-squares scalar flux is continuous at a cell edge. Therefore we can define a cell edge scalar flux as given in Eq. .

$$\phi_{i+1/2,n} \equiv \bar{\phi}_{i,n}^{(0)} + \phi_{i,n}^{x,(0)} = \bar{\phi}_{i+1,n}^{(0)} - \phi_{i+1,n}^{x,(0)} \tag{3.62}$$

Investigation of what happens on the boundary of the problem should be similar to the steady-state LC derivation. Equation (3.61) as applied to the boundaries yields the following result.

$$\begin{aligned}
&\sum_{\mu_m>0} w_m \mu_m \psi_{m,n,inc} = \sum_{\mu_m<0} w_m |\mu_m| \frac{1}{2} \phi_{1/2,n}^{(0)} \\
&\Rightarrow \phi_{1/2,n}^{(0)} = \sum_{\mu_m>0} w_m \frac{4\mu_m}{\rho} \psi_{m,n,inc} \\
&\sum_{\mu_m<0} w_m |\mu_m| \psi_{m,n,inc} = \sum_{\mu_m>0} w_m |\mu_m| \frac{1}{2} \phi_{I+1/2,n}^{(0)} \\
&\Rightarrow \phi_{I+1/2,n}^{(0)} = \sum_{\mu_m<0} w_m \frac{4|\mu_m|}{\rho} \psi_{m,n,inc}
\end{aligned} \tag{3.63}$$

It will be advantageous to determine an expression for the first order current in all cells that will use the previous two equations. Multiplying Eq. (3.55) by a quadrature cosine before performing the angular summation, the following equation is found.

$$\begin{aligned}
&\frac{1}{v} \sum_{m=1}^{M} w_m \mu_m \sum_{k=\text{type 1}} \omega_k \sqrt{1+\mu_m^2} \left(\Psi_{m,k}^{(0)} (\Delta s_k) - \Psi_{m,k}^{(0)} (0) \right) \\
&+ \frac{\sigma_t}{v} \sum_{m=1}^{M} w_m \mu_m \sum_{k=\text{type 1}} \omega_k \sqrt{1+\mu_m^2} \int_0^{\Delta s_k} ds \left(\Psi_{m,k}^{(1)} (s) - \frac{1}{2} \phi_k^{(1),SS} \right) = 0
\end{aligned} \tag{3.64}$$

Simplifying with the relations found in Eq. (3.46), Eq. (3.64) can be written as given in Eq. (3.65).

$$\begin{aligned}
&\sum_{m=1}^{M} w_m \mu_m \sum_{k=\text{type 1}} |\mu_m| \delta t \left(\Psi_{m,k}^{(0)} (\Delta s_k) - \Psi_{m,k}^{(0)} (0) \right) \\
&+ \sigma_t \sum_{m=1}^{M} w_m \mu_m \sum_{k=\text{type 1}} |\mu_m| \delta t \Delta s_k \left(\bar{\Psi}_{m,k}^{(1)} (s) - \frac{1}{2} \bar{\phi}_k^{(1),SS} \right) = 0
\end{aligned} \tag{3.65}$$

Again applying Eq. (3.46), the term on the second line of Eq. (3.65) can be simplified for tracks of type 1 as shown in Eq. (3.66).

$$\begin{aligned}&\sum_{m=1}^{M} w_m \mu_m^2 \sum_{k=\text{type 1}} \delta t\left(\Psi_{m,k}^{(0)}\left(\Delta s_k\right)-\Psi_{m,k}^{(0)}\left(0\right)\right)\\&+\sigma_t \sum_{m=1}^{M} w_m \mu_m \sum_{k=\text{type 1}} \Delta x_i \delta t\left(\bar{\Psi}_{m,k}^{(1)}\left(s\right)-\frac{1}{2}\bar{\phi}_k^{(1),SS}\right)=0\end{aligned} \tag{3.66}$$

We see from this equation that the angular summation over the scalar flux term will be zero. Applying the definition of the current and performing the track summation in Eq. (3.66) leads to Eq. (3.67).

$$\sum_{m=1}^{M} w_m \mu_m^2 \Delta t_n\left(\Psi_{i+1/2,n}^{(0)}-\Psi_{i-1/2,n}^{(0)}\right)+\sigma_t \Delta x_i \Delta t_n \bar{J}_{i,n}^{(1)}=0 \tag{3.67}$$

Finally, rearranging Eq. (3.67) leads to a relation for the first order current.

$$\bar{J}_{i,n}^{(1)}=-\frac{1}{\sigma_t \Delta x_i \Delta t_n}\sum_{m=1}^{M} w_m \mu_m^2 \Delta t_n\left(\Psi_{i+1/2,n}^{(0)}-\Psi_{i-1/2,n}^{(0)}\right) \tag{3.68}$$

This equation for the current has different representations for interior and boundary cells. Applying the boundary relation found in Eq. (3.63) and the expression for the leading order angular flux in Eq. (3.54) to the first term in Eq. (3.68), the following relation is found.

$$\sum_{m=1}^{M} w_m \mu_m^2\left(\Psi_{i+1/2,m,n}^{(0)}\right)=\begin{Bmatrix}\sum_{\mu_m>0} w_m \mu_m^2 \psi_{m,n,inc}+\frac{1}{6}\phi_{1/2,n}^{(0)}, & i=0,\\ \frac{1}{3}\phi_{i+1/2,n}, & i=1,\ldots,I-1,\\ \sum_{\mu_m<0} w_m \mu_m^2 \psi_{m,n,inc}+\frac{1}{6}\phi_{I+1/2,n}^{(0)}, & i=I\end{Bmatrix} \tag{3.69}$$

Therefore, Eq. (3.68) becomes the following relation for the first order current density.

$$J_{i,n}^{(1)}=\left\{\begin{array}{ll}-\dfrac{1}{3\sigma_t\Delta x_i}\left(\phi_{3/2,n}-\sum\limits_{\mu_m>0}w_m\left(3\mu_m^2+\dfrac{2|\mu_m|}{\rho}\right)\psi_{m,n,inc}\right), & i=1,\\ -\dfrac{1}{3\sigma_t\Delta x_i}\left(\phi_{i+1/2,n}-\phi_{i-1/2,n}\right), & i=2,...,I-1,\\ -\dfrac{1}{3\sigma_t\Delta x_i}\left(\sum\limits_{\mu_m<0}w_m\left(3\mu_m^2+\dfrac{2|\mu_m|}{\rho}\right)\psi_{m,n,inc}-\phi_{I-1/2,n}\right), & i=I\end{array}\right\} \tag{3.70}$$

Finally the O(1) terms from Eq. (3.43) will be analyzed. These terms are given in Eq. (3.71) where again, only tracks of type 1contribute.

$$\begin{aligned}&\frac{1}{v}\sum_{m=1}^{M}w_m\sum_{k=\text{type 1}}\omega_k\sqrt{1+\mu_m^2}\left[\begin{array}{l}\left(\dfrac{2\left(t_{k,0}-t_n\right)}{\Delta t_n}\right)\left(\psi_{m,k}^{(0)}\left(\Delta s_k\right)-\psi_{m,k}^{(0)}\left(0\right)\right)\\ +\dfrac{2\varepsilon}{v\Delta t_n}\Delta s_k\left(\psi_{m,k}^{(0)}\left(\Delta s_k\right)-\bar{\psi}_{m,k}^{(0)}\right)\end{array}\right]\\ &+\frac{\sigma_t}{v}\sum_{m=1}^{M}w_m\sum_{k=\text{type 1}}\omega_k\sqrt{1+\mu_m^2}\int_0^{\Delta s_k}ds\left(\frac{2\left(t-t_n\right)}{\Delta t_n}\right)\left(\psi_{m,k}^{(1)}(s)-\frac{1}{2}\phi_k^{(1),SS}\right)=0\end{aligned} \tag{3.71}$$

From the least squares definition in Eq. (2.17), the second term in Eq. (3.71) is zero. Applying the relations in Eq. (3.46) the first term in Eq. (3.71) becomes the following relation found in Eq. (3.72). The second term in the square brackets is of higher order so it is ignored.

$$\sum_{m=1}^{M}w_m\sum_{k=\text{type 1}}|\mu_m|\delta t\left[\left(\frac{2\left(t_{k,0}-t_n\right)}{\Delta t_n}\right)\left(\Psi_{m,k}^{(0)}\left(\Delta s_k\right)-\Psi_{m,k}^{(0)}\left(0\right)\right)\right]=0 \tag{3.72}$$

As Eq. (3.72), the sum over tracks becomes an integral over time, and the time moment of the current at cell edges appears as given in Eq. (3.73).

$$\begin{aligned} &\Delta t_n \left(J^{t,(0)}_{i+1/2,n} - J^{t,(0)}_{i-1/2,n} \right) = 0 \\ &\Rightarrow \\ &J^{t,(0)}_{i+1/2,n} = J^{t,(0)}_{i-1/2,n} \end{aligned} \tag{3.73}$$

Eq. (3.73) means that the time moment of the current is constant across the spatial domain for a given time step. However, this relation does not prove the time moment of the angular flux is constant across the spatial domain for a given time. Equation (3.75) shows how the time moment of the current in Eq. (3.74) can be written in terms of the angular flux.

$$J^{t,(0)}_{i-1/2,n} = J^{t,(0)}_{i+1/2,n} = J^{t,(0)}_{(i+1)-1/2,n} \tag{3.74}$$

$$\sum_{m=1}^{M} w_m \mu_m \Psi^{t,(0)}_{i-1/2,m,n} = \sum_{m=1}^{M} w_m \mu_m \Psi^{t,(0)}_{i+1/2,m,n} = \sum_{m=1}^{M} w_m \mu_m \Psi^{t,(0)}_{(i+1)-1/2,m,n} \tag{3.75}$$

Also, from the leading-order relation of the angular and scalar fluxes found previously, Eq. (3.75) can be rewritten in terms of the time moment of the scalar flux as given in Eq. (3.76).

$$\frac{1}{2} \sum_{\mu_m>0} w_m \mu_m \phi^{t,(0),SS}_{(i-1)R,n} - \frac{1}{2} \sum_{\mu_m<0} w_m \left|\mu_m\right| \phi^{t,(0),SS}_{iL,n} = \frac{1}{2} \sum_{\mu_m>0} w_m \mu_m \phi^{t,(0),SS}_{iR,n} - \frac{1}{2} \sum_{\mu_m<0} w_m \left|\mu_m\right| \phi^{t,(0),SS}_{(i+1)L,n} \tag{3.76}$$

Equation (3.76) can be simplified due to the fact that the time moment is the same for a given time across a spatial cell. Equation (3.77) gives this simplified and rearranged version of Eq. (3.76).

$$\phi^{t,(0),SS}_{(i-1),n} \sum_{\mu_m>0} w_m \mu_m - 2\phi^{t,(0),SS}_{i,n} \sum_{\mu_m>0} w_m \left|\mu_m\right| + \phi^{t,(0),SS}_{(i+1),n} \sum_{\mu_m<0} w_m \left|\mu_m\right| = 0 \tag{3.77}$$

The quadrature summations in Eq. (3.77) are just constants based upon the quadrature set and divide out; therefore this relation holds for each cell with a different relation for the boundary cells. The definition of the time-slope on the boundaries is given in Eq. (3.78).

$$\begin{aligned}\phi_{0,n}^{t,(0)} &\equiv \sum_{\mu_m>0} w_m \frac{4\mu_m}{\rho}\psi_{m,n,inc}^{t} \\ \phi_{I+1,n}^{t,(0)} &\equiv \sum_{\mu_m<0} w_m \frac{4|\mu_m|}{\rho}\psi_{m,n,inc}^{t}\end{aligned} \tag{3.78}$$

Applying these boundary definitions and dividing Eq. (3.78) by the quadrature summations leads to a set of equations for every cell as shown in Eq. (3.79). This set of equations leads to the realization that the time moment of the scalar flux in each cell is an interpolation between known boundary values for every time value. Since this interpolation is not based upon actual spatial distance as evident from Eq. (3.79), it is merely an interpolation between values.

$$\left\{\begin{array}{ll} \displaystyle\sum_{\mu_m>0} w_m \frac{4\mu_m}{\rho}\psi_{m,n,inc}^{t} - 2\phi_{1,n}^{t,(0),SS} + \phi_{2,n}^{t,(0),SS} = 0, & i=1 \\ \phi_{(i-1),n}^{t,(0),SS} - 2\phi_{i,n}^{t,(0),SS} + \phi_{(i+1),n}^{t,(0),SS} = 0, & i=2,\ldots,I-1 \\ \phi_{(I-1),n}^{t,(0),SS} - 2\phi_{I,n}^{t,(0),SS} + \displaystyle\sum_{\mu_m<0} w_m \frac{4|\mu_m|}{\rho}\psi_{m,n,inc}^{t} = 0, & i=I \end{array}\right\} \tag{3.79}$$

Next the O(ε) terms from the asymptotic expansions of Eqs. (3.37), (3.40), and (3.43) will be analyzed. These are the O(ε) portions of Eq. (3.37):

$$\begin{aligned}&\frac{\varepsilon}{v}\sum_{m=1}^{M} w_m \sum_{k=1}^{\#\text{ in (i,n,m)}} \omega_k \sqrt{1+\mu_m^2}\left(\Psi_{m,k}(\Delta s_k) - \Psi_{m,k}(0)\right) \\ &+\frac{\varepsilon^2}{v}\sum_{m=1}^{M} w_m \sum_{k=1}^{\#\text{ in (i,n,m)}} \omega_k \sqrt{1+\mu_m^2}\int_0^{\Delta s_k} ds\left(\frac{\sigma_a}{2}\phi_k^{SS} - \frac{1}{2}q_k\right) = 0\end{aligned}. \tag{3.80}$$

Tracks of types 1, 3, and 4 must be considered in this analysis. The first term in Eq. (3.80) will be split up for different types of tracks. For tracks of type 3, the following definition holds for the track spacing in the x-direction.

$$\omega_k \sqrt{1+\mu_m^2} = \delta x \tag{3.81}$$

Applying this definition to the beginning angular flux in the first term of Eq. (3.80) and the leading-order angular flux definition found previously, the summation over tracks of type 3 becomes the following.

$$\begin{aligned} &\sum_{k=\text{type 3}} \omega_k \sqrt{1+\mu_m^2} \Psi_{m,k}(0) = \Delta x_i \psi_{i,m,n-1/2} \\ &\Rightarrow \left\{ \frac{\varepsilon}{v} \sum_{m=1}^{M} w_m \sum_{k=\text{type 3}} \omega_k \sqrt{1+\mu_m^2} \left(-\Psi_{m,k}(0) \right) \right\}^{(1)} \\ &= -\frac{1}{v} \Delta x_i \phi_{i,n-1/2}^{(0),SS} \end{aligned} \tag{3.82}$$

This same definition can be applied to the ending of tracks of type 4, therefore yielding the summation given in Eq. (3.83).

$$\left\{ \frac{\varepsilon}{v} \sum_{m=1}^{M} w_m \sum_{k=\text{type 4}} \omega_k \sqrt{1+\mu_m^2} \left(\Psi_{m,k}(\Delta s_k) \right) \right\}^{(1)} = \frac{1}{v} \Delta x_i \phi_{i,n+1/2}^{(0),SS} \tag{3.83}$$

Using the definition in Eq. (3.46), the corresponding summations of beginning and ending angular fluxes of tracks of type 1 and types 3 and 4 are shown in Eq. (3.84).

$$\begin{aligned} &\left\{ \frac{\varepsilon}{v} \sum_{m=1}^{M} w_m \sum_{k=\text{type 1 and type 3}} \omega_k \sqrt{1+\mu_m^2} \left(\Psi_{m,k}(\Delta s_k) \right) \right\}^{(1)} = \Delta t_n \left(J_{i+1/2,n}^{+,(1)} + J_{i-1/2,n}^{-,(1)} \right) \\ &\left\{ \frac{\varepsilon}{v} \sum_{m=1}^{M} w_m \sum_{k=\text{type 1 and type 4}} \omega_k \sqrt{1+\mu_m^2} \left(-\Psi_{m,k}(0) \right) \right\}^{(1)} = \Delta t_n \left(-J_{i-1/2,n}^{+,(1)} - J_{i+1/2,n}^{-,(1)} \right) \end{aligned} \tag{3.84}$$

Combining the relations found in Eqs. (3.82), (3.83), and (3.84), the first term in Eq. (3.80) becomes the following:

$$\begin{aligned}&\frac{\varepsilon}{v}\sum_{m=1}^{M} w_m \sum_{k=1}^{\#\text{ in (i,n,m)}} \omega_k \sqrt{1+\mu_m^2}\left(\Psi_{m,k}\left(\Delta s_k\right)-\Psi_{m,k}\left(0\right)\right)\\&=\frac{\Delta x_i}{v}\left(\phi_{i,n+1/2}^{(0),SS}-\phi_{i,n-1/2}^{(0),SS}\right)+\Delta t_n\left(J_{i+1/2,n}^{(1)}-J_{i-1/2,n}^{(1)}\right)\end{aligned} \quad . \tag{3.85}$$

The second term in Eq. (3.80) is more difficult to analyze in terms of the tracks that have been defined. If there were symmetry in the track pattern in a cell about 180°, the following would be true.

$$\frac{\sum_{k=1}^{\#\text{ in (i,m,n)}} \phi_k^{SS}}{\sum_{k=1}^{\#\text{ in (i,m,n)}} k}=\bar{\phi}_{i,n} \tag{3.86}$$

As $\varepsilon \to 0$, there are an infinite number of tracks in a cell, and tracks of types 2-4 are O(ε) smaller in number. From Eq. (3.80) only terms of leading order are of interest due to the epsilon that is present in the first and second lines. Therefore, only tracks of type 1 contribute. The functional form of the scattering source as given in Eq. (2.16) can be re-expressed for tracks of type 1 and in this asymptotic limit. Due to symmetry of the tracks, the $\phi_{i,n}^{x,SS}$ term will cancel, and the average scalar flux along a track, *k*, is defined as in Eq. (3.87).

$$\bar{\phi}_k = \bar{\phi}_{i,n}^{SS}+\phi_{i,n}^{t,SS}\left(\frac{2\left(t_{o,1}+\frac{\delta t}{2}+\left(k-1\right)\delta t-t_n\right)}{\Delta t_n}\right) \tag{3.87}$$

In this previous relation the definition of the starting track position for type 1 tracks is used as given in Eq. (3.88).

$$t_{o,1} = t_{n-1/2} + O(\varepsilon) \tag{3.88}$$

Substituting Eqs. (3.86) and (3.87) into the second line of Eq. (3.80) with a similar relation for the fixed source term leads to the following expression to evaluate.

$$\begin{aligned} &\frac{\varepsilon^2}{v}\sum_{m=1}^{M} w_m \sum_{k=\text{type 1}} \omega_k \sqrt{1+\mu_m^2}\,\Delta s_k \frac{1}{2}\left(\sigma_a \bar{\phi}_{i,n}^{(0),SS} - \bar{q}_{i,n}\right) \\ &+\frac{\varepsilon^2}{v}\sum_{m=1}^{M} w_m \sum_{k=\text{type 1}} \omega_k \sqrt{1+\mu_m^2}\,\Delta s_k \frac{1}{2}\left(\sigma_a \phi_{i,n}^{t,(0),SS} - q_{i,n}^{t}\right)\frac{2}{\Delta t_n}\left(t_{o,1} + \frac{\delta t}{2} + (k-1)\,\delta t - t_n\right) \end{aligned} \tag{3.89}$$

The second line in Eq. (3.89) will be analyzed first. The number of tracks of type 1 and type 4 can be defined as given in Eq. (3.90).

$$\begin{aligned} N_4 &= \frac{\Delta x_i}{\delta x} = \frac{\varepsilon \Delta x_i}{v \delta t \left|\mu_m\right|} \\ N_1 &= \frac{\Delta t_n}{\delta t} - N_4 = N_4\left(\frac{v\left|\mu_m\right|\Delta t_n}{\varepsilon \Delta x_i} - 1\right) \end{aligned} \tag{3.90}$$

Also we will note that the following are true for tracks of type 1.

$$\begin{aligned} \Delta s_k &= \Delta x_i \left|\mu_m\right| \\ \omega_k &= \omega \end{aligned} \tag{3.91}$$

With these definitions, the second term of Eq. (3.89) can be re-written and simplified.

$$\begin{aligned} &\omega \Delta x_i \left|\mu_m\right| \sum_{k=1}^{N_1} \frac{2}{\Delta t_n}\left(t_{o,1} + \frac{\delta t}{2} + (k-1)\,\delta t - t_n\right) \\ &= \omega \Delta x_i \left|\mu_m\right| \left[\frac{2}{\Delta t_n} N_1 \left(t_{o,1} + \frac{\delta t}{2} - t_n\right) + \frac{\delta t}{\Delta t_n}(N_1 - 1) N_1\right] \end{aligned} \tag{3.92}$$

Equation (3.92) can be further simplified by substituting the relations defined in Eqs. (3.90) and (3.88),

$$\begin{aligned}&\omega\Delta x_i\left|\mu_m\right|\left[\frac{2}{\Delta t_n}N_1\left(t_{o,1}+\frac{\delta t}{2}-t_n\right)+\frac{\delta t}{\Delta t_n}\left(N_1-1\right)N_1\right]\\&=\omega\Delta x_i\left|\mu_m\right|\left[\frac{2}{\Delta t_n}N_1\left(t_{n-1/2}+O(\varepsilon)+\frac{\delta t}{2}-t_n\right)+\left(\frac{\varepsilon\Delta x_i}{N_4 v\left|\mu_m\right|\Delta t_n}\right)\left(N_1-1\right)N_1\right]\end{aligned} \tag{3.93}$$

where

$$\frac{\delta t}{\Delta t_n}=\frac{1}{N_1+N_4}=\frac{\varepsilon\Delta x_i}{N_4 v\left|\mu_m\right|\Delta t_n} \tag{3.94}$$

Performing some more simplifications of Eq.(3.93), it is found that the second term in Eq. (3.89) is zero to O(ε). Therefore, when this term is inserted back into the angular summation in the second line of Eq. (3.89) it can be ignored because it is higher-order.

$$\begin{aligned}&=\omega\Delta x_i\left|\mu_m\right|\left[\frac{2}{\Delta t_n}N_1\left(0+O(\varepsilon)\right)+O(\varepsilon)\right]\\&=0+O(\varepsilon)\end{aligned} \tag{3.95}$$

To address the first term of Eq. (3.89) a short proof of the approximate volume integral over a cell is needed and will also be used later in the derivation. A representation of the volume integral is defined as given in Eq. (3.96).

$$\varepsilon\left[\Delta x_i\Delta t_n\right]_{tracks}=\frac{\varepsilon^2}{v}\frac{1}{2}\sum_{m=1}^{M}w_m\sum_{k=1}^{\#\text{ in (i,m,n)}}\omega_k\sqrt{1+\mu_m^2}\,\Delta s_k \tag{3.96}$$

Since the numbers of tracks of types 3 and 4 do not change with epsilon, the summation over tracks in Eq. (3.96) can be split up as given in Eq. (3.97).

$$\varepsilon\left[\Delta x_i\Delta t_n\right]_{tracks}=\frac{\varepsilon^2}{v}\frac{1}{2}(2)\left(\sum_{k=\text{type 1}}\omega_k\sqrt{1+\mu_m^2}\,\frac{\Delta x_i}{\left|\mu_m\right|}+\sum_{k=\text{type 2}}\omega_k\sqrt{1+\mu_m^2}\,v\Delta t_n+O(1)\right) \tag{3.97}$$

Applying the definition of tracks of type 1 and type 2, it is found that the approximate volume integral over the cell as defined in Eq. (3.96) is exact to O(ε) as given in Eq. (3.98).

$$\begin{aligned}\varepsilon\left[\Delta x_i \Delta t_n\right]_{tracks} &= \frac{\varepsilon^2}{v}\left\{\sum_{k=\text{type 1}} \frac{v\delta t \Delta x_i}{\varepsilon} + \sum_{k=\text{type 2}} v\delta x \Delta t_n + O(1)\right\} \\ \varepsilon\left[\Delta x_i \Delta t_n\right]_{tracks} &= \varepsilon \Delta t_n \Delta x_i + \varepsilon^2 \Delta t_n \Delta x_i + \varepsilon^2 O(1)\end{aligned} \tag{3.98}$$

With the results of Eqs. (3.95) and (3.98), the second term of Eq. (3.80) has become the following.

$$\frac{\varepsilon^2}{v}\sum_{m=1}^{M} w_m \sum_{k=1}^{\#\text{ in (i,n,m)}} \omega_k \sqrt{1+\mu_m^2} \int_0^{\Delta s_k} ds \left(\frac{\sigma_a}{2}\phi_k^{SS} - \frac{1}{2}q_k\right) = \Delta x_i \Delta t_n \left(\sigma_a \bar{\phi}_{i,n}^{(0),SS} - \bar{q}_{i,n}\right)\left(1+O(\varepsilon)\right) \tag{3.99}$$

All together, it is found that the O(ε) terms from the balance equation, Eq. (3.37), yields the equation given in Eq. (3.100).

$$\frac{\Delta x_i}{v}\left(\phi_{i,n+1/2}^{(0)} - \phi_{i,n-1/2}^{(0)}\right) + \Delta t_n \left(J_{i+1/2,n}^{(1)} - J_{i-1/2,n}^{(1)}\right) + \Delta x_i \Delta t_n \left(\sigma_a \bar{\phi}_{i,n}^{(0),SS} - \bar{q}_{i,n}\right) = 0 \tag{3.100}$$

The O(ε) terms from Eq. (3.40) are given in Eq. (3.101). These terms will eventually yield a spatial moment equation.

$$\begin{aligned}&\frac{\varepsilon}{v}\sum_{m=1}^{M} w_m \sum_{k=1}^{\#\text{ in (i,n,m)}} \omega_k \sqrt{1+\mu_m^2} \left[\begin{array}{l} \dfrac{2\left(x_{k,0}-x_i\right)}{\Delta x_i}\left(\Psi_{m,k}\left(\Delta s_k\right) - \Psi_{m,k}\left(0\right)\right) \\ + \dfrac{2\mu_m}{\Delta x_i}\Delta s_k \left(\Psi_{m,k}\left(\Delta s_k\right) - \bar{\Psi}_{m,k}\right) \end{array}\right] \\ &+ \frac{\varepsilon^2}{v}\sum_{m=1}^{M} w_m \sum_{k=1}^{\#\text{ in (i,n,m)}} \omega_k \sqrt{1+\mu_m^2} \int_0^{\Delta s_k} ds \frac{2\left(x-x_i\right)}{\Delta x_i}\left(\frac{\sigma_a}{2}\phi_k^{SS} - \frac{1}{2}q_k\right) = 0\end{aligned} \tag{3.101}$$

Considering tracks of type 1, the first term of Eq. (3.101) can be written as in Eq. (3.102)

.

$$\begin{aligned}
&\left[\frac{2\left(x_{k,0}-x_i\right)}{\Delta x_i}\left(\Psi_{m,k}\left(\Delta s_k\right)-\Psi_{m,k}\left(0\right)\right)+\frac{2\mu_m}{\Delta x_i}\Delta s_k\left(\Psi_{m,k}\left(\Delta s_k\right)-\bar{\Psi}_{m,k}\right)\right] \\
&=\mp(1)\left(\Psi_{m,k}\left(\Delta s_k\right)-\Psi_{m,k}\left(0\right)\right)\pm(2)\left(\Psi_{m,k}\left(\Delta s_k\right)-\bar{\Psi}_{m,k}\right) \\
&=\begin{Bmatrix}\Psi_{m,k}\left(\Delta s_k\right)+\Psi_{m,k}\left(0\right)-2\bar{\Psi}_{m,k}, & \mu_m>0, \\ -\Psi_{m,k}\left(\Delta s_k\right)-\Psi_{m,k}\left(0\right)+2\bar{\Psi}_{m,k}, & \mu_m<0\end{Bmatrix}
\end{aligned} \tag{3.102}$$

Performing the summation over tracks and angles the terms in Eq. (3.102) will be split up among different track types. With the relations in Eq. (3.46), the summation over the ending points of type 1 and type 3 tracks yields the result given in Eq. (3.103).

$$\begin{aligned}
&\left\{\frac{\varepsilon}{v}\sum_{m=1}^{M}w_m\sum_{k=\text{type 1 and type 3}}\omega_k\sqrt{1+\mu_m^2}\left(\Psi_{m,k}\left(\Delta s_k\right)\right)\right\}^{(1)} \\
&=\sum_{m=1}^{M}w_m\sum_{k=\text{type 1 and type 3}}\left|\mu_m\right|\delta t\Psi_{m,k}\left(\Delta s_k\right) \\
&=\Delta t_n\left(J_{i+1/2,n}^{+,(1)}-J_{i-1/2,n}^{-,(1)}\right)
\end{aligned} \tag{3.103}$$

Similarly, the summation over the beginning point of type 1 and type 4 tracks yields the result given in Eq. (3.104).

$$\left\{\frac{\varepsilon}{v}\sum_{m=1}^{M}w_m\sum_{k=\text{type 1 and type 4}}\omega_k\sqrt{1+\mu_m^2}\left(\Psi_{m,k}\left(0\right)\right)\right\}^{(1)}=\Delta t_n\left(J_{i-1/2,n}^{+,(1)}-J_{i+1/2,n}^{-,(1)}\right) \tag{3.104}$$

For the beginning point of tracks of type 3 there are contributions from two terms in Eq. (3.101) which can be simplified easily as given in Eq. (3.105). Contribution from the average angular flux term will be discussed below.

$$
\begin{aligned}
&\left\{\frac{\varepsilon}{v}\sum_{m=1}^{M} w_m \sum_{k=\text{type 3}} \omega_k \sqrt{1+\mu_m^2}\left[\frac{2\left(x_{k,0}-x_i\right)}{\Delta x_i}\left(-\Psi_{m,k}\left(0\right)\right)\right]\right\}^{(1)} \\
&=\left\{\frac{\varepsilon}{v}\sum_{m=1}^{M} w_m \sum_{k=\text{type 3}} \delta x\left[\frac{2\left(x_{k,0}-x_i\right)}{\Delta x_i}\left(-\Psi_{m,k}\left(0\right)\right)\right]\right\}^{(1)} \\
&\approx\left\{\frac{\varepsilon}{v}\sum_{m=1}^{M} w_m \int_{x_{i-1/2}}^{x_{i+1/2}} dx\left[\frac{2\left(x-x_i\right)}{\Delta x_i}\left(-\Psi_{m,k,n-1/2}\right)\right]\right\}^{(1)} \\
&=-\frac{\Delta x_i}{v}\phi_{i,n-1/2}^{(0),SS,x}
\end{aligned}
\tag{3.105}
$$

There is also a similar relation for the ending point of tracks of type 4 as given in Eq. (3.106).

$$
\begin{aligned}
&\left\{\frac{\varepsilon}{v}\sum_{m=1}^{M} w_m \sum_{k=\text{type 4}} \omega_k \sqrt{1+\mu_m^2}\left[\frac{2\left(x_{k,0}-x_i\right)}{\Delta x_i}\left(\Psi_{m,k}\left(\Delta s_k\right)\right)+\frac{2\mu_m}{\Delta x_i}\Delta s_k\left(\Psi_{m,k}\left(\Delta s_k\right)\right)\right]\right\}^{(1)} \\
&=\left\{\frac{\varepsilon}{v}\sum_{m=1}^{M} w_m \sum_{k=\text{type 4}} \omega_k \sqrt{1+\mu_m^2}\left[\frac{2\left(x_{k,0}-x_i+\Delta x_k\right)}{\Delta x_i}\left(\Psi_{m,k}\left(\Delta s_k\right)\right)\right]\right\}^{(1)} \\
&=\left\{\frac{\varepsilon}{v}\sum_{m=1}^{M} w_m \sum_{k=\text{type 4}} \delta x\frac{2\left(x_{k,end}-x_i\right)}{\Delta x_i}\Psi_{m,k}\left(\Delta s_k\right)\right\}^{(1)} \\
&\approx\frac{1}{v}\sum_{m=1}^{M} w_m \int_{x_{i-1/2}}^{x_{i+1/2}} dx\frac{2\left(x\ -x_i\right)}{\Delta x_i}\psi_{i,m,n+1/2}^{(0)} \\
&=\frac{\Delta x_i}{v}\phi_{i,n+1/2}^{(0),SS,x}
\end{aligned}
\tag{3.106}
$$

The average angular flux term in Eq. (3.101) turns into an average current density in the *x*-*vt* cell. Only tracks of type 1 need to be considered when analyzing this term, because tracks of type 3 and type 4 lead to terms of higher order. Equation (3.107) shows the summation over the angular flux and its simplification for tracks of type 1.

$$
\begin{aligned}
&\left\{\frac{\varepsilon}{v}\sum_{m=1}^{M} w_m \sum_{k=\text{type 1}} \omega_k \sqrt{1+\mu_m^2}\left[-\frac{2\mu_m}{\Delta x_i}\Delta s_k \bar{\Psi}_{m,k}\right]\right\}^{(1)} \\
&= \pm\sum_{m=1}^{M} w_m \sum_{k=\text{type 1}} |\mu_m| \delta t 2\bar{\Psi}^{(1)}_{m,k} \\
&= -2\sum_{k=\text{type 1}} \delta t \left(\frac{\sum_{k=\text{type 1}} \delta t \bar{J}^{(1)}_k}{\sum_{k=\text{type 1}} \delta t}\right) \\
&= -2\Delta t_n \bar{J}^{(1)}_{i,n} + O(\varepsilon)
\end{aligned}
\tag{3.107}
$$

In the previous equation, the summation over tracks in the time-variable definition given in Eq. (3.108) is applied.

$$
\sum_{k=\text{type 1}} \delta t = \Delta t_n + O(\varepsilon) \tag{3.108}
$$

Combining the results of Eq. (3.103), Eq. (3.104), Eq. (3.105), Eq. (3.106), and Eq. (3.107) the first term of Eq. (3.101) has simplified to the expression given in Eq. (3.109).

$$
\begin{aligned}
&\frac{\varepsilon}{v}\sum_{m=1}^{M} w_m \sum_{k=1}^{\#\text{ in (i,n,m)}} \omega_k \sqrt{1+\mu_m^2}\left[\begin{array}{l}\frac{2\left(x_{k,0}-x_i\right)}{\Delta x_i}\left(\Psi_{m,k}\left(\Delta s_k\right)-\Psi_{m,k}\left(0\right)\right) \\ +\frac{2\mu_m}{\Delta x_i}\Delta s_k\left(\Psi_{m,k}\left(\Delta s_k\right)-\bar{\Psi}_{m,k}\right)\end{array}\right] \\
&= \frac{\Delta x_i}{v}\left(\phi^{(0),SS,x}_{i,n+1/2} - \phi^{(0),SS,x}_{i,n-1/2}\right) + \Delta t_n\left(J^{(1)}_{i+1/2,n} + J^{(1)}_{i-1/2,n} - 2\bar{J}^{(1)}_{i,n}\right)
\end{aligned}
\tag{3.109}
$$

A similar analysis for the source term of Eq. (3.101) is now done as was done for the previous terms. Again only tracks of type 1 will contribute because the others are of higher order. The integral over the s variable is converted to an integral in the x-dimension as shown in Eq. (3.110).

$$\begin{aligned}&\frac{\varepsilon^2}{v}\sum_{m=1}^{M} w_m \sum_{k=1}^{\#\text{ in (i,n,m)}} \omega_k \sqrt{1+\mu_m^2} \int_0^{\Delta s_k} ds \frac{2\left(x-x_i\right)}{\Delta x_i}\left(\frac{\sigma_a}{2}\phi_k^{SS}-\frac{1}{2}q_k\right)\\&=\frac{1}{v}\sum_{m=1}^{M} w_m \sum_{k=\text{type 1}} \omega_k \sqrt{1+\mu_m^2}\frac{1}{|\mu_m|}\int_{x_{i\mp1/2}}^{x_{i\pm1/2}} dx \frac{2\left(x-x_i\right)}{\Delta x_i}\left(\frac{\sigma_a}{2}\phi_k^{(0),SS}-\frac{1}{2}q_k\right)\end{aligned} \tag{3.110}$$

If the functional form of the scattering source and the fixed source are substituted into this integral, it is obvious that the average term will cancel in the integral. Also, if there is symmetry of the type 1 tracks about the time step midpoint, the time term in the integral is also cancelled. With these cancellations and the use of Eq. (3.98), Eq. (3.110) simplifies to the result given in Eq. (3.111) which only includes the spatial moment terms.

$$\begin{aligned}&\frac{1}{v}\sum_{m=1}^{M} w_m \sum_{k=\text{type 1}} \omega_k \sqrt{1+\mu_m^2}\frac{1}{|\mu_m|}\int_{x_{i\mp1/2}}^{x_{i\pm1/2}} dx \frac{2\left(x-x_i\right)}{\Delta x_i}\left(\frac{\sigma_a}{2}\phi_k^{(0),SS}-\frac{1}{2}q_k\right)\\&=\frac{1}{v}\sum_{m=1}^{M} w_m \sum_{k=\text{type 1}} \omega_k \sqrt{1+\mu_m^2}\frac{1}{|\mu_m|}\frac{1}{3}\Delta x_i\left(\frac{\sigma_a}{2}\phi_{i,n}^{x,(0),SS}-\frac{1}{2}q_{i,n}^{x}\right)\\&=\frac{1}{v}\sum_{m=1}^{M} w_m \sum_{k=\text{type 1}} \omega_k \sqrt{1+\mu_m^2}\frac{1}{3}\Delta s_k\left(\frac{\sigma_a}{2}\phi_{i,n}^{x,(0),SS}-\frac{1}{2}q_{i,n}^{x}\right)\\&=\Delta x_i\Delta t_n\left(\frac{1}{3}\sigma_a\phi_{i,n}^{x,(0),SS}-\frac{1}{3}q_{i,n}^{x}\right)\end{aligned} \tag{3.111}$$

Combining Eq. (3.109) and Eq. (3.111), the O(ε) terms from Eq. (3.40) are simplified and given in Eq. (3.112) which gives a spatial moment equation for the scalar flux.

$$\begin{aligned}&\frac{\Delta x_i}{v}\left(\phi_{i,n+1/2}^{(0),SS,x}-\phi_{i,n-1/2}^{(0),SS,x}\right)+\Delta t_n\left(J_{i+1/2,n}^{(1)}+J_{i-1/2,n}^{(1)}-2\overline{J}_{i,n}^{(1)}\right)\\&+\frac{1}{3}\Delta x_i\Delta t_n\left(\sigma_a\phi_{i,n}^{x,(0),SS}-q_{i,n}^{x}\right)=0\end{aligned} \tag{3.112}$$

Finally the O(ε) terms from Eq. (3.43) are analyzed. The terms of interest are given in Eq. (3.113).

$$\frac{\varepsilon}{v}\sum_{m=1}^{M} w_m \sum_{k=1}^{\#\text{ in (i,n,m)}} \omega_k \sqrt{1+\mu_m^2}\left[\begin{array}{l}\dfrac{2\left(t_{k,0}-t_n\right)}{\Delta t_n}\left(\Psi_{m,k}\left(\Delta s_k\right)-\Psi_{m,k}\left(0\right)\right)\\ +\dfrac{2\varepsilon}{v\Delta t_n}\Delta s_k\left(\Psi_{m,k}\left(\Delta s_k\right)-\bar{\Psi}_{m,k}\right)\end{array}\right] \qquad (3.113)$$
$$+\frac{\varepsilon^2}{v}\sum_{m=1}^{M} w_m \sum_{k=1}^{\#\text{ in (i,n,m)}} \omega_k \sqrt{1+\mu_m^2}\int_0^{\Delta s_k} ds\,\frac{2\left(t-t_n\right)}{\Delta t_n}\left(\frac{\sigma_a}{2}\phi_k^{SS}-\frac{1}{2}q_k\right)=0$$

Considering the first term in Eq. (3.113), first the beginning point of tracks of type 3 is analyzed. As from the previous derivation, Eq. (3.114) gives the simplification of the summation over these beginning points.

$$\begin{aligned}&\frac{\varepsilon}{v}\sum_{m=1}^{M} w_m \sum_{k=\text{type 3}} \omega_k \sqrt{1+\mu_m^2}\left[\frac{2\left(t_{k,0}-t_n\right)}{\Delta t_n}\left(-\Psi_{m,k}\left(0\right)\right)\right]\\ &=\frac{1}{v}\sum_{m=1}^{M} w_m \sum_{k=\text{type 3}} \delta x \Psi^{(0)}_{m,k,n-1/2}\\ &=\frac{1}{v}\Delta x_i \phi^{(0),SS}_{i,n-1/2}\end{aligned} \qquad (3.114)$$

Similarly, the ending points of tracks of type 4 yield the result given in Eq. (3.115).

$$\begin{aligned}&\frac{\varepsilon}{v}\sum_{m=1}^{M} w_m \sum_{k=\text{type 4}} \omega_k \sqrt{1+\mu_m^2}\left[\left(\frac{2\left(t_{k,0}-t_n\right)}{\Delta t_n}+\frac{2\varepsilon}{v\Delta t_n}\Delta s_k\right)\Psi_{m,k}\left(\Delta s_k\right)\right]\\ &=\frac{1}{v}\sum_{m=1}^{M} w_m \sum_{k=\text{type 4}} \delta x\left[\left(\frac{2\left(t_{k,end}-t_n\right)}{\Delta t_n}\right)\Psi^{(0)}_{m,k,n+1/2}\right]\\ &=\frac{1}{v}\Delta x_i \phi^{(0),SS}_{i,n+1/2}\end{aligned} \qquad (3.115)$$

The summation over beginning points of type 4 and type 1 tracks gives a time moment of the partial currents as shown in Eq. (3.116).

$$
\begin{aligned}
&\frac{\varepsilon}{v}\sum_{m=1}^{M} w_m \sum_{k=\text{type 1 and type 4}} \omega_k \sqrt{1+\mu_m^2}\left[\frac{2\left(t_{k,0}-t_n\right)}{\Delta t_n}\left(-\Psi_{m,k}\left(0\right)\right)\right] \\
&=\left\{\sum_{m=1}^{M} w_m \sum_{k=\text{type 1 and type 4}} \left|\mu_m\right|\delta t\left[\frac{2\left(t_{k,0}-t_n\right)}{\Delta t_n}\left(-\Psi_{m,k}\left(0\right)\right)\right]\right\}^{(1)} \\
&\approx -\sum_{m=1}^{M} w_m \left|\mu_m\right| \int_{t_{n-1/2}}^{t_{n+1/2}} dt \frac{2\left(t-t_n\right)}{\Delta t_n}\Psi_{m,i\pm 1/2,n}^{(1)} \\
&=-\Delta t_n\left(J_{i-1/2,n}^{(1),t,+}+J_{i+1/2,n}^{(1),t,-}\right)
\end{aligned}
\tag{3.116}
$$

Similarly, the summation over the ending point of type 3 and type 1 tracks gives a time moment of the partial currents as shown in Eq. (3.117).

$$
\begin{aligned}
&\frac{\varepsilon}{v}\sum_{m=1}^{M} w_m \sum_{k=\text{type 1 and type 3}} \omega_k \sqrt{1+\mu_m^2}\left[\left(\frac{2\left(t_{k,0}-t_n\right)}{\Delta t_n}+\frac{2\varepsilon}{v\Delta t_n}\Delta s_k\right)\Psi_{m,k}\left(\Delta s_k\right)\right] \\
&=\left\{\sum_{m=1}^{M} w_m \sum_{k=\text{type 1 and type 3}} \left|\mu_m\right|\delta t\left[\frac{2\left(t_{k,0}-t_n\right)}{\Delta t_n}\left(-\Psi_{m,k}\left(\Delta s_k\right)\right)\right]\right\}^{(1)} \\
&\approx \sum_{m=1}^{M} w_m \left|\mu_m\right| \int_{t_{n-1/2}}^{t_{n+1/2}} dt \frac{2\left(t-t_n\right)}{\Delta t_n}\Psi_{m,i\pm 1/2,n}^{(1)} \\
&=\Delta t_n\left(J_{i-1/2,n}^{(1),t,-}+J_{i+1/2,n}^{(1),t,+}\right)
\end{aligned}
\tag{3.117}
$$

The track summation over the average angular flux term in Eq. (3.113) becomes an average scalar flux in the *x-vt* cell.

$$
\begin{aligned}
&\left\{\frac{\varepsilon}{v}\sum_{m=1}^{M} w_m \sum_{k=1}^{\#\text{ in (i,m,n)}} \omega_k \sqrt{1+\mu_m^2}\Delta s_k \frac{2\varepsilon}{v\Delta t_n}\bar{\Psi}_{m,k}\right\}^{(1)} \\
&=\left\{\frac{\varepsilon}{v}\frac{2\varepsilon}{v\Delta t_n}\frac{v}{\varepsilon}\Delta t_n \Delta x_i\left(\bar{\phi}_{i,n}^{SS}\right)\right\}^{(1)} \\
&=2\frac{\Delta x_i}{v}\bar{\phi}_{i,n}^{(0),SS}
\end{aligned}
\tag{3.118}
$$

Combining the results of Eq. (3.114), Eq. (3.115), Eq. (3.116), Eq. (3.117), and Eq. (3.118), the first term in Eq. (3.113) simplifies to the result given in Eq. (3.119).

$$\begin{aligned}&\frac{\varepsilon}{v}\sum_{m=1}^{M} w_m \sum_{k=1}^{\#\text{ in (i,n,m)}} \omega_k \sqrt{1+\mu_m^2}\left[\begin{array}{l}\dfrac{2\left(t_{k,0}-t_n\right)}{\Delta t_n}\left(\Psi_{m,k}\left(\Delta s_k\right)-\Psi_{m,k}\left(0\right)\right)\\ +\dfrac{2\varepsilon}{v\Delta t_n}\Delta s_k\left(\Psi_{m,k}\left(\Delta s_k\right)-\overline{\Psi}_{m,k}\right)\end{array}\right] \\ &=\frac{1}{v}\Delta x_i\left(\phi_{i,n+1/2}^{(0),SS}+\phi_{i,n-1/2}^{(0),SS}-2\overline{\phi}_{i,n}^{(0),SS}\right)+\Delta t_n\left(J_{i+1/2,n}^{(1),t}-J_{i-1/2,n}^{(1),t}\right)\end{aligned} \tag{3.119}$$

The source term in Eq. (3.113) is more difficult to analyze. Equation (3.120) shows this source term with the functional form of the scattering source and fixed source.

$$\left\{\frac{\varepsilon^2}{v}\sum_{m=1}^{M} w_m \sum_{k=\text{type 1}} \omega_k \sqrt{1+\mu_m^2}\,\frac{1}{2}\int_0^{\Delta s_k} ds\,\frac{2\left(t-t_n\right)}{\Delta t_n}\left[\begin{array}{l}\left(\sigma_a\overline{\phi}_{i,n}^{SS}-\overline{q}_{i,n}\right)\\ +\left(\dfrac{2\left(x-x_i\right)}{\Delta x_i}\right)\left(\sigma_a\phi_{i,n}^{x,SS}-q_{i,n}^{x}\right)\\ +\left(\dfrac{2\left(t-t_n\right)}{\Delta t_n}\right)\left(\sigma_a\phi_{i,n}^{t,SS}-q_{i,n}^{t}\right)\end{array}\right]\right\}^{(1)} \tag{3.120}$$

Again, only tracks of type 1 need to be considered to find the O(ε) terms. Assuming symmetry of the type 1 tracks about the time midpoint of the cell, the average terms will cancel when performing the integration and summation over all of these tracks in the cell as given in Eq. (3.121).

$$\frac{\varepsilon^2}{v}\sum_{m=1}^{M} w_m \sum_{k=\text{type 1}} \omega_k \sqrt{1+\mu_m^2}\,\frac{1}{2}\int_0^{\Delta s_k} ds\,\frac{2\left(t-t_n\right)}{\Delta t_n}\left[\sigma_a\overline{\phi}_{i,n}^{SS}-\overline{q}_{i,n}\right]=0 \tag{3.121}$$

The terms involving the spatial moment will also cancel if there is symmetry about the midpoint of the time step and a symmetric quadrature set is used. Therefore, for a

positive angle, the integration over two sibling tracks is positive, with the integration over the corresponding siblings in its negative counterpart is the same value with an opposite sign which is evident in Eq. (3.122).

$$\frac{\varepsilon^2}{v}\sum_{m=1}^{M} w_m \sum_{k=\text{type 1}} \omega_k \sqrt{1+\mu_m^2}\,\frac{1}{2}\int_0^{\Delta s_k} ds\left(\frac{2\left(t-t_n\right)}{\Delta t_n}\right)\left(\frac{2\left(x-x_i\right)}{\Delta x_i}\right)\left[\sigma_a \phi_{i,n}^{x,SS} - q_{i,n}^{x}\right] = 0 \tag{3.122}$$

The time moment term in Eq. (3.120) requires more careful consideration. For tracks of type 1, this integration can be rewritten and performed as shown in Eq. (3.123).

$$\begin{aligned}\int_0^{\Delta s_k} ds\left(\frac{2\left(t-t_n\right)}{\Delta t_n}\right)^2\left[\sigma_a \phi_{i,n}^{t,SS} - q_{i,n}^{t}\right] &= \int_0^{\Delta s_k} ds\,\frac{4\left(t_{k,0}+\frac{\varepsilon}{v}s-t_n\right)^2}{\Delta t_n^2}\left[\sigma_a \phi_{i,n}^{t,SS} - q_{i,n}^{t}\right] \\ = \frac{4}{\Delta t_n^2}\left(\sigma_a \phi_{i,n}^{t,SS} - q_{i,n}^{t}\right)&\left[\Delta s_k\left(t_{k,0}-t_n\right)^2 + \frac{\varepsilon}{v}\Delta s_k^2\left(t_{k,0}-t_n\right) + \frac{\varepsilon^2}{3v^2\Delta t_n^2}\Delta s_k^3\right]\end{aligned} \tag{3.123}$$

Each of these terms in Eq. (3.123) is now considered in the full summation of Eq. (3.120). From symmetry about the time midpoint, the summation over tracks of the second term will be zero as shown in Eq. (3.124).

$$\frac{1}{v}\sum_{m=1}^{M} w_m \sum_{k=\text{type 1}} \omega_k \sqrt{1+\mu_m^2}\,\frac{1}{2}\frac{4}{\Delta t_n^2}\left(\sigma_a \phi_{i,n}^{t,(0),SS} - q_{i,n}^{t,(0)}\right)\frac{\varepsilon}{v}\Delta s_k^2\left(t_{k,0}-t_n\right) = 0 \tag{3.124}$$

The last term in Eq. (3.123), when summed over all tracks and angles yields a term that is higher order as given in Eq. (3.125).

$$\begin{aligned}&\left\{\frac{\varepsilon^2}{v}\sum_{m=1}^{M} w_m \sum_{k=\text{type 1}} \omega_k \sqrt{1+\mu_m^2}\,\Delta s_k\,\frac{1}{2}\frac{4}{3}\left(\sigma_a \phi_{i,n}^{t,SS} - q_{i,n}^{t}\right)\left(\frac{\varepsilon}{v\Delta t_n}\right)^2 \Delta s_k^2\right\}^{(1)} \\ &= \Delta x_i \Delta t_n \left(\sigma_a \phi_{i,n}^{t,SS} - q_{i,n}^{t}\right) N_1 \frac{4}{3}\left(\frac{\varepsilon}{v\Delta t_n}\right)^2\left(\frac{\Delta x_i}{|\mu_m|}\right)^2 \\ &\Rightarrow O(\varepsilon^2)\end{aligned} \tag{3.125}$$

Finally the full summation over type 1 tracks of the first term in Eq. (3.120) is performed below. First, it is easy to recognize the doubling of terms due to symmetry about the time midpoint. Also, the squared difference in this term can be expanded as given in Eq. (3.126).

$$\begin{aligned}
&\frac{\varepsilon^2}{v}\sum_{m=1}^{M} w_m \sum_{k=\text{type 1}} \omega_k \sqrt{1+\mu_m^2}\,\Delta s_k \,\frac{1}{2}\frac{4}{\Delta t_n^2}\left(\sigma_a \phi_{i,n}^{t,SS} - q_{i,n}^{t}\right)\left(t_{k,0} - t_n\right)^2 \\
&= \frac{\varepsilon^2}{v}\sum_{m=1}^{M} w_m \sum_{t_{k,0}<t_n} \omega_k \sqrt{1+\mu_m^2}\,\Delta s_k \,\frac{1}{2}\frac{8}{\Delta t_n^2}\left(\sigma_a \phi_{i,n}^{t,SS} - q_{i,n}^{t}\right)\left(t_{k,0} - t_n\right)^2 \\
&= \frac{\varepsilon^2}{v}\sum_{m=1}^{M} w_m \omega_k \sqrt{1+\mu_m^2}\,\Delta s_k \,\frac{1}{2}\frac{8}{\Delta t_n^2}\left(\sigma_a \phi_{i,n}^{t,SS} - q_{i,n}^{t}\right)\left[\begin{array}{l}\left(\dfrac{\Delta t_n}{2}\right)^2 \\ +\left(\dfrac{\Delta t_n}{2} - \delta t\right)^2 \\ +\left(\dfrac{\Delta t_n}{2} - 2\delta t\right)^2 + \ldots\end{array}\right]
\end{aligned} \tag{3.126}$$

Simplifying this expansion into summations and performing these summations yields the result obtained in Eq. (3.127).

$$\begin{aligned}
&\Delta x_i \Delta t_n \left(\sigma_a \phi_{i,n}^{t,(0),SS} - q_{i,n}^{t,(0)}\right)\frac{8}{\Delta t_n^2}\left[\frac{N_1}{2}\left(\frac{\Delta t_n}{2}\right)^2 + \sum_{k=1}^{\frac{N_1}{2}-1} k^2 \delta t^2 - \sum_{k=1}^{\frac{N_1}{2}-1} 2k\,\frac{\Delta t_n}{2}\,\delta t\right] \\
&= \Delta x_i \Delta t_n \left(\sigma_a \phi_{i,n}^{t,(0),SS} - q_{i,n}^{t,(0)}\right)\frac{8}{\Delta t_n^2}\left[\frac{1}{24}\left(N_1 \Delta t_n^2 + 2\Delta t_n \delta t\ \right) + \frac{\Delta t_n^2}{8}\right] \\
&= \Delta x_i \Delta t_n \left(\sigma_a \phi_{i,n}^{t,(0),SS} - q_{i,n}^{t,(0)}\right)\left[\frac{1}{3}\left(N_1 + 3\right) + \frac{2\delta t}{3\Delta t_n}\right] \\
&= \frac{1}{3}\Delta x_i \Delta t_n \left(\sigma_a \phi_{i,n}^{t,(0),SS} - q_{i,n}^{t,(0)}\right)
\end{aligned} \tag{3.127}$$

Therefore it is shown that the O(ε) terms from the source term in Eq. (3.113) yields the following time moment terms.

$$\left\{\frac{\varepsilon^2}{v}\sum_{m=1}^{M} w_m \sum_{k=1}^{\#\text{ in (i,n,m)}} \omega_k \sqrt{1+\mu_m^2} \int_0^{\Delta s_k} ds \frac{2\left(t-t_n\right)}{\Delta t_n}\left(\frac{\sigma_a}{2}\phi_k^{SS}-\frac{1}{2}q_k\right)\right\}^{(1)}$$
$$= \Delta x_i \Delta t_n \frac{1}{3}\left(\sigma_a \phi_{i,n}^{t,(0),SS} - q_{i,n}^{t,(0)}\right) \tag{3.128}$$

Overall, combining the results from Eq. (3.119) and Eq. (3.128), the O(ε) terms from Eq. (3.43) are simplified and given in Eq. (3.129).

$$\frac{1}{v}\Delta x_i\left(\phi_{i,n+1/2}^{(0),SS}+\phi_{i,n-1/2}^{(0),SS}-2\overline{\phi}_{i,n}^{(0),SS}\right)+\Delta t_n\left(J_{i+1/2,n}^{(1),t}-J_{i-1/2,n}^{(1),t}\right)$$
$$+\Delta x_i \Delta t_n \frac{1}{3}\left(\sigma_a \phi_{i,n}^{t,(0),SS} - q_{i,n}^{t,(0)}\right) = 0 \tag{3.129}$$

Finally the important equations determined in the previous derivation can be combined to produce the desired diffusion equation. First the functional form of the scattering source will be substituted into Eqs. (3.100) and (3.112) where needed yielding Eqs. (3.130) and (3.131).

$$\frac{\Delta x_i}{v}\left(\overline{\phi}_{i,n}^{(0),SS}+\phi_{i,n}^{t,(0),SS}-\overline{\phi}_{i,n-1}^{(0),SS}-\phi_{i,n-1}^{t,(0),SS}\right)+\Delta t_n\left(J_{i+1/2,n}^{(1)}-J_{i-1/2,n}^{(1)}\right)$$
$$+\Delta x_i \Delta t_n\left(\sigma_a \overline{\phi}_{i,n}^{(0),SS} - \overline{q}_{i,n}\right) = 0 \tag{3.130}$$

$$\frac{\Delta x_i}{v}\frac{1}{3}\left(\phi_{i,n}^{x,(0),SS}-\phi_{i,n-1}^{x,(0),SS}\right)+\Delta t_n\left(J_{i+1/2,n}^{(1)}+J_{i-1/2,n}^{(1)}-2\overline{J}_{i,n}^{(1)}\right)$$
$$+\Delta x_i \Delta t_n \frac{1}{3}\left(\sigma_a \phi_{i,n}^{x,(0),SS} - q_{i,n}^{x}\right) = 0 \tag{3.131}$$

Next, Eq. (3.130) is added to Eq. (3.131) for cell *i* as shown in Eq. (3.132).

$$\frac{\Delta x_i}{v}\left(\overline{\phi}_{i,n}^{(0),SS}+\phi_{i,n}^{t,(0),SS}+\frac{1}{3}\phi_{i,n}^{x,(0),SS}-\overline{\phi}_{i,n-1}^{(0),SS}-\phi_{i,n-1}^{t,(0),SS}-\frac{1}{3}\phi_{i,n-1}^{x,(0),SS}\right)$$
$$+\Delta t_n 2\left(J_{i+1/2,n}^{(1)}-\overline{J}_{i,n}^{(1)}\right)$$
$$+\Delta x_i \Delta t_n\left(\sigma_a \overline{\phi}_{i,n}^{(0),SS}+\frac{1}{3}\sigma_a\phi_{i,n}^{x,(0),SS}-\overline{q}_{i,n}-\frac{1}{3}q_{i,n}^{x}\right)=0 \tag{3.132}$$

Also, Eq. (3.131) is subtracted from Eq. (3.130) for cell *i+1* as shown in Eq. (3.133).

$$\begin{aligned}&\frac{\Delta x_{i+1}}{v}\left(\overline{\phi}_{i+1,n}^{(0),SS}+\phi_{i+1,n}^{t,(0),SS}-\frac{1}{3}\phi_{i+1,n}^{x,(0),SS}-\overline{\phi}_{i+1,n-1}^{(0),SS}-\phi_{i+1,n-1}^{t,(0),SS}+\frac{1}{3}\phi_{i+1,n-1}^{x,(0),SS}\right)\\&+\Delta t_n\left(2\overline{J}_{i+1,n}^{(1)}-2J_{i+1/2,n}^{(1)}\right)\\&+\Delta x_{i+1}\Delta t_n\left(\sigma_a\overline{\phi}_{i+1,n}^{(0),SS}-\frac{1}{3}\sigma_a\phi_{i+1,n}^{x,(0),SS}-\overline{q}_{i+1,n}+\frac{1}{3}q_{i+1,n}^{x}\right)=0\end{aligned}\tag{3.133}$$

Adding Eq. (3.132) and Eq. (3.133) gives the following equation.

$$\begin{aligned}&\frac{\Delta x_i}{v}\left(\overline{\phi}_{i,n}^{(0),SS}+\phi_{i,n}^{t,(0),SS}+\frac{1}{3}\phi_{i,n}^{x,(0),SS}-\overline{\phi}_{i,n-1}^{(0),SS}-\phi_{i,n-1}^{t,(0),SS}-\frac{1}{3}\phi_{i,n-1}^{x,(0),SS}\right)\\&+\frac{\Delta x_{i+1}}{v}\left(\overline{\phi}_{i+1,n}^{(0),SS}+\phi_{i+1,n}^{t,(0),SS}-\frac{1}{3}\phi_{i+1,n}^{x,(0),SS}-\overline{\phi}_{i+1,n-1}^{(0),SS}-\phi_{i+1,n-1}^{t,(0),SS}+\frac{1}{3}\phi_{i+1,n-1}^{x,(0),SS}\right)\\&+\Delta t_n\left(2\overline{J}_{i+1,n}^{(1)}-2\overline{J}_{i,n}^{(1)}\right)+\Delta x_i\,\Delta t_n\left(\sigma_a\overline{\phi}_{i,n}^{(0),SS}+\frac{1}{3}\sigma_a\phi_{i,n}^{x,(0),SS}-\overline{q}_{i,n}-\frac{1}{3}q_{i,n}^{x}\right)\\&+\Delta x_{i+1}\Delta t_n\left(\sigma_a\overline{\phi}_{i+1,n}^{(0),SS}-\frac{1}{3}\sigma_a\phi_{i+1,n}^{x,(0),SS}-\overline{q}_{i+1,n}+\frac{1}{3}q_{i+1,n}^{x}\right)=0\end{aligned}\tag{3.134}$$

Dividing Eq. (3.134) by two and substituting the known relations gives the relation shown in Eq. (3.135). In this equation the source term has been redefined as given in Eq. (3.136).

$$\begin{aligned}&\frac{\Delta x_i}{2v}\left(\overline{\phi}_{i,n}^{(0),SS}+\phi_{i,n}^{t,(0),SS}+\frac{1}{3}\phi_{i,n}^{x,(0),SS}-\overline{\phi}_{i,n-1}^{(0),SS}-\phi_{i,n-1}^{t,(0),SS}-\frac{1}{3}\phi_{i,n-1}^{x,(0),SS}\right)\\&+\frac{\Delta x_{i+1}}{2v}\left(\overline{\phi}_{i+1,n}^{(0),SS}+\phi_{i+1,n}^{t,(0),SS}-\frac{1}{3}\phi_{i+1,n}^{x,(0),SS}-\overline{\phi}_{i+1,n-1}^{(0),SS}-\phi_{i+1,n-1}^{t,(0),SS}+\frac{1}{3}\phi_{i+1,n-1}^{x,(0),SS}\right)\\&+\Delta t_n\left(\overline{J}_{i+1,n}^{(1)}-\overline{J}_{i,n}^{(1)}\right)+\sigma_a\Delta x_i\,\Delta t_n\left(\frac{1}{3}\phi_{i+1/2,n}+\frac{1}{6}\phi_{i-1/2,n}\right)\\&+\sigma_a\Delta x_{i+1}\Delta t_n\left(\frac{1}{3}\phi_{i+1/2,n}+\frac{1}{6}\phi_{i+3/2,n}\right)=\left(Q\Delta x\Delta t\right)_{i+1/2,n}\end{aligned}\tag{3.135}$$

$$\left(Q\Delta x\Delta t\right)_{i+1/2,n}=\frac{\Delta x_i\,\Delta t_n}{2}\left(\overline{q}_{i,n}+\frac{1}{3}q_{i,n}^{x}\right)+\frac{\Delta x_{i+1}\Delta t_n}{2}\left(\overline{q}_{i+1,n}-\frac{1}{3}q_{i+1,n}^{x}\right)\tag{3.136}$$

Before substituting the relationship for the first-order current, we will further simplify the time terms shown in the first two lines of Eq. (3.135). In order to compare with known discretization methods, it would be advantageous to express all cell-centered values in Eq. (3.135) in terms of cell edge or near-edge values. The time-slope scalar flux terms will not be changed since these are known from Eq. (3.79). Equation (3.137) reiterates some previously found relations and presents other known relations.

$$\begin{aligned}\overline{\phi}_{i,n}^{(0)} &= \frac{1}{2}\left(\phi_{i+1/2,n} + \phi_{i-1/2,n}\right) \\ \phi_{i,n}^{x,(0)} &= \frac{1}{2}\left(\phi_{i+1/2,n} - \phi_{i-1/2,n}\right) \\ \phi_{i,n+1/2}^{(0)} &= \overline{\phi}_{i,n}^{(0)} + \phi_{i,n}^{t,(0)}\end{aligned} \tag{3.137}$$

Applying these relations to several of the terms in Eq. (3.135) gives the simplification shown in Eq. (3.138) and Eq. (3.139).

$$\begin{aligned}&\frac{\Delta x_i}{2v}\left(\overline{\phi}_{i,n}^{(0),SS} + \phi_{i,n}^{t,(0),SS} + \frac{1}{3}\phi_{i,n}^{x,(0),SS}\right) \\ &= \frac{\Delta x_i}{2v}\left(\frac{2}{3}\phi_{i+1/2,n} + \frac{1}{3}\phi_{i-1/2,n} + \phi_{i,n}^{t,(0),SS}\right)\end{aligned} \tag{3.138}$$

$$\begin{aligned}&\frac{\Delta x_{i+1}}{2v}\left(\overline{\phi}_{i+1,n}^{(0),SS} + \phi_{i+1,n}^{t,(0),SS} - \frac{1}{3}\phi_{i+1,n}^{x,(0),SS}\right) \\ &= \frac{\Delta x_{i+1}}{2v}\left(\frac{1}{3}\phi_{i+3/2,n} + \frac{2}{3}\phi_{i+1/2,n} + \phi_{i+1,n}^{t,(0),SS}\right)\end{aligned} \tag{3.139}$$

Finally, substituting Eq. (3.138) and Eq. (3.139) into Eq. (3.135) along with similar relations for the previous time step values yields the diffusion equation for each cell in the problem shown in Eq. (3.140).

$$\begin{aligned}
&\frac{\Delta x_i}{2v}\left(\frac{2}{3}\phi_{i+1/2,n}+\frac{1}{3}\phi_{i-1/2,n}+\phi^t_{i,n}-\frac{2}{3}\phi_{i+1/2,n-1}-\frac{1}{3}\phi_{i-1/2,n-1}-\phi^t_{i,n-1}\right)\\
&+\frac{\Delta x_{i+1}}{2v}\left(\frac{1}{3}\phi_{i+3/2,n}+\frac{2}{3}\phi_{i+1/2,n}+\phi^t_{i+1,n}-\frac{1}{3}\phi_{i+3/2,n-1}-\frac{2}{3}\phi_{i+1/2,n-1}-\phi^t_{i+1,n-1}\right)\\
&+\Delta t_n\left(\overline{J}^{(1)}_{i+1,n}-\overline{J}^{(1)}_{i,n}\right)+\sigma_a\Delta x_i\,\Delta t_n\left(\frac{1}{3}\phi_{i+1/2,n}+\frac{1}{6}\phi_{i-1/2,n}\right)\\
&+\sigma_a\Delta x_{i+1}\Delta t_n\left(\frac{1}{3}\phi_{i+1/2,n}+\frac{1}{6}\phi_{i+3/2,n}\right)=\left(Q\Delta x\Delta t\right)_{i+1/2,n}
\end{aligned} \tag{3.140}$$

The relationship found for the first order current in Eq. (3.70) is now substituted into Eq. (3.140) along with the other known boundary terms. For the left boundary, this substitution leads to the following equation.

$$\begin{aligned}
&\frac{\Delta x_1}{2v}\left(\frac{2}{3}\phi_{3/2,n}+\frac{1}{3}\sum_{\mu_m>0}w_m\left(\frac{4|\mu_m|}{\rho}\right)\psi_{m,n,inc}+\phi^t_{1,n}-\frac{2}{3}\phi_{3/2,n-1}-\frac{1}{3}\sum_{\mu_m>0}w_m\left(\frac{4|\mu_m|}{\rho}\right)\psi_{m,n-1,inc}-\phi^t_{1,n-1}\right)\\
&+\frac{\Delta x_2}{2v}\left(\frac{1}{3}\phi_{5/2,n}+\frac{2}{3}\phi_{3/2,n}+\phi^t_{2,n}-\frac{1}{3}\phi_{5/2,n-1}-\frac{2}{3}\phi_{3/2,n-1}-\phi^t_{2,n-1}\right)\\
&+\Delta t_n\left(-\frac{1}{3\sigma_t\Delta x_2}\left(\phi_{5/2,n}-\phi_{3/2,n}\right)+\frac{1}{3\sigma_t\Delta x_1}\left(\phi_{3/2,n}-\sum_{\mu_m>0}w_m\left(3\mu_m^2+\frac{2|\mu_m|}{\rho}\right)\psi_{m,n,inc}\right)\right)\\
&+\sigma_a\Delta x_1\,\Delta t_n\left(\frac{1}{3}\phi_{3/2,n}+\frac{1}{6}\sum_{\mu_m>0}w_m\left(\frac{4|\mu_m|}{\rho}\right)\psi_{m,n,inc}\right)\\
&+\sigma_a\Delta x_2\Delta t_n\left(\frac{1}{3}\phi_{3/2,n}+\frac{1}{6}\phi_{5/2,n}\right)=\left(Q\Delta x\Delta t\right)_{3/2,n}
\end{aligned} \tag{3.141}$$

To make this previous equation look more like a spatially discretized FEM diffusion equation, a scalar flux quantity can be defined for the left boundary to satisfy the definition in Eq. (3.142), where the Marshak boundary condition for the previous time step has been replaced with its scalar flux representation.

$$
\begin{aligned}
&\frac{\Delta x_1}{2v}\frac{1}{3}\sum_{\mu_m>0} w_m\left(\frac{4|\mu_m|}{\rho}\right)\psi_{m,n,inc} - \frac{\Delta x_1}{2v}\frac{1}{3}\phi_{1/2,n-1} \\
&-\frac{\Delta t_n}{3\sigma_t\Delta x_1}\sum_{\mu_m>0} w_m\left(3\mu_m^2+\frac{2|\mu_m|}{\rho}\right)\psi_{m,n,inc} + \sigma_a\Delta x_1\Delta t_n\frac{1}{6}\sum_{\mu_m>0} w_m\left(\frac{4|\mu_m|}{\rho}\right)\psi_{m,n,inc} \\
&\equiv \frac{\Delta x_1}{2v}\frac{1}{3}\Phi_{1/2,n} - \frac{\Delta x_1}{2v}\frac{1}{3}\Phi_{1/2,n-1} - \frac{\Delta t_n}{3\sigma_t\Delta x_1}\Phi_{1/2,n} + \sigma_a\Delta x_1\Delta t_n\frac{1}{6}\Phi_{1/2,n} \\
&\Rightarrow \Phi_{1/2,n} = \frac{\displaystyle\sum_{\mu_m>0} w_m\left[3\mu_m^2+\frac{2|\mu_m|}{\rho}\left(1-\sigma_t\Delta x_1^2\left(\sigma_a+\frac{1}{v\Delta t_n}\right)\right)\right]\psi_{m,n,inc} + \frac{\sigma_t\Delta x_1^2}{2v\Delta t_n}\left(\phi_{1/2,n-1}-\Phi_{1/2,n-1}\right)}{\left(1-\dfrac{\sigma_t\Delta x_1^2}{2}\left(\sigma_a+\dfrac{1}{v\Delta t_n}\right)\right)}
\end{aligned}
\tag{3.142}
$$

With this scalar flux quantity substituted into Eq. (3.141), the following diffusion equation for the left cell is produced as given in Eq. (3.143).

$$
\begin{aligned}
&\frac{\Delta x_1}{2v}\left(\frac{2}{3}\phi_{3/2,n}+\frac{1}{3}\Phi_{1/2,n}+\phi^t_{1,n}-\frac{2}{3}\phi_{3/2,n-1}-\frac{1}{3}\Phi_{1/2,n-1}-\phi^t_{1,n-1}\right) \\
&+\frac{\Delta x_2}{2v}\left(\frac{1}{3}\phi_{5/2,n}+\frac{2}{3}\phi_{3/2,n}+\phi^t_{2,n}-\frac{1}{3}\phi_{5/2,n-1}-\frac{2}{3}\phi_{3/2,n-1}-\phi^t_{2,n-1}\right) \\
&-\frac{\Delta t_n\left(\phi_{5/2,n}-\phi_{3/2,n}\right)}{3\sigma_t\Delta x_2}+\frac{\Delta t_n\left(\phi_{3/2,n}-\Phi_{1/2,n}\right)}{3\sigma_t\Delta x_1}+\sigma_a\Delta x_1\Delta t_n\left(\frac{1}{3}\phi_{3/2,n}+\frac{1}{6}\Phi_{1/2,n}\right) \\
&+\sigma_a\Delta x_2\Delta t_n\left(\frac{1}{3}\phi_{3/2,n}+\frac{1}{6}\phi_{5/2,n}\right)=\left(Q\Delta x\Delta t\right)_{3/2,n}
\end{aligned}
\tag{3.143}
$$

The scalar flux quantity in Eq. (3.142) can be defined for all cells as shown in Eq. (3.144) where we note that this scalar flux quantity is defined recursively and can be expressed explicitly in terms of the initial conditions. Also, note the similarity to the corresponding steady-state LC flux definition found in Eq. (3.30).

$$\Phi_{i+1/2,n}=\begin{cases}\dfrac{\sum\limits_{\mu_m>0} w_m\left[3\mu_m^2+\dfrac{2|\mu_m|}{\rho}\left(1-\sigma_t\Delta x_1^2\left(\sigma_a+\dfrac{1}{v\Delta t_n}\right)\right)\right]\psi_{m,n,inc}+\dfrac{\sigma_t\Delta x_1^2}{2v\Delta t_n}\left(\phi_{1/2,n-1}-\Phi_{1/2,n-1}\right)}{\left(1-\dfrac{\sigma_t\Delta x_1^2}{2}\left(\sigma_a+\dfrac{1}{v\Delta t_n}\right)\right)} & i=0,\\ \phi_{i+1/2,n}+\dfrac{\dfrac{\sigma_t\Delta x_i^2}{2v\Delta t_n}\left(\phi_{i+1/2,n-1}-\Phi_{i+1/2,n-1}\right)}{1-\dfrac{\sigma_t\Delta x_i^2}{2}\left(\sigma_a+\dfrac{1}{v\Delta t_n}\right)} & i=1,\ldots,I-1,\\ \dfrac{\sum\limits_{\mu_m<0} w_m\left[3\mu_m^2+\dfrac{2|\mu_m|}{\rho}\left(1-\sigma_t\Delta x_I^2\left(\sigma_a+\dfrac{1}{v\Delta t_n}\right)\right)\right]\psi_{m,n,inc}+\dfrac{\sigma_t\Delta x_I^2}{2v\Delta t_n}\left(\phi_{I+1/2,n-1}-\Phi_{I+1/2,n-1}\right)}{\left(1-\dfrac{\sigma_t\Delta x_I^2}{2}\left(\sigma_a+\dfrac{1}{v\Delta t_n}\right)\right)} & i=I\end{cases} \tag{3.144}$$

Finally, similar to Eq. (3.143), a diffusion equation for all cells, $i=1,\ldots I-1$, is defined as given in Eq. (3.145).

$$\begin{aligned}&\frac{\Delta x_i}{2v}\left(\frac{2}{3}\Phi_{i+1/2,n}+\frac{1}{3}\Phi_{i-1/2,n}+\phi_{i,n}^t-\frac{2}{3}\Phi_{i+1/2,n-1}-\frac{1}{3}\Phi_{i-1/2,n-1}-\phi_{i,n-1}^t\right)\\&+\frac{\Delta x_{i+1}}{2v}\left(\frac{1}{3}\Phi_{i+3/2,n}+\frac{2}{3}\Phi_{i+1/2,n}+\phi_{i+1,n}^t-\frac{1}{3}\Phi_{i+3/2,n-1}-\frac{2}{3}\Phi_{i+1/2,n-1}-\phi_{i+1,n-1}^t\right)\\&-\frac{\Delta t_n\left(\Phi_{i+3/2,n}-\Phi_{i+1/2,n}\right)}{3\sigma_t\Delta x_{i+1}}+\frac{\Delta t_n\left(\Phi_{i+1/2,n}-\Phi_{i-1/2,n}\right)}{3\sigma_t\Delta x_i}+\sigma_a\Delta x_i\,\Delta t_n\left(\frac{1}{3}\Phi_{i+1/2,n}+\frac{1}{6}\Phi_{i-1/2,n}\right)\\&+\sigma_a\Delta x_{i+1}\Delta t_n\left(\frac{1}{3}\Phi_{i+1/2,n}+\frac{1}{6}\Phi_{i+3/2,n}\right)=\left(Q\Delta x\Delta t\right)_{i+1/2,n}\end{aligned} \tag{3.145}$$

This set of diffusion equations, along with the determined relation about the time moment of the scalar fluxes from Eq. (3.79) form a complete set. Overall it has been shown that this STLC method produces a diffusion equation in the asymptotic limit that is accurate to first order. The "flaw" in the leading-order time-slope does not allow for this method to be accurate to second order in the thick diffusion limit. In the following section it will be noted how this diffusion limit result relates to a FEM in space and an implicit method in time.

3.5 Comparison with Analytic Limit and Steady-State Limit

If the STLC method is to be accurate in thick diffusive problems, its leading-order solution should satisfy a discretized version of the analytic diffusion-limit equation. The analytic diffusion limit for a time-dependent 1D slab problem is given in Eq. (3.146).

$$\frac{1}{v}\frac{\partial\phi^{(0)}(x,\mu,t)}{\partial t}-\frac{\partial}{\partial x}\left(\frac{1}{3\sigma_t}\frac{\partial\phi^{(0)}(x,t)}{\partial x}\right)+\sigma_a\phi^{(0)}(x,t)-q(x,t)=0 \tag{3.146}$$

Dividing Eq. (3.145) by the time step leads to Eq. (3.147). The discretized spatial derivative is clearly shown on the second line of this equation with the discretized collision term shown on the third and fourth lines. The discretized source term is also shown on the fourth line of Eq. (3.147). The discretized time derivative is not as clear to distinguish. Combining the first and last lines of Eq. (3.147) yields an implicit time discretization of the time derivative term with the addition of several time-slope terms. If these time-slopes were not present, this equation would show a fully implicit time differencing where the scalar flux at the midpoint of the time step is the same as the end of the time step.

$$\begin{aligned}
&\frac{\Delta x_i}{2v\Delta t_n}\left(\frac{2}{3}\Phi_{i+1/2,n}+\frac{1}{3}\Phi_{i-1/2,n}+\phi^t_{i,n}\right)+\frac{\Delta x_{i+1}}{2v\Delta t_n}\left(\frac{1}{3}\Phi_{i+3/2,n}+\frac{2}{3}\Phi_{i+1/2,n}+\phi^t_{i+1,n}\right)\\
&-\frac{\left(\Phi_{i+3/2,n}-\Phi_{i+1/2,n}\right)}{3\sigma_t\Delta x_{i+1}}+\frac{\left(\Phi_{i+1/2,n}-\Phi_{i-1/2,n}\right)}{3\sigma_t\Delta x_i}\\
&+\sigma_a\Delta x_i\left(\frac{1}{3}\Phi_{i+1/2,n}+\frac{1}{6}\Phi_{i-1/2,n}\right)\\
&+\sigma_a\Delta x_{i+1}\left(\frac{1}{3}\Phi_{i+1/2,n}+\frac{1}{6}\Phi_{i+3/2,n}\right)=\left(Q\Delta x\Delta t\right)_{i+1/2,n}\\
&+\frac{\Delta x_i}{2v\Delta t_n}\left(\frac{2}{3}\Phi_{i+1/2,n-1}+\frac{1}{3}\Phi_{i-1/2,n-1}+\phi^t_{i,n-1}\right)+\frac{\Delta x_{i+1}}{2v\Delta t_n}\left(\frac{1}{3}\Phi_{i+3/2,n-1}+\frac{2}{3}\Phi_{i+1/2,n-1}+\phi^t_{i+1,n-1}\right)
\end{aligned} \tag{3.147}$$

It is expected that this STLC method should produce a discretized diffusion equation in space that is the same as FEM with a linear basis [13]. Comparing Eq. (3.145) to this linear FEM discretized time-independent diffusion equation on a 1D slab, the spatial terms have the same discretization. Also, considering Eq. (3.145), if the time-slope is zero, a discretized diffusion equation is produced that is the same as LFEM with fully implicit time discretization. Equation (3.148) rearranges Eq. (3.145) and drops the time-slope terms. This equation clearly shows the relationship between the STLC diffusion limit and the aforementioned standard discretization.

$$\begin{aligned}
&\frac{\Delta x_i}{2v}\left(\frac{2}{3}\left(\Phi_{i+1/2,n}-\Phi_{i+1/2,n-1}\right)+\frac{1}{3}\left(\Phi_{i-1/2,n}-\Phi_{i-1/2,n-1}\right)\right)\\
&+\frac{\Delta x_{i+1}}{2v}\left(\frac{1}{3}\left(\Phi_{i+3/2,n}-\Phi_{i+3/2,n-1}\right)+\frac{2}{3}\left(\Phi_{i+1/2,n}-\Phi_{i+1/2,n-1}\right)\right)\\
&-\frac{\Delta t_n\left(\Phi_{i+3/2,n}-\Phi_{i+1/2,n}\right)}{3\sigma_t\Delta x_{i+1}}+\frac{\Delta t_n\left(\Phi_{i+1/2,n}-\Phi_{i-1/2,n}\right)}{3\sigma_t\Delta x_i}\\
&+\sigma_a\Delta x_i\,\Delta t_n\left(\frac{1}{3}\Phi_{i+1/2,n}+\frac{1}{6}\Phi_{i-1/2,n}\right)\\
&+\sigma_a\Delta x_{i+1}\Delta t_n\left(\frac{1}{3}\Phi_{i+1/2,n}+\frac{1}{6}\Phi_{i+3/2,n}\right)=\left(Q\Delta x\Delta t\right)_{i+1/2,n}
\end{aligned} \tag{3.148}$$

The effect of including the time-slope term in the discretized equation will be shown through several test problems further in this paper. Although the unphysical representation of this time-slope still yields a desirable solution for most problems, it can reduce the accuracy of solutions for certain problems. In the final section we discuss the ramifications of this result and the possible ways to address them.

This time-dependent diffusion equation should collapse to the steady-state diffusion limit found in Section 3.3 if the problem is steady. Equation (3.149) shows the division of Eq. (3.145) by the time step and the limit as the time step becomes large.

Performing this limit collapses the equation to steady-state and yields the result given in Eq. (3.150).

$$\lim_{\Delta t_n \to \infty} \left[\begin{array}{l} \frac{\Delta x_i}{2v\Delta t_n}\left(\frac{2}{3}\Phi_{i+1/2,n}+\frac{1}{3}\Phi_{i-1/2,n}+\phi^t_{i,n}\right) \\ +\frac{\Delta x_{i+1}}{2v\Delta t_n}\left(\frac{1}{3}\Phi_{i+3/2,n}+\frac{2}{3}\Phi_{i+1/2,n}+\phi^t_{i+1,n}\right) \\ -\frac{\left(\Phi_{i+3/2,n}-\Phi_{i+1/2,n}\right)}{3\sigma_t\Delta x_{i+1}}+\frac{\left(\Phi_{i+1/2,n}-\Phi_{i-1/2,n}\right)}{3\sigma_t\Delta x_i}+\sigma_a\Delta x_i\left(\frac{1}{3}\Phi_{i+1/2,n}+\frac{1}{6}\Phi_{i-1/2,n}\right) \\ +\sigma_a\Delta x_{i+1}\left(\frac{1}{3}\Phi_{i+1/2,n}+\frac{1}{6}\Phi_{i+3/2,n}\right)=\left(Q\Delta x\Delta t\right)_{i+1/2,n} \\ +\frac{\Delta x_i}{2v\Delta t_n}\left(\frac{2}{3}\Phi_{i+1/2,n-1}+\frac{1}{3}\Phi_{i-1/2,n-1}+\phi^t_{i,n-1}\right)+\frac{\Delta x_{i+1}}{2v\Delta t_n}\left(\frac{1}{3}\Phi_{i+3/2,n-1}+\frac{2}{3}\Phi_{i+1/2,n-1}+\phi^t_{i+1,n-1}\right) \end{array} \right] \tag{3.149}$$

$$\begin{array}{l} -\frac{\left(\Phi_{i+3/2}-\Phi_{i+1/2}\right)}{3\sigma_t\Delta x_{i+1}}+\frac{\left(\Phi_{i+1/2}-\Phi_{i-1/2}\right)}{3\sigma_t\Delta x_i}+\sigma_a\Delta x_i\left(\frac{1}{3}\Phi_{i+1/2}+\frac{1}{6}\Phi_{i-1/2}\right) \\ +\sigma_a\Delta x_{i+1}\left(\frac{1}{3}\Phi_{i+1/2}+\frac{1}{6}\Phi_{i+3/2}\right)=\left(Q\Delta x\right)_{i+1/2} \end{array} \tag{3.150}$$

The collapsed time-dependent diffusion equation shown in Eq. (3.150) is the same as the steady-state diffusion limit found in Eq. (3.32) as expected for this STLC method.

In summary, the previous section has shown an analysis of the STLC method for several problem models. From these analyses, it is expected that the STLC method will find the exact solution for a problem that has a linear solution and find "conservative" solutions for most transport problems. This STLC method should also find a solution accurate to first-order for problems that are "thick" and highly scattering similar to a continuous linear FEM discretization in space with time differencing. The result that the leading-order time-slope of the solution is not dependent on physical properties of the problem means that this method may not be as accurate for certain problems in the thick diffusion limit.

4. RESULTS

In order to show the properties of the new STLC method several different test problems were run. The results from the STLC code were compared to analytical solutions and to an LD method with two different FD discretizations for the time variable. All of these test problems are time-dependent, slab-geometry problems, which have one spatial variable and one temporal variable.

4.1 Test Problem 1: Linear in Space and Time

This test problem consists of a multi-cell rectangular grid of a total width X = 5 cm and a cell width of $\Delta x_i = 0.5$ cm. The method of manufactured solutions was used to produce the desired solution that is linear in x, μ, and t as shown in Eq. (4.1). Therefore the initial and incident angular flux values as well as the fixed source were set accordingly. The scattering ratio for this problem is taken to be $\sigma_s / \sigma_t = 0.9$ with non-varying cross sections. A uniform time step of $\Delta t_n = 0.5$ s was used up to a maximum time of T = 5 s. The track width defined by $\Delta\omega_k$ was varied in order to determine the sensitivity of the STLC solution to the track width.

$$\psi(x,\mu,t) = C_0 + C_1 t + C_2\left(x - \frac{\mu}{\sigma_t}\right) \tag{4.1}$$

The following results show how STLC can capture the linear solution of this problem. These results were generated with a four point Gauss-Legendre quadrature set, but almost any quadrature set would produce the same result. The non-TWC least-squares scalar flux for this problem is shown in Fig. 4 where it can be seen that this solution approaches the analytic linear solution within the iterative convergence

tolerance. All of the following figures show a linear function plotted in each cell that is independent of other cells. As expected, the resulting solution is independent of track width, on the condition that at least two tracks cross each space-time cell.

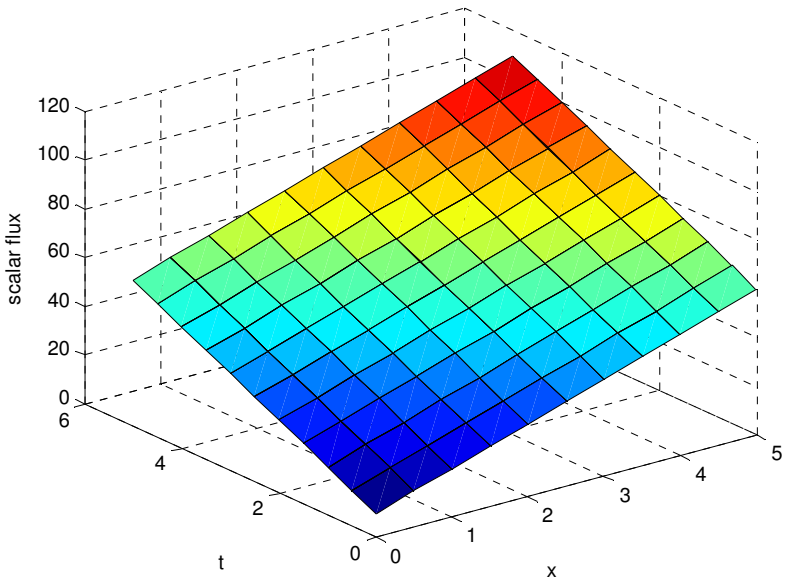

Figure 4: Non-TWC Scalar Flux- TP #1

Figures 5 and 6 show the TWC scalar flux values for this test problem with coarse track spacing, $\Delta\omega_k = 0.5$ cm, and fine track spacing of $\Delta\omega_k = 0.05$ cm. These TWC flux values can be used in reaction-rate calculations as well as in comparison with the least-squares flux values. As expected, these TWC flux values are not the exact linear solution and show a lack of smoothness. Despite the very coarse track spacing the overall shape and magnitude of the flux is correct even though the gradient within many cells is relatively far from the gradient of the analytic solution as shown in Fig. 5. The

global correctness is because exiting fluxes from each cell do not know anything about the un-smooth TWC scalar fluxes, but instead employ a scattering source that uses the (smooth) non-TWC least-squares scalar fluxes. As seen in Fig. 6, as the track spacing is refined, the TWC flux solution approaches the smooth analytic solution as expected.

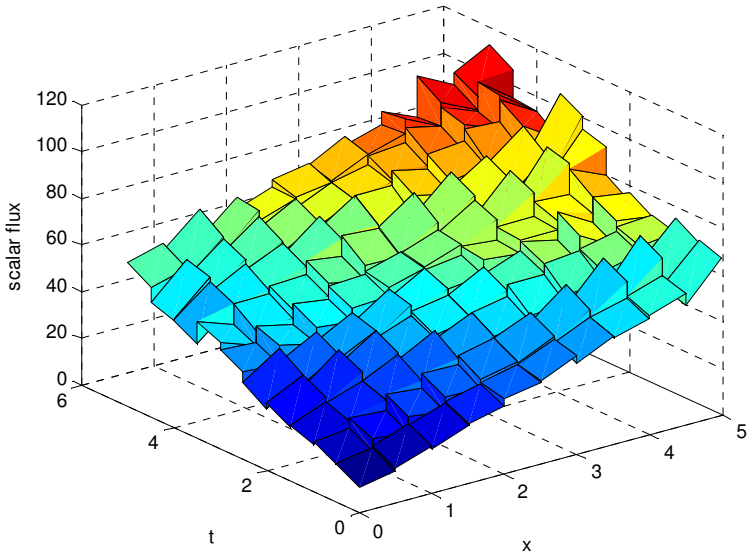

Figure 5: TWC Scalar Flux with Coarse Track Spacing ($\Delta\omega_k$ = 0.5 cm)

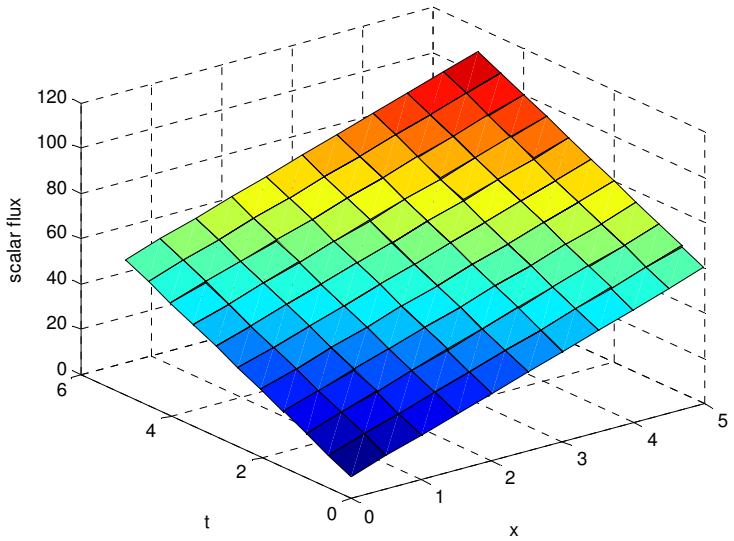

Figure 6: TWC Scalar Flux with Fine Track Spacing ($\Delta\omega_k$ = 0.05 cm)

4.2 Test Problem 2: Streaming from an Incident Beam

The following test problem demonstrates properties of the STLC method when applied to a streaming problem. The two methods used for comparison with the STLC method use a LD discretization for the spatial variable with one using implicit Euler in time and the other using Crank-Nicholson. This problem consists of a multi-cell rectangular grid of uniform spatial cell width and a uniform time step up to a maximum time of T = 1 s. An S_4 quadrature set was used for both the STLC method and the LD methods. Also, the track width defined by $\Delta\omega_k$ was varied for the STLC method to determine its effect on the solution. The source of particles was from an incident beam on the left side of the slab; the initial and boundary conditions are given in Eq. (4.2).

$$\begin{aligned} &\psi_{inc}^{m} = \psi_0, \quad \mu_m > 0, \\ &\psi_{inc}^{m} = 0, \quad \mu_m < 0, \\ &\psi(x,0) = 0, \quad x \in (0,L) \end{aligned} \tag{4.2}$$

Based upon these boundary conditions, this problem can be viewed as the superposition of two beam problems, one for each positive value of μ. The scattering ratio for this problem is $\sigma_s/\sigma_t = 0.2$ with the value of the total cross section being very small, σ_t = 1E-4. Therefore, the domain can be thought of as approximately vacuum. Also it should be noted that at least two tracks per cell were needed for this problem in order for both the TWC and non-TWC methods to build the linear functions of x and t with sufficient information.

The solution of this problem is expected to be zero in part of the space-time domain, a constant in the part of the domain reached by the beam in the direction of the largest μ, and a larger constant in the rest of the domain (where both beams have

reached). Figure 7 shows the STLC solution for the TWC and non-TWC least-square scalar flux methods for this problem with a cell width of $\Delta x = 0.05$ cm, a time step of $\Delta t = 0.1$ s, and a track spacing of $\Delta\omega_k = 0.01$ cm. Figure 8 shows the same STLC solution but with only the average scalar flux value in each cell plotted without the spatial and time gradients as shown in Fig. 7. Figure 9 shows the LD scalar flux solutions using the implicit Euler and Crank-Nicholson methods. From Figs. 7 and 8 it can be seen that the STLC method clearly defines the expected regions of constant solution for both the TWC and non-TWC methods. This STLC method produces a smooth solution for this problem except in the cells that contain discontinuities in the analytic solution. In these cells, the linear fit naturally exhibits some under- and over-shoot. However, this does not affect the solution in other cells because scattering is negligible. Also, notice that this STLC method does not suffer the effects of smearing in time that is associated with the fully implicit solution shown in Fig. 9(a), nor the oscillations that occur in the Crank-Nicholson solution shown in Fig. 9(b).

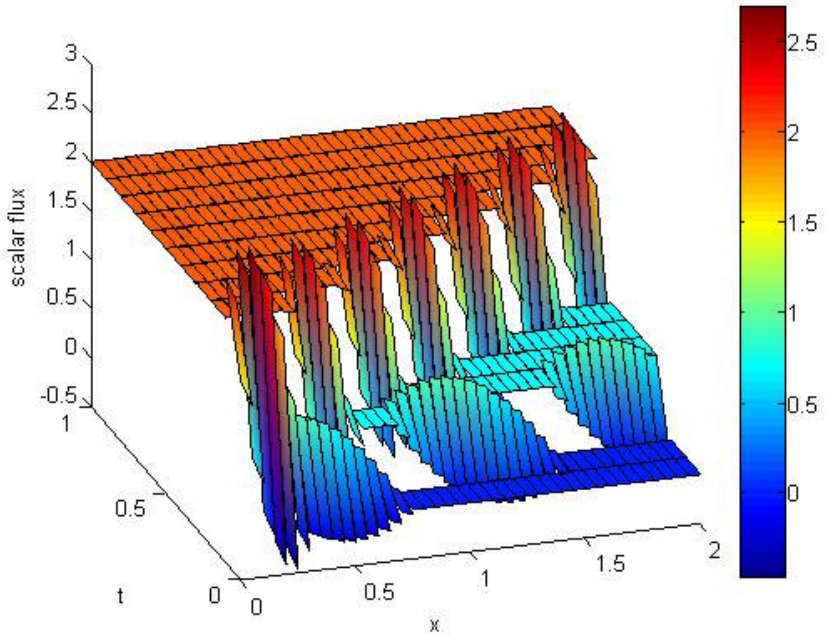

(a)

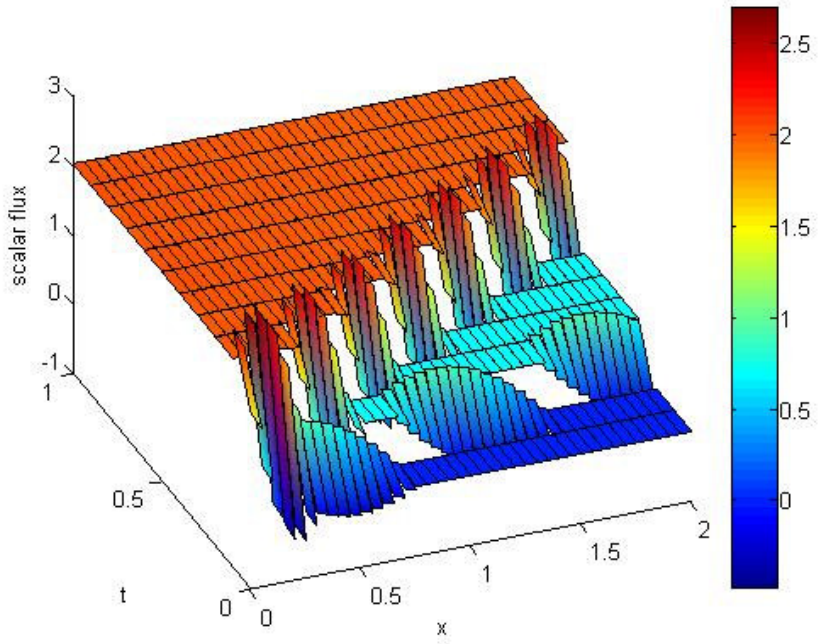

(b)

Figure 7: (a) STLC TWC Scalar Flux –TP #2; (b) STLC Non-TWC Scalar Flux – TP #2

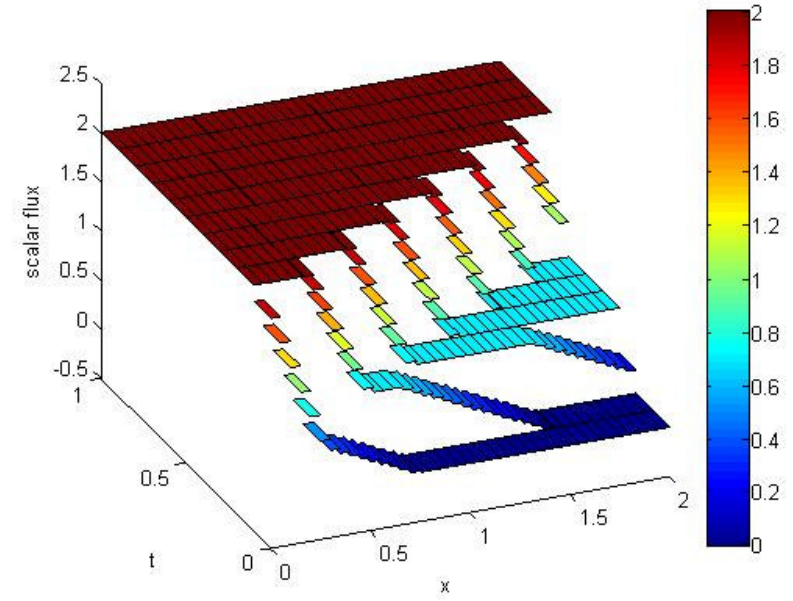

(a)

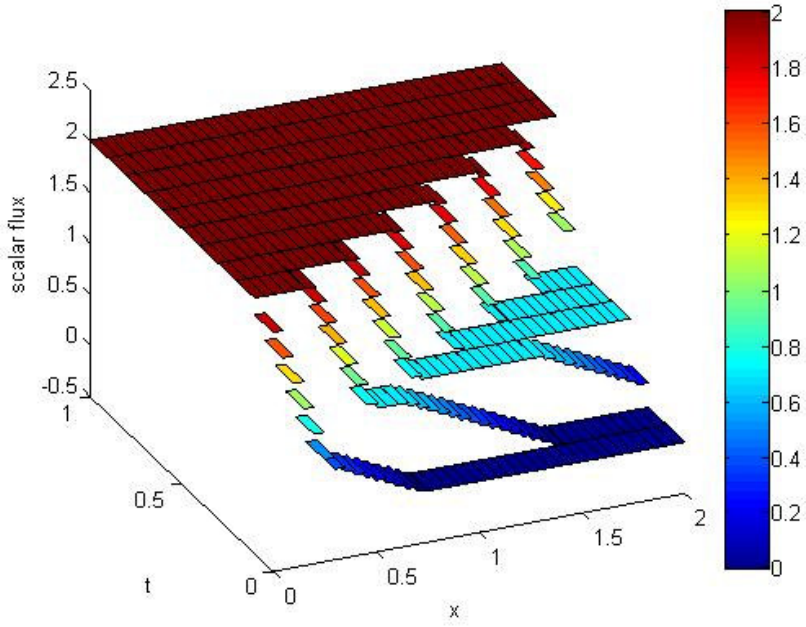

(b)

Figure 8: (a) STLC TWC Average Scalar Flux –TP #2; (b) STLC Non-TWC Average Scalar Flux –TP #2

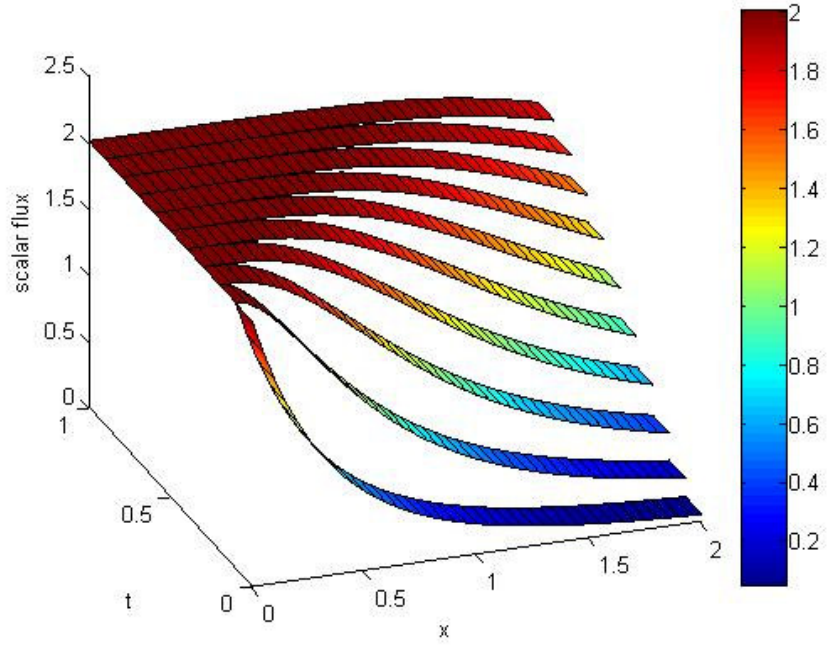

(a)

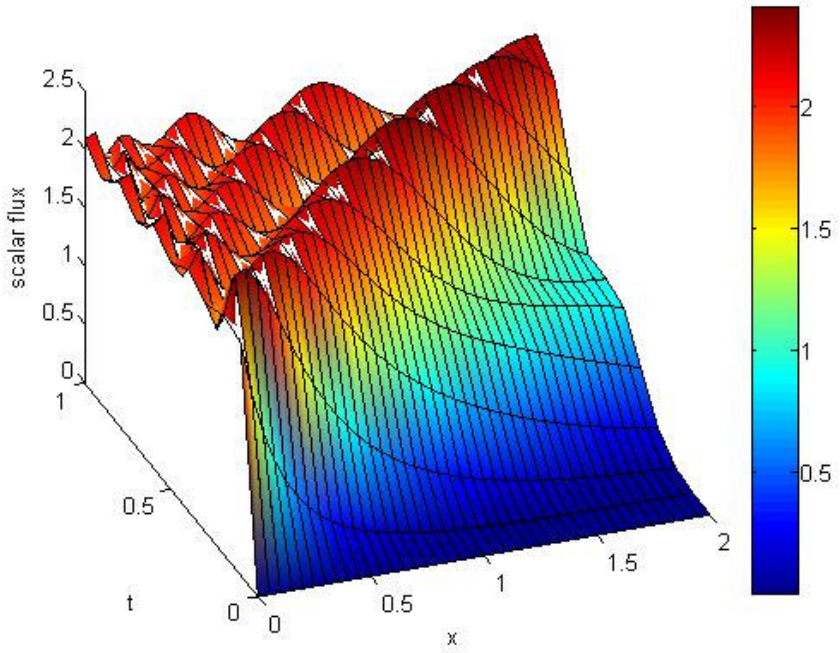

(b)

Figure 9: (a) Fully Implicit Scalar Flux Solution – TP #2; (b) Crank Nicholson Scalar Flux Solution – TP #2

4.3 Test Problem 3: Diffusion from a Surface Source

This test problem is designed to determine how the STLC method handles a diffusion problem as compared to LD in space and FD methods in time. The LD methods used previously, with implicit Euler and Crank-Nicholson, were again used for comparison. Figure 10 shows the geometry of the problem, which consists of a multi-cell rectangular grid with a total width of X = 10.1 cm and a constant isotropic source in the center of the material. The properties of the material and source are given in Eq. (4.3).

$$
\begin{aligned}
&\frac{\sigma_s}{\sigma_t} = 1.0 \\
&\psi^m_{inc} = 0, \quad \mu_m > 0, \\
&\psi^m_{inc} = 0, \quad \mu_m < 0, \\
&\psi(x,0) = 0, \quad x \in (0, L) \\
&\text{Source Region:} \\
&q(x,\mu_m) = C, \qquad x \in (5, 5.1)\, cm, \quad m = 1, ..., M \\
&\frac{\sigma_s}{\sigma_t} = 1.0 \\
&\Delta x_{source} = 1\ mm
\end{aligned}
\tag{4.3}
$$

The time step and cell width in the problem, excluding the small source region, were uniform up to a maximum time of T = 2 s.

The analytic solution of the diffusion equation for this problem can be found easily if we ignore boundaries. The diffusion equation representing this problem is given in Eq. (4.4).

$$
\begin{aligned}
&\frac{1}{v}\frac{\partial \phi}{\partial t} - D\frac{\partial^2 \phi}{\partial x^2} = 0 \qquad x, t \neq 0 \\
&\phi(x,0) = 0, \qquad x \neq 0
\end{aligned}
\tag{4.4}
$$

The general solution to this problem is given in Eq. (4.5).

$$\phi(x,t) = C\frac{\exp\left(-\frac{x^2}{4vDt}\right)}{\sqrt{t}} \tag{4.5}$$

To find the particular solution we apply the source condition as given in Eq. (4.6). In this source condition the thin source region has been approximated as a delta function plane source.

$$S(x,t) = \begin{cases} S_0\delta(x), & t > 0 \\ 0, & t \le 0 \end{cases} \tag{4.6}$$

This δ-function source produces a discontinuity in the spatial derivative, $d\phi / dx$, which can be used as a "boundary" condition to find the constant C. Performing the integration shown in Eq. (4.7), the full analytic diffusion solution is given in terms of the complementary error function as given in Eq. (4.8) with the correct proportionality constant.

$$\phi(x,t) = S_0 C\int_0^t dt' \frac{e^{-\frac{x^2}{4vD(t-t')}}}{\sqrt{t-t'}}, \qquad t > 0, \quad x \neq 0 \tag{4.7}$$

$$\phi(x,t) = S_0\sqrt{\frac{v}{4\pi D}}\left[2\sqrt{t}e^{-\frac{x^2}{4vDt}} - x\sqrt{\frac{\pi}{vD}}\operatorname{Erfc}\left(\sqrt{\frac{x^2}{4vDt}}\right)\right], \qquad t > 0, \quad x \neq 0 \tag{4.8}$$

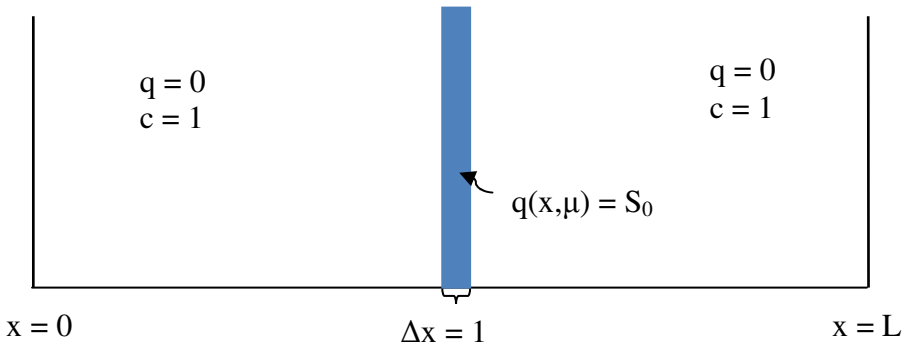

Figure 10: Geometry of TP #3: Diffusion

The analytic diffusion scalar flux solution is shown in Fig. 11. If the associated transport problem is solved with an S_2 quadrature, the results should be very similar to the diffusion solution. There should be a small difference, because although the S_2 solution is equivalent to the P_1 solution, the P_1 solution differs from the diffusion solution because it does not ignore the time derivative of the net current density like diffusion does.

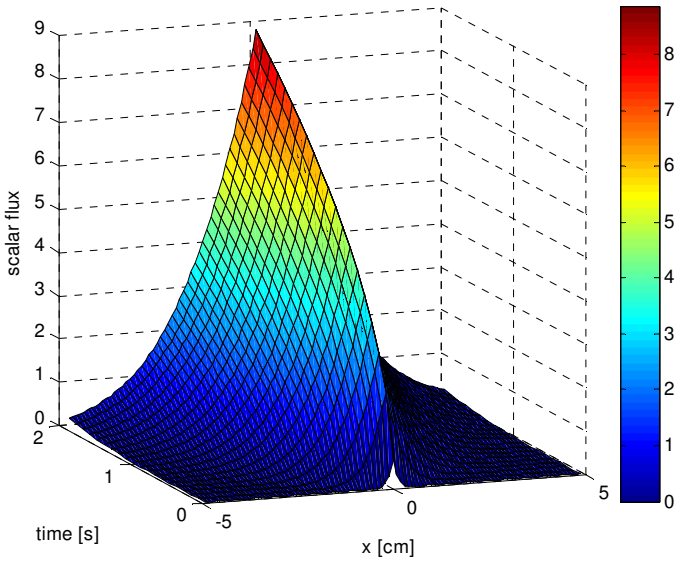

Figure 11: Analytic Scalar Flux for TP #3

Figure 12 shows the TWC and non-TWC least-square scalar flux solutions from the STLC code using a cell width of $\Delta x = 0.25$ cm, a time step of $\Delta t = 0.1$ s, and a track width of $\Delta\omega_k = 0.01$ cm. Figure 13 shows the scalar flux solutions from the LD methods using implicit Euler and Crank-Nicholson with the same cell width and time step. Comparing these figures to the analytical solution that is shown in Fig. 11, the STLC and LD codes both produce the correct flux shape using these relatively fine spatial and temporal grids. However, the STLC method seems to not over-diffuse the solution as much as the FD methods. It should be noted that for early time values, when the spatial gradient of the solution near the source is high, the spatial grid used cannot resolve these gradients and therefore the linear STLC functions dip negative in the cells adjacent to this centered source, as evident in Fig. 12. Overall, the main result from this test problem is that the STLC method is accurate for this kind of diffusive problem.

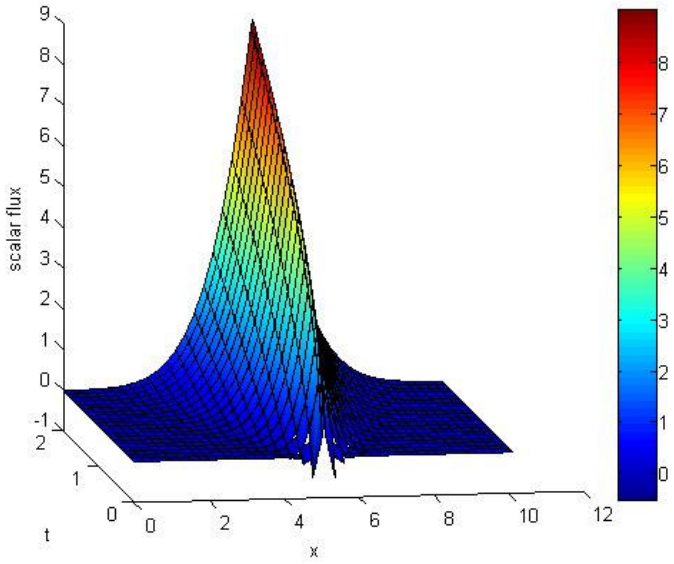

(a)

Figure 12: (a) STLC TWC Scalar Flux –TP #3; (b) STLC Non-TWC Scalar Flux – TP #3

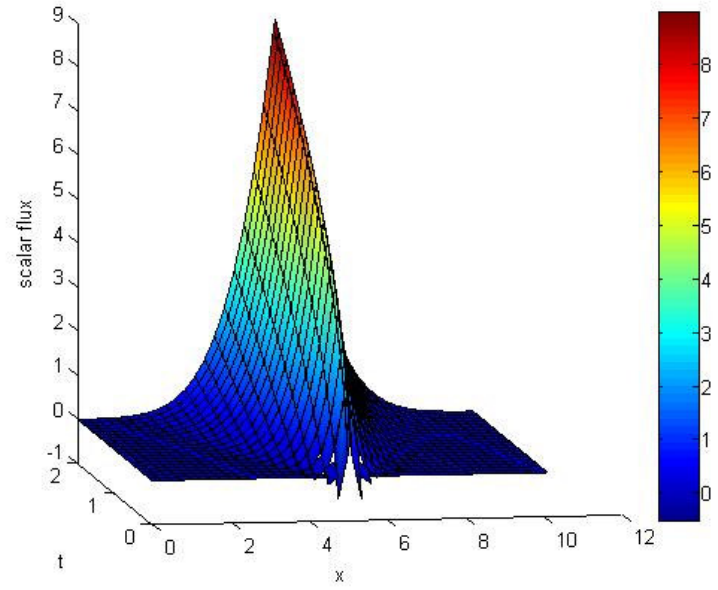

(b)

Figure 12: cont.

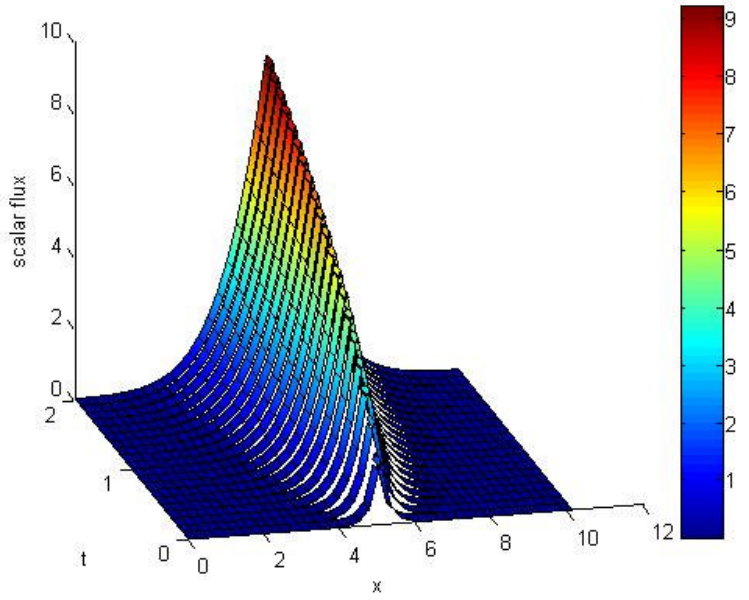

(a)

Figure 13: (a) Fully Implicit Scalar Flux Solution – TP #3; (b) Crank Nicholson Scalar Flux Solution – TP #3

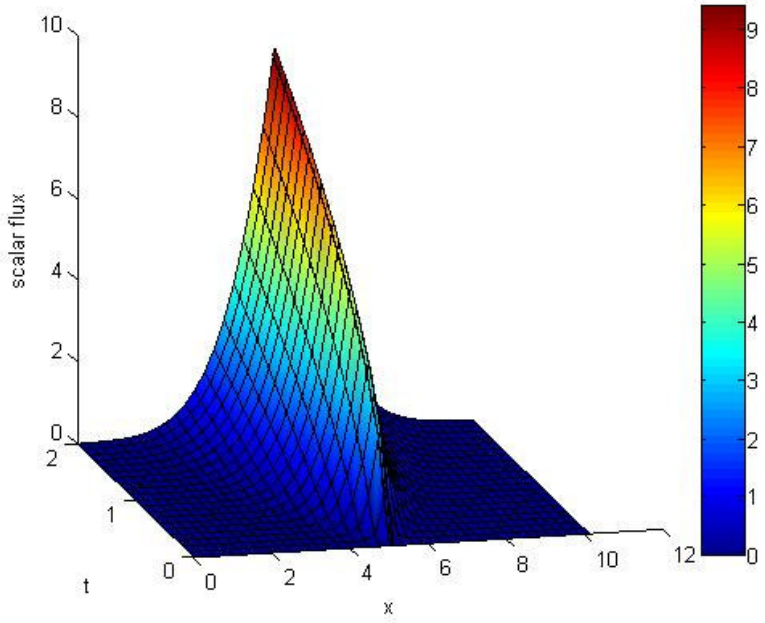

(b)

Figure 13: cont.

4.3.1: Diffusion from Linear-in-Time Surface Source

This test problem is a variation of the previous test problem and seeks to test certain results obtained from the asymptotic analysis of the STLC method. It consists of an isotropic surface source whose strength is linear in time, with the geometry of the problem given in Figure 14. A family of transport problems was tested by changing the value of ε to tend toward zero with the specifications given in Eq. (4.9).

$$\sigma_t = \frac{\sigma_{t,0}}{\varepsilon} = \frac{0.2}{\varepsilon}$$

$$c = \frac{\sigma_s}{\sigma_t} = 1 - \varepsilon^2$$

$$v = \frac{v_0}{\varepsilon} = \frac{8.6603}{\varepsilon}$$

$$\psi^m_{inc}(x,t) = 0, \quad \mu_m > 0,$$

$$\psi^m_{inc}(x,t) = 0, \quad \mu_m < 0, \tag{4.9}$$

$$\psi(x,0) = 0, \quad x \in (0,L)$$

Source Region:

$$q(x,\mu_m,t) = \varepsilon S_0 (1+2t) = 200\varepsilon(1+2t)$$

$$\Delta x_{source} = 0.0001 \ cm$$

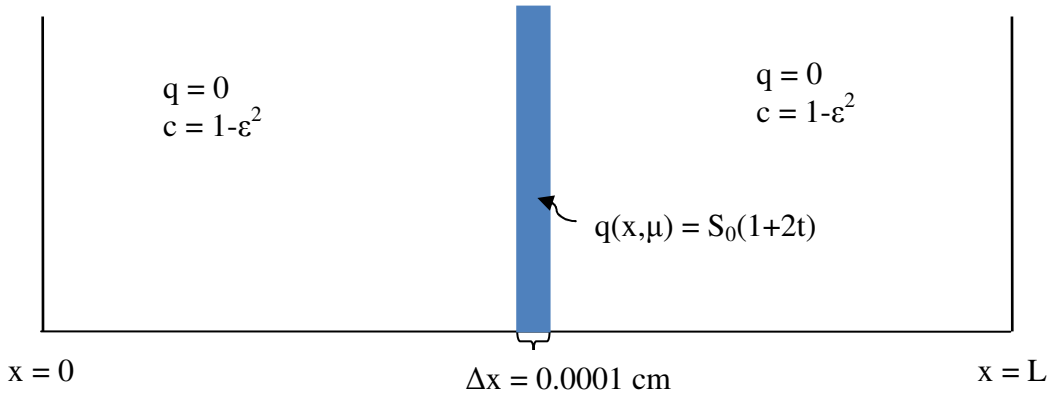

Figure 14: Geometry of Linear in Time Surface Source Test Problem

The analytic diffusion solution to this problem is also similar to the previous test problem, but in this case absorption must be considered. The source condition that simulates this linear-in-time surface source is given in Eq. (4.10).

$$q(x,t) = \delta(x - x_0)(S_0 + tS_t), \quad t > 0 \tag{4.10}$$

Solving the diffusion equation on an infinite slab as given in Eq. (4.4) with this source condition yields the general solution found in Eq. (4.11).

$$\phi(x,t) = C\int_0^t dt' S_0 \frac{e^{-\left(\frac{x^2}{4vD(t-t')}+v\Sigma_a(t-t')\right)}}{\sqrt{t-t'}} + C\int_0^t dt' S_t t' \frac{e^{-\left(\frac{x^2}{4vD(t-t')}+v\Sigma_a(t-t')\right)}}{\sqrt{t-t'}}, \qquad t>0, x\neq 0 \tag{4.11}$$

The proportionality constant in this solution is the same as that determined in the previous test problem. The analytic solution was produced by numerically integrating Eq. (4.11) with an adaptive Simpson quadrature function in Matlab with an absolute tolerance of tol = 1E-6. Figure 15 shows a plot of this analytic scalar flux solution in the region of interest for this test problem. It is important to note that this diffusion solution is independent of the value of ε, as one can see by inserting the definitions in Eq. (4.9) into the solution given in Eq. (4.11).

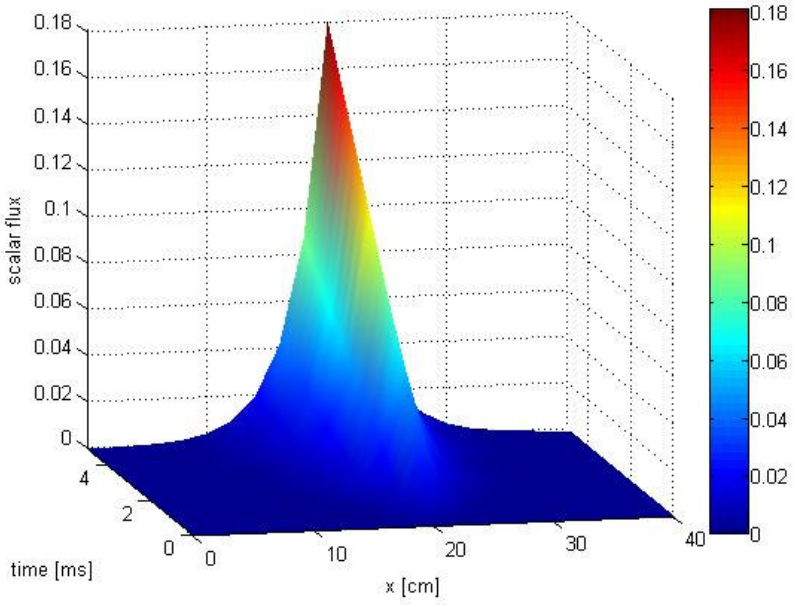

Figure 15: Analytic Diffusion Scalar Flux Solution

For the family of problems solved with this STLC method, several parameters were kept constant. Besides the specifications given in Eq. (4.9), the problem width is X = 40.0001 cm with a cell width of Δx = 2.0 cm and coincides to the geometry shown in Figure 14. Also the maximum time value used in the calculations is T = 5 ms with a time step of Δt_n = 0.25 ms. An S_4 quadrature set was used with a convergence tolerance in GMRES of tol = 1E-10. That is, GMRES declared convergence when $\|r\|_2 < (1E-10)\|b\|_2$, where r is the residual and b is the source vector for the GMRES iteration as described in section 2.3. The planar surface source was modeled by a very thin region made up of two cells with the same material properties as the rest of the problem domain as shown in Fig. 14. For the highly diffusive problems run in this family, GMRES is used to accelerate this STLC method to achieve convergence as explained in section 2.3. Also, in order to run problems with increasing scattering ratio the preconditioner described in section 2.3 was used to accelerate GMRES.

The following figures show the transport solution from STLC for various scattering ratios. Figure 16 shows the non-TWC scalar flux solution from the STLC code along with a time profile for a scattering ratio of c = 0.999. Figures 17 and 18 show the solution from the STLC code for scattering ratios of c = 0.99999 and c = 0.9999999. These plots show that the transport solution for the scalar flux varies only slightly as the scattering ratio becomes closer to unity. Figure 19 shows a cross section of the non-TWC solutions as compared to the analytic diffusion solution for a specific time step. As evident in the zoomed in section in Fig. 19, the transport solution agrees well with the analytic diffusion solution as the scattering ratio approaches unity.

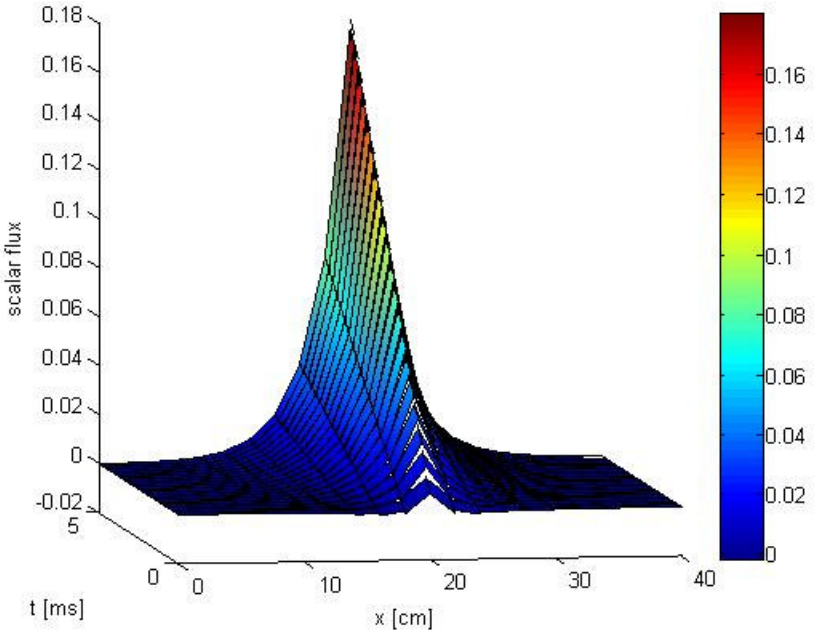

(a)

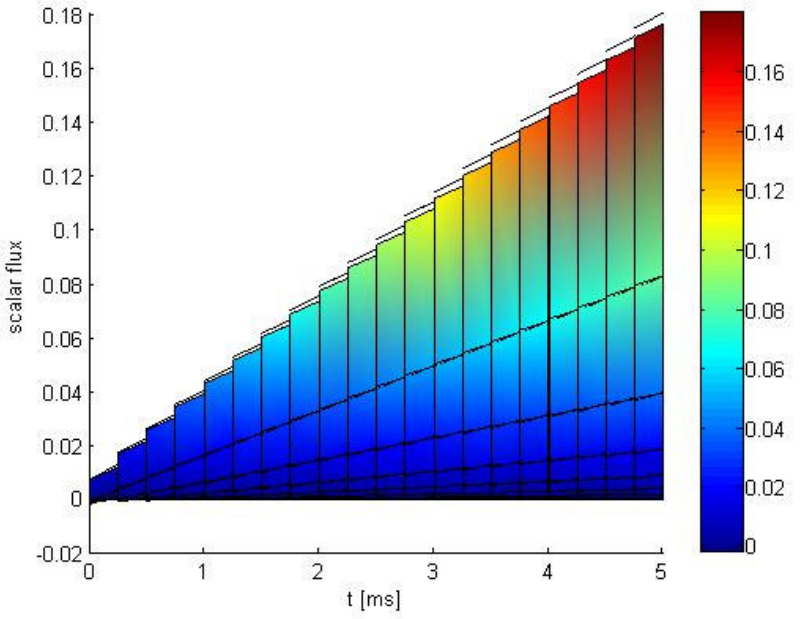

(b)

Figure 16: STLC Scalar Flux Solution (c = 0.999) (a) Non-TWC (b) Time Profile

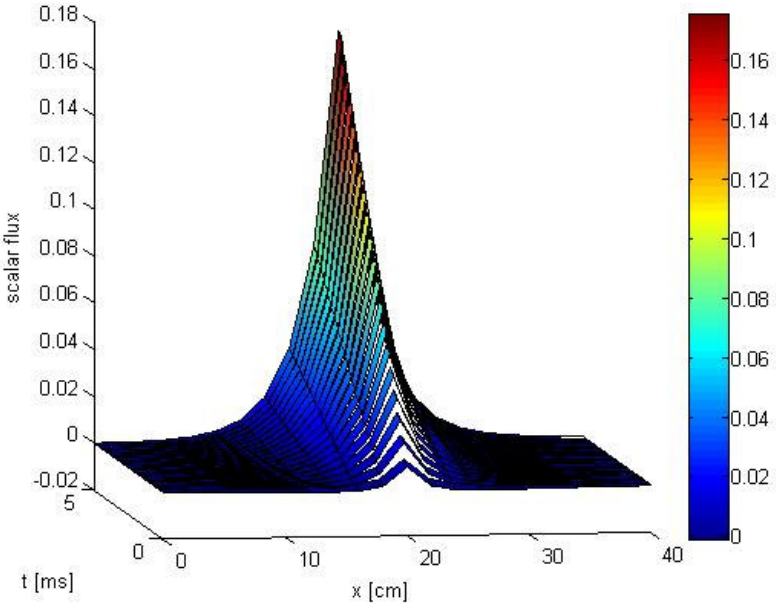

(a)

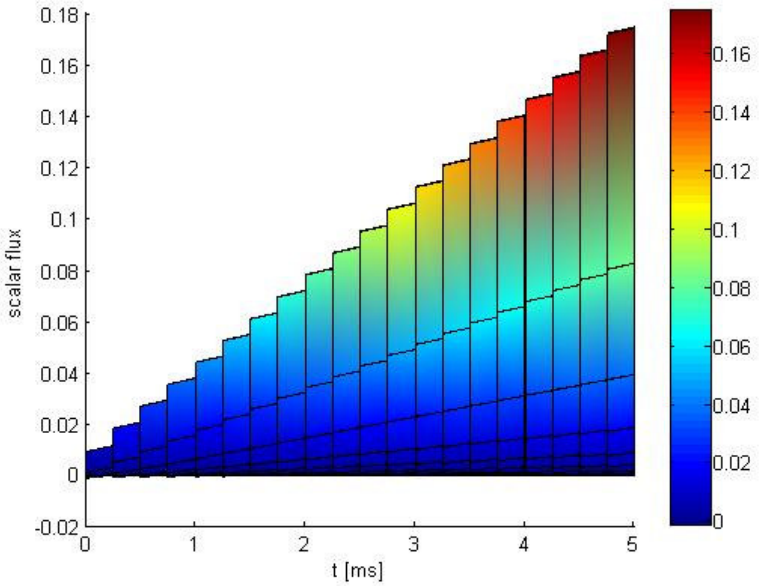

(b)

Figure 17: STLC Scalar Flux Solution (c = 0.99999) (a) Non-TWC (b) Time Profile

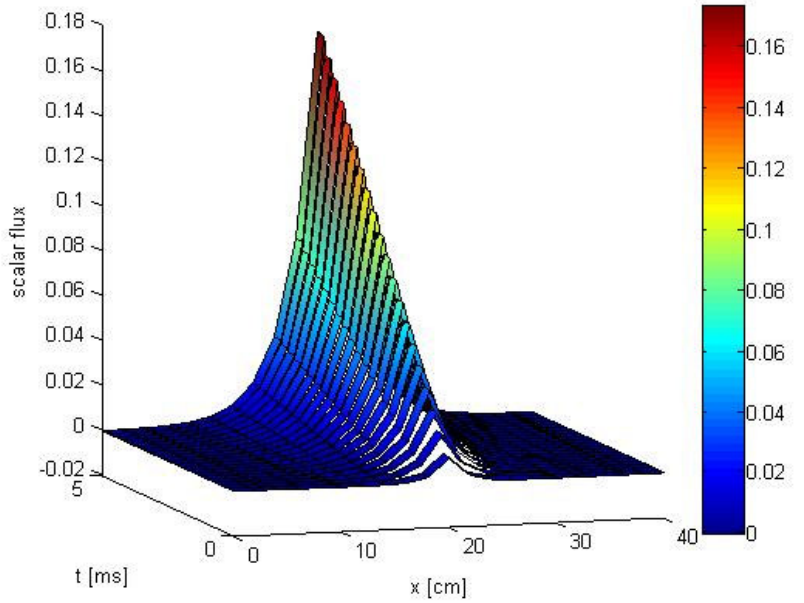

(a)

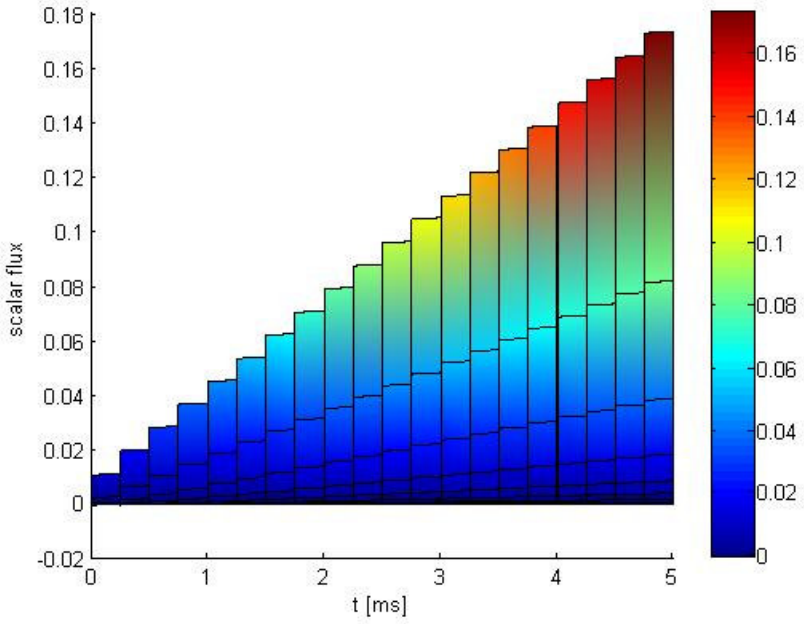

(b)

Figure 18: STLC Scalar Flux Solution (c = 0.9999999) (a) Non-TWC (b) Time Profile

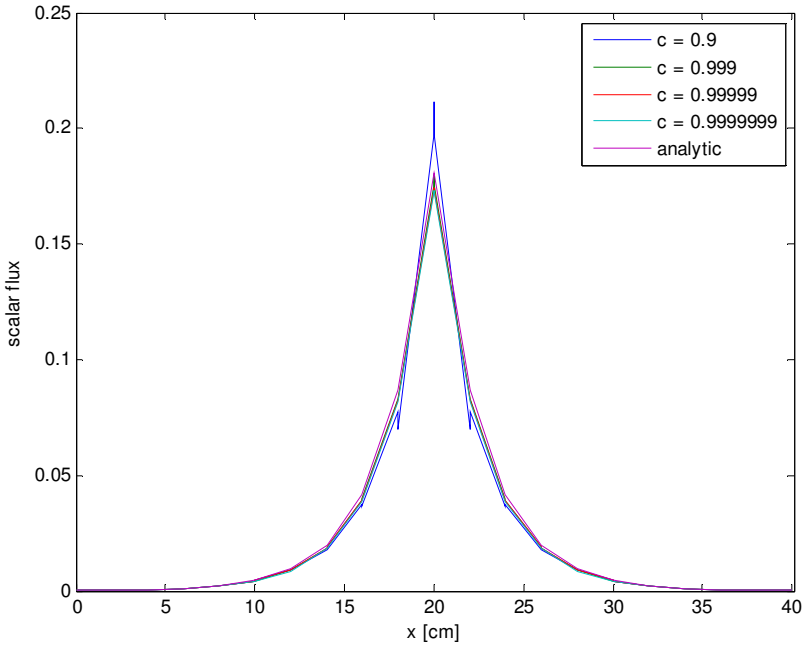

(a)

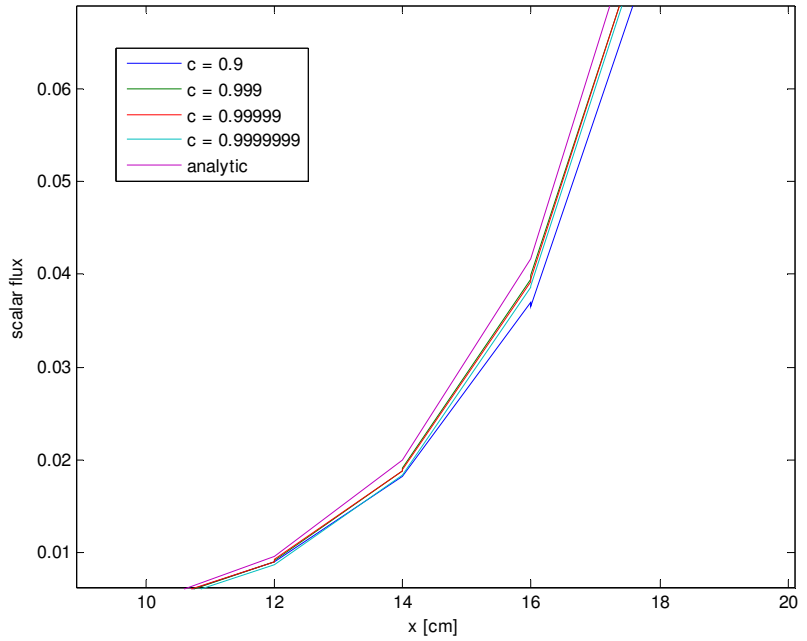

(b)

Figure 19: Comparison of Solutions at T = 5 ms (a) Full Domain (b) Zoom to Part of Domain

From the asymptotic diffusion limit analysis, it was found in Eq. (3.79) that the time-slope in each cell is an interpolation of the boundary time-slopes. From this analysis, for this problem, it would be expected for the time profile to be piecewise constant and approaching zero with the difference between successive cells equal to a constant across the problem. The time profiles of Figs. 16-18 clearly show that the time-slope approaches zero as the scattering ratio approaches unity which coincides with the results from the diffusion limit analysis of this method. Figures 20 and 21 show time profiles of the non-TWC scalar flux solution for various scattering ratios in a cell next to the source region and a cell 3rd from the source region. The analytic diffusion time profile solution is also plotted at these locations for comparison in Fig. 20 and 21. As can be seen in the zoomed in views of these plots, the solution approaches a piecewise constant in time (zero time-slope) in both of these cells as the scattering ratio approaches unity, as predicted by analysis.

For further comparison, Table 1 shows the values of the time moment of the non-TWC scalar flux for various scattering ratios at a specific time. These numbers show that as the scattering ratio approaches unity, the time-slope values approach zero as expected. Table 2 gives the difference of the time moments of the non-TWC scalar flux between successive cells at a given time. From these values, it can be seen that this difference between cells is approaching a constant value as the scattering ratio approaches unity which is expected from the diffusion limit analysis. There is a deviation from the expected values near the source region for these time-slope values which requires further investigation.

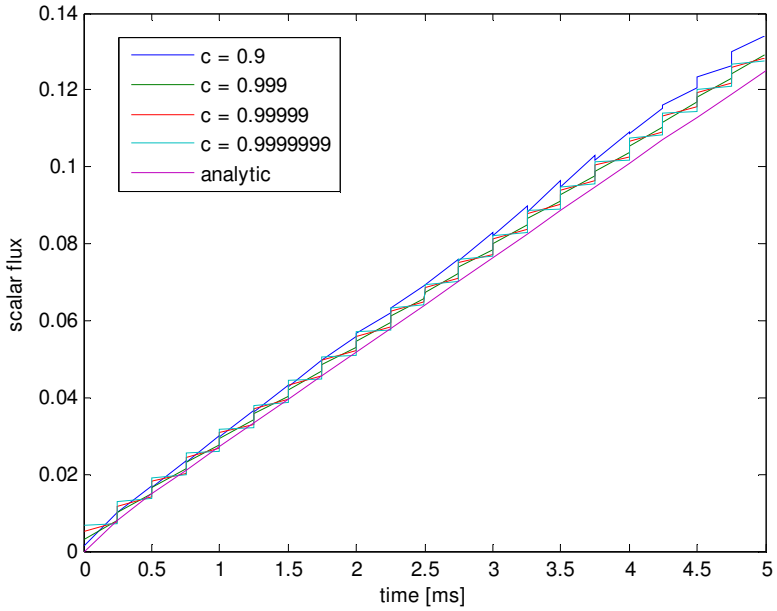

(a)

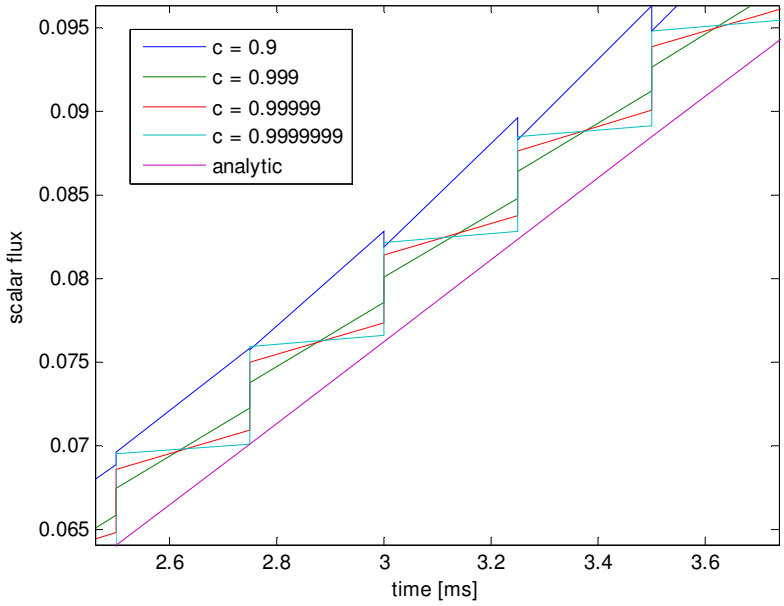

(b)

Figure 20: Time Profile of Solution in Cell Adjacent to Source (a) Full Time Domain (b) Zoom to Partial Time Domain

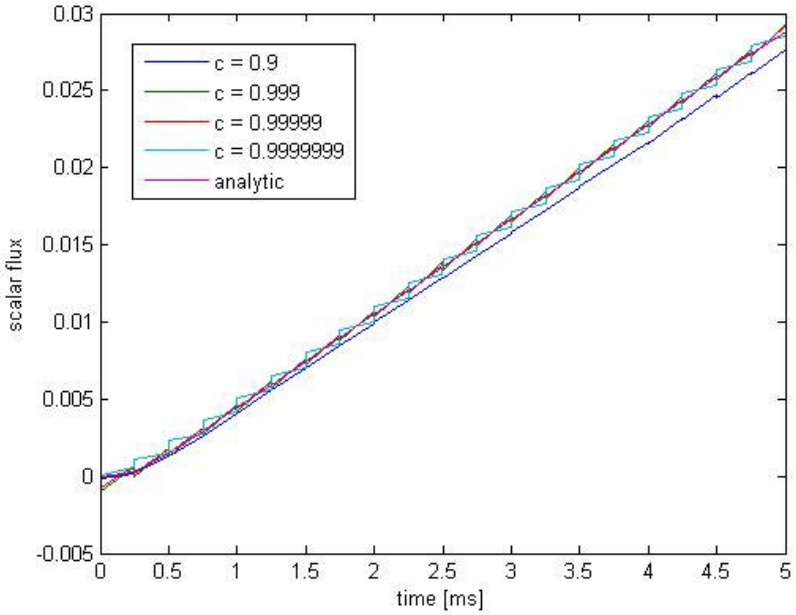

(a)

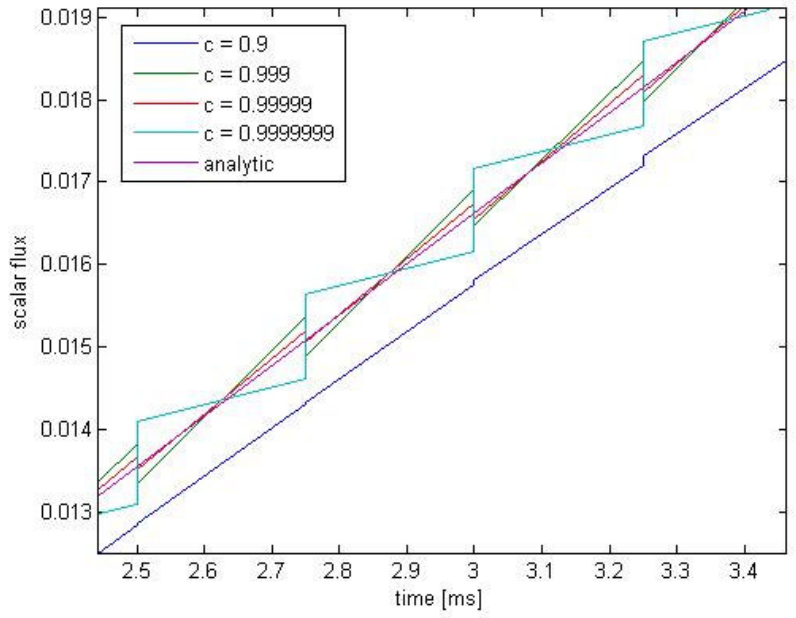

(b)

Figure 21: Time Profile of Solution in 3rd Cell from Source (a) Full Time Domain (b) Zoom to Partial Time Domain

Table 1: Non-TWC Time-slope Values at T = 4 ms

Cell	c = 0.999	c = 0.99999	c = 0.9999999
1	9.36E-06	6.17E-05	3.04E-05
2	2.35E-05	1.29E-04	6.09E-05
3	4.82E-05	2.03E-04	9.18E-05
4	9.59E-05	2.91E-04	1.23E-04
5	1.79E-04	3.97E-04	1.55E-04
6	3.25E-04	5.23E-04	1.88E-04
7	5.84E-04	6.78E-04	2.21E-04
8	1.02E-03	8.55E-04	2.53E-04
9	1.70E-03	1.04E-03	2.81E-04
10	2.47E-03	1.20E-03	3.00E-04

Table 2: Difference Between Non-TWC Time-slope Values at T = 4 ms

Cell	c = 0.999	c = 0.99999	c = 0.9999999
1-2	1.41E-05	6.68E-05	3.06E-05
2-3	2.48E-05	7.49E-05	3.09E-05
3-4	4.77E-05	8.77E-05	3.15E-05
4-5	8.31E-05	1.06E-04	3.21E-05
5-6	1.46E-04	1.27E-04	3.26E-05
6-7	2.59E-04	1.55E-04	3.26E-05
7-8	4.37E-04	1.77E-04	3.20E-05
8-9	6.79E-04	1.86E-04	2.80E-05
9-10	7.70E-04	1.58E-04	1.97E-05
10-11	2.02E-04	2.35E-05	1.86E-06

4.4 Test Problem 4: Interface Problem

This test problem is designed to determine how the STLC method can handle the solution with an unresolved boundary layer at an interface. Figure 22 shows the properties and geometry of this problem which consists of a thin region followed by an optically thick region. The boundary and initial condition on the left is an incident beam at the largest positive quadrature cosine (approximately normal incidence). This

beam is present for all 20 time steps with length $\Delta t_n = 10$ s. As denoted in Fig. 22 the total length of the problem is L = 2 cm with uniform cell spacing in each region of Δx = 0.1 cm. Due to the long time step in comparison to the mean free path, the track spacing is determined by this time step length which leads to a track spacing of $\Delta\omega_k = 0.27305$ cm. An S_{16} quadrature set was used with a desired convergence tolerance of tol = 1E-07. The steady-state analytic diffusion solution is found for the diffusive region from the LD equations for comparison. This general solution is given in Eq. (4.12). The conditions needed to find the constants in the general solution are given in Eq. (4.13).

$$\phi(x) = A\exp\left(-x\sqrt{\frac{\Sigma_a}{D}}\right) + B\exp\left(x\sqrt{\frac{\Sigma_a}{D}}\right) \tag{4.12}$$

$$\begin{aligned}
&\frac{1}{4}\phi(x_R) = \frac{1}{2}D_R\left.\frac{d\phi}{dx}\right|_{x=x_L} + \frac{1}{2}w_{16}\left(\frac{3}{2}\mu_{16}^2 + \frac{\mu_{16}}{\sum_{\mu_m>0} 2w_m\mu_m}\right)\exp\left(\frac{-x_L\Sigma_{tL}}{\mu_{16}}\right)\\
&\frac{1}{4}\phi(x_R) = -\frac{1}{2}D_R\left.\frac{d\phi}{dx}\right|_{x=x_R}\\
&x_L = 1cm\\
&x_R = 2cm\\
&\Sigma_{tL} = 1cm^{-1}\\
&D_R = \frac{1}{3\Sigma_{tR}} = \frac{1}{3000}cm
\end{aligned} \tag{4.13}$$

As explained in Section 2.3, GMRES is used to accelerate the STLC method for this problem due to the highly diffusive region. Figures 23 and 24 show the STLC scalar flux solutions, TWC and non-TWC, at various time steps along with the analytic steady-state LD diffusion solution. The boundary layer is not resolved in this case, but it would be resolved as the cell width is refined. As seen from these results, the STLC method approaches this steady-state diffusion limit to within the desired tolerance. This result is

expected from the asymptotic analysis of the STLC method performed in Section 3.4. Also it is encouraging to note that in this slab geometry, a bilinear representation of the source was not needed to produce accurate results, but this is only because this solution is in steady-state. For non-steady-state solutions, the bilinear terms must be included to produce an accurate time-slope result as was illustrated in the previous test problem.

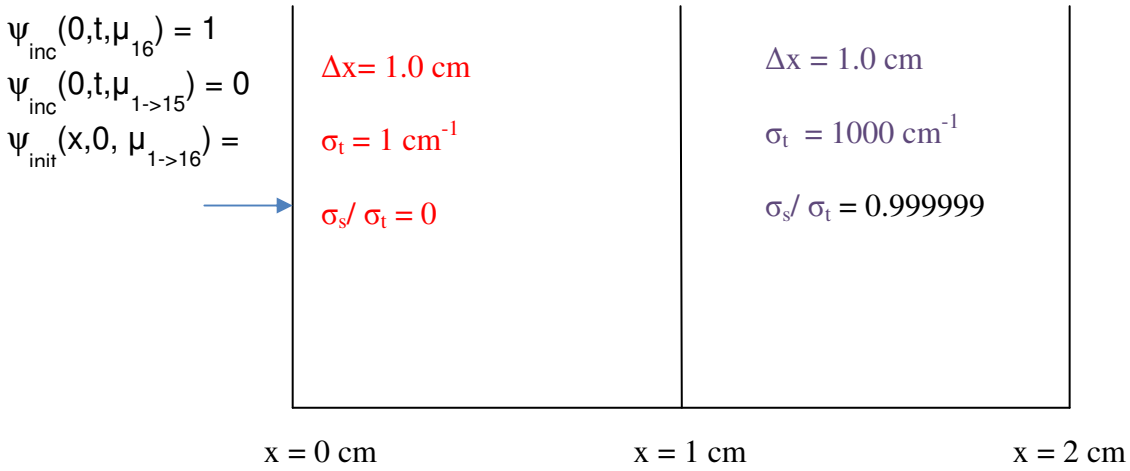

Figure 22: Geometry of TP #4: Interface Problem

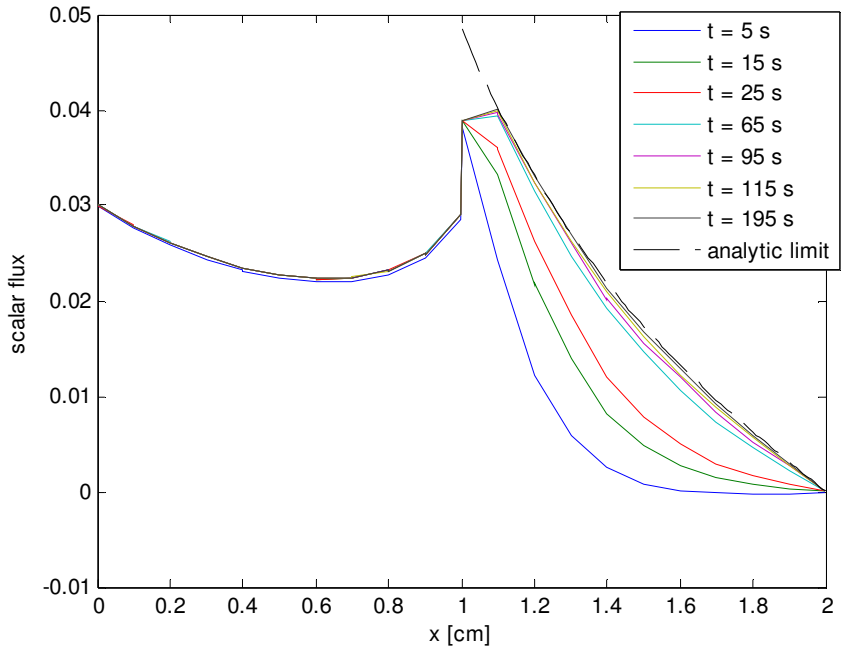

Figure 23: STLC TWC Scalar Flux Solution for Different Time Levels and the Analytic LD Diffusion Solution

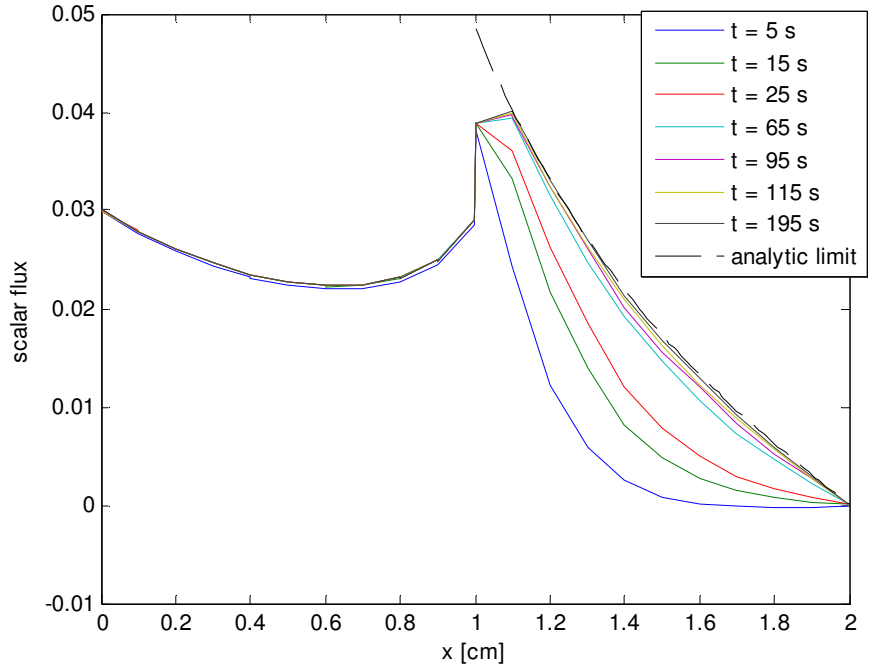

Figure 24: STLC Non-TWC Scalar Flux Solution for Different Time Levels and the Analytic LD Diffusion Solution

5. SUMMARY AND CONCLUSIONS

5.1 Summary

The motivation of this work was to develop and understand a discrete ordinate method that uses an accurate discretization in space and time, with the only approximation being in the representation of the collision source. The result is our STLC least-square method, which in this work employed a linear function for the collision source in each space-time cell. Two different linear solutions are plausible in each cell. One is smoothly varying; the other yields cell-wise and track-wise conservation. The smooth least-square solution is exact if the exact solution is linear in space and time.

An asymptotic analysis of the STLC method in the thick diffusion limit was performed. This analysis showed that the leading-order STLC solution satisfies a diffusion discretization similar to a linear continuous FEM discretization in space with time differencing that is the same as fully implicit (Backward Euler) except for an extra "time-slope" term. If the time-slope term were accurate, this time discretization would be better than fully implicit. However the analysis showed that the time-slope term satisfies, to leading-order, unphysical equations: it depends only on boundary conditions and not on sources or material properties.

Results from various test problems showed the viability of this STLC method as applied to streaming and diffusive problems. These test problems are all consistent with the prediction from the asymptotic analysis both as the solution approaches steady-state and regarding the time-slope term in time-dependent problems. There are several

options to address the "flaw" with the time-slope term. One option is to force the time-slope of the incident angular flux to zero in 1D thick diffusive problems. Another and better option is to use a bilinear collision source representation. Part of this work has been presented and summarized in Pandya & Adams [14].

5.2 Conclusions

We have developed a long characteristic method in space and time that can accurately find the solution of both diffusive and streaming problems. This STLC method is exact for problems with linear solution in space and time and only makes one approximation: the distribution of the collisional source term. The capability to produce two different results, TWC and non-TWC, allows this method to attain the following properties:

- Cell-wise reaction rate equal to the sum of track-wise reaction rates,
- Exact solution along each ray,
- Possible unsmooth cell-to-cell variation in reaction rates for problems whose correct reaction rates are smoothly varying.

Also, from the asymptotic analysis results in the thick diffusion limit, this STLC method is applicable to a large range of problems including radiation transport in very diffusive media. STLC behaves much like an implicit linear FEM discretization in such problems. In application to higher dimensions it should be noted that the "flaw" due to the time-slope term must be addressed. Overall, this method shows great promise for several applications and should be further developed.

6. RECOMMENDATIONS

There are many further research areas surrounding the application and development of this STLC method. First would be to extend this method to higher spatial dimensions so it can be applied to realistic transport problems. This extension is relatively straightforward. Based upon the results of the diffusion limit analysis in 1D, a bilinear representation of the scattering source will be needed to achieve accurate solutions in 1D, trilinear in time-dependent 2D (x,y,t), and quadrilinear in time-dependent 3D (x,y,z,t).

With the extension to higher dimensions comes the need to make this STLC method adaptive. For regions of particular interest requiring finer resolution, the track width should be refined for only this region and incorporated into the full solution process. A method for performing a negative fix up should also be developed to fix the possible negativity of solution that can occur due to the linear representation of the source. This negative fix up can either change the solution or the source representation.

With this expansion to higher dimensions also comes the motivation to devise a parallel algorithm for massively parallel computing. Since the solution along each ray in a problem can be found separately, the division among many processors seems logical. However, the details of this parallel scheme are rather complicated.

REFERENCES

[1] K. S. Smith and J. D. Rhodes, CASMO-4 Characteristics Method for Two-Dimensional PWR and BWR Core Calculations, Trans. Am. Nucl. Soc. 83 (2000) 294.

[2] G. S. Lee, *et al*., Acceleration and Parallelization of the Method of Characteristics for Lattice and Whole-Core Heterogeneous Calculations, Proc. Int. Mtg. Advances in Reactor Physics and Mathematics and Computations into the new Millenium, Pittsburgh, PA, American Nuclear Society, 2000.

[3] M. R. Zika and M. L. Adams, Transport Synthetic Acceleration for Long-Characteristics Assembly-Level Transport Problems, Nucl. Sci. Eng. 134 (2000) 135-158.

[4] K. S. Smith and J. D. Rhodes, Full-Core, 2-D, LWR Core Calculations with CASMO-4E, Proc. Int. Conf. on the New Frontiers of Nuclear Technology: Reactor Physics, Safety and High-Performance Computing, Seoul, Korea, 2002.

[5] M. L. Adams, E. W. Larsen, Fast iterative methods for discrete-ordinates particle transport calculations, Prog. Nucl. Energy 40 (2002) 3-159.

[6] M. Dahmani, R. Le Tellier, R. Roy, A. Hebert, An efficient preconditioning technique using Krylov subspace methods for 3D characteristic solvers, Annals of Nuclear Energy 32 (2005) 876-896.

[7] Y. Saad, Iterative Methods for Sparse Linear Systems, second ed., Society for Industrial and Applied Mathematics, Pittsburgh, PA, 2003.

[8] M. Adams, N. Amato, P. Nelson, and L. Rauchwerger, Efficient Massively-Parallel Implementation of Modern Deterministic Transport Calculations, Report to the Department of Energy, Texas A&M University, College Station, TX, October 2002.

[9] M. Mathis, N. Amato, M. L. Adams, A General Performance Model for Parallel Sweeps

on Orthogonal Grids for Particle Transport Calculations, Proc. Intl. Conf. on Supercomputing, Santa Fe, New Mexico, 2000.

[10] S. Pautz, M. Adams, T. Pandya, Scalable Parallel Prefix Solvers for Discrete Ordinates Transport, Proc. Intl. Conf. on Mathematics, Computational Methods, and Reactor Physics, Saratoga Springs, NY, American Nuclear Society, 2009.

[11] E. W. Larsen, J. E. Morel, W. F. Miller Jr., Asymptotic Solutions of Numerical Transport Problems in Optically Thick, Diffusive Regimes, J. Comp. Phys., 69 (1987) 283-324.

[12] E. W. Larsen, J. E. Morel, Asymptotic Solutions of Numerical Transport Problems in Optically Thick, Diffusive Regimes II, J. Comp. Phys., 83 (1989) 212-236.

[13] M. L. Adams, T. A. Wareing, W. F. Walters, Characteristic Methods in Thick Diffusive Problems, Nucl. Sci. Eng. 130 (1998)18-46.

[14] T. Pandya, M. Adams, Method of Long Characteristics Applied in Space and Time, Proc. Intl. Conf. on Mathematics, Computational Methods, and Reactor Physics, Saratoga Springs, NY, American Nuclear Society, 2009.

APPENDIX A

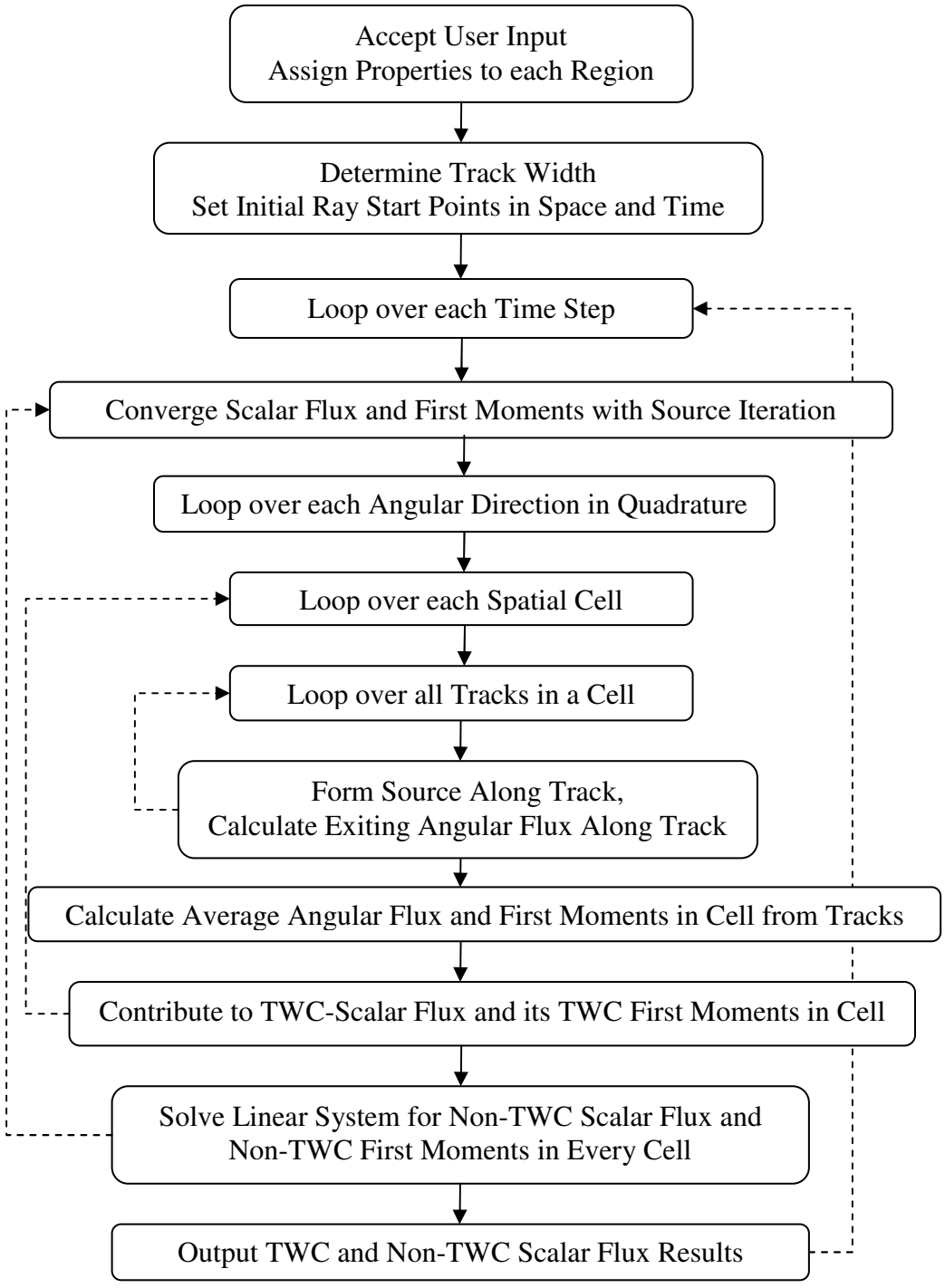

Figure A.1: Layout of STLC Method Implementation with Source Iteration

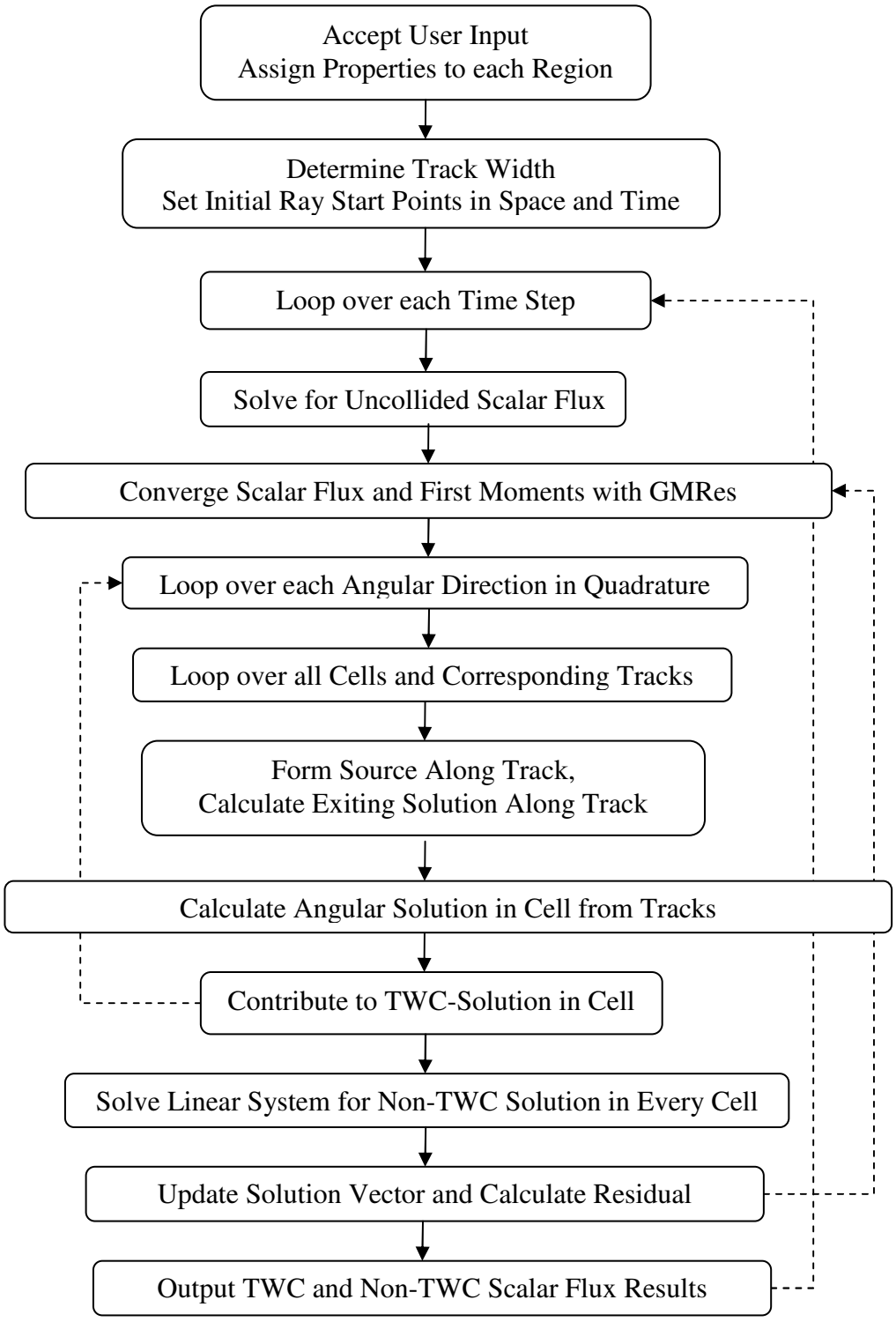

Figure A.2: Layout of STLC Method Implementation with GMRes

VITA

Name:	Tara Marie Pandya
Address:	Nuclear Engineering Department, Texas A&M University, 3133 TAMU, College Station, TX, 77843
Email Address:	tarapandya@tamu.edu
Education:	B.S., Nuclear Engineering, Texas A&M University, 2006
	M.S. Nuclear Engineering, Texas A&M University, 2009